AD-A217 366

F-15B HIGH ANGLE-OF-ATTACK PHENOMENA
AND SPIN PREDICTION USING
BIFURCATION ANALYSIS

THESIS

Daniel D. Baumann
Captain, USAF

AFIT/GAE/ENY/89D-01

DEPARTMENT OF THE AIR FORCE

AIR UNIVERSITY

AIR FORCE INSTITUTE OF TECHNOLOGY

Wright-Patterson Air Force Base, Ohio

89 12 29 037

AFIT/GAE/ENY/89D-01

DTIC
ELECTE
JAN 3 1 1990
S B D

F-15B HIGH ANGLE-OF-ATTACK PHENOMENA
AND SPIN PREDICTION USING
BIFURCATION ANALYSIS

THESIS

Daniel D. Baumann
Captain, USAF

AFIT/GAE/ENY/89D-01

AFIT/GAE/ENY/89D-01

F-15B HIGH ANGLE-OF-ATTACK PHENOMENA
AND SPIN PREDICTION USING BIFURCATION ANALYSIS

THESIS

Presented to the Faculty of the School of Engineering
of the Air Force Institute of Technology
Air University
In Partial Fulfillment of the
Requirements for the Degree of
Master of Science of Aeronautical Engineering

Daniel D. Baumann, B.S., P.E.
Captain, USAF

December 1989

Acknowledgements

The purpose of this study was to develop a complete nonlinear analytical model of the F-15B aircraft accurate throughout the entire angle-of-attack range (-20 degrees to 90 degrees) in order to study in-depth high angle-of-attack phenomena such as flat spins. This thesis would not have been possible without a great deal of help from a number of individuals who gave unselfishly of their time and/or expertise. I would like to recognize their support and contributions at this time.

I would like to thank my advisor, Capt. James Planeaux of the Air Force Institute of Technology, who provided a great deal of insight and guidance on Bifurcation Theory as well as to the kinematic relationships of the aerodynamic coefficients. I would be remiss not to mention appreciating his ability to come up with some necessary special curve fitting techniques as well as help with AUTO. I would also like to thank Jeff Beck as an unofficial committee member for his invaluable help and advice during this study. A large debt of gratitude and thanks is due to Jeff Priem of Aeronautical Systems Division (ASD) F-15 System Programming Office (SPO) for providing me with Aerodynamic Data which was used as the basis for my project as well as providing me with much needed general information. I wish to thank Dr. Reynolds for a number of critical lessons and help on

ii

STATEMENT "A" per Ms. K. Criner
AFIT-GAE-ENY
TELECON   1/31/90   CG

by _per telecon_

Distribution/
Availability Codes

Dist	Avail and/or Special
A-1	

running SAS. A special thanks goes to Major Bob Papka for helpful hints on using Word Perfect. I would like to thank the Audio Visual library at Edwards AFB, AFFTC/HO, for providing me with the motivational film used in my thesis defense. I also offer special thanks to Captain Thomas J. Barth for the help he provided above and beyond the call of duty. His work once realized and appreciated provided a great deal of inspiration. Thanks Kathee for your endless patience, understanding, good humor and above all great hugs. It is now time for me to return to the raison d'etre for this diversion - flying.

Finally I would like to dedicate this work to the memory of Adele Baumann, a much missed friend and confidant.

Captain Daniel D. Baumann

Table of Contents

List of Figures

List of Figures
(Continued)

List of Tables

List of Symbols

Symbol	Definition	Units
b	wing span	ft
c	wing mean aerodyamic chord	ft
CG	center of gravity, % mean aerodynamic chord	
C_D	drag coefficient	
C_L	lift coefficient	
C_l	rolling moment coefficient	
$C_{l\beta}$	rolling moment derivative with respect to sideslip angle	1/deg
$C_{l\delta a}$	aileron effectiveness derivative	1/deg
$C_{l\delta e}$	stabilator effectiveness derivative	1/deg
$C_{l\delta\Delta e}$	differential stabilator effectiveness derivative	1/deg
$C_{l\delta r}$	rudder effectiveness derivative	1/deg
C_{lp}	roll damping derivative	1/rad
C_{lr}	rolling moment derivative with respect to yaw rate	1/rad
C_m	pitching moment coefficient	
C_{mo}	basic pitching moment coefficient	
C_{mq}	pitching moment derivative with respect to pitch rate	1/rad
C_n	yawing moment coefficient	
$C_{n\beta}$	yawing moment derivative with respect to sideslip angle	1/rad
$C_{n\beta*}$	yawing moment derivative high angle-of-attack increment with respect to sideslip angle	1/rad

List of Symbols
(continued)

Symbol	Definition	Units
$C_{n\delta a}$	yawing moment derivative with respect to aileron deflection	1/deg
$C_{n\delta e}$	yawing moment derivative with respect to stabilator deflection	1/deg
$C_{n\delta\Delta e}$	yawing moment derivative with respect to differential stabilator deflection	1/deg
$C_{n\delta r}$	rudder effectiveness derivative	1/deg
C_{np}	yawing moment derivative with respect to roll rate	1/rad
C_{nr}	yaw damping derivative	1/rad
C_x	longitudinal force coefficient	
C_y	side force coefficient	
$C_{y\beta}$	side force derivative with respect to sideslip angle	1/deg
$C_{y\beta*}$	asymmetric side force derivative high angle-of-attack increment with respect to sideslip angle	1/deg
$C_{y\delta a}$	side force derivative with respect to aileron deflection	1/deg
$C_{y\delta e}$	side force derivative with respect to stabilator deflection	1/deg
$C_{y\Delta e}$	side force derivative with respect to differential stabilator deflection	1/deg
$C_{y\delta r}$	side force derivative with respect to rudder deflection	1/deg
C_{yp}	side force derivative with respect to roll rate	1/rad
C_{yr}	side force derivative with respect to yaw rate	1/rad

x

Symbol	Definition	Units
C_z	normal force coefficient	
g	gravitational constant, 32.2 ft/sec^2	ft/sec^2
I_x, I_y, I_z, I_{xz}	body axis moments and product of inertia, taken about the center of mass	slugft^2
LHP	Left Half Plane	
p,q,r	roll, pitch, and yaw angular rates about body axis	rad/sec
$\bar{q}$	dynamic pressure, $(1/2)\rho V^2$	slug/ft
RHP	Right Half Plane	
S_{ref}	wing reference area	ft^2
t	time	sec
$\bar{u}$	vector of state variables; e.g., for n=8 $\bar{u} = (\alpha,\beta,p,q,r,\theta,\phi,V)^T$	
V	true airspeed	ft/sec
α	angle-of-attack	degrees
β	sideslip angle	degrees
δ_a	aileron surface deflection	degrees
δ_e	stabilator surface deflection	degrees
$\delta_{\Delta e}$	differential stabilator surface deflection	degrees
δ_r	rudder surface deflection	degrees
$\Delta C_{l\beta}$	Rolling Moment Increment due to 2-Place Canopy	
$\Delta C n_\beta$	Yawing Moment Increment due to 2-Place Canopy	

List of Symbols
(continued)

Symbol	Definition	Units
ΔCn_{β°	Asymmetric Yawing Moment Increment	
ΔCy_{β°	Asymmetric Side Force Increment	
Δz_{offset}	Thrust offset ($= 0.25/12.0$)	ft
γ	flight path angle	degrees
λ	free parameter	
ϕ	bank angle	degrees
ρ	period	seconds
θ	pitch angle	degrees

Abstract

Modern fighter aircraft are being designed to be operated at higher and higher angles-of-attack. The resulting increase in maneuverability is offset however by an increase in susceptibility to departure from controlled flight. An investigation of the F-15B fighter aircraft was undertaken to predict high angle-of-attack phenomena such as flat spins. Aerodynamic forces and moments as a function of control surface deflections (δ_a, δ_e, $\delta_{\Delta e}$, δ_r) were modeled over a wide angle-of-attack range ($-20° \leq \alpha \leq +90°$) and were then used to formulate a non-linear eight state (α, β, p, q, r, θ, ϕ, V) aircraft model. Equilibrium and periodic solutions to the resulting equations of motion were then computed using a bifurcation analysis package. A number of bifurcation points, limit points and Hopf bifurcation points were detected indicating changes in flight stability. Several stable equilibrium solution branches at angles-of-attack greater than 70 degrees were observed which correspond to flat spin behavior. Theoretically predicted flat spin conditions correlated well with empirical flight test data. In addition stable equilibrium and periodic solutions other than those corresponding to spin behavior were surveyed resulting in a global map of stability as a function of control surface deflection for the F-15B.

I. Introduction

The capability of modern fighter aircraft to operate in the high angle-of-attack (> 40°) flight regime has markedly improved in the past few years. The enhancement of this capability however has lead to an increase in the susceptibility to departure from controlled flight. Analysis of high angle-of-attack phenomena such as stall, departure, spin entry, flat and steep spin, nose slice and wing rock is complicated by the highly nonlinear nature of the governing equations of motion. Analysis of these types of phenomena would be greatly enhanced by a mathematical tool which would be able to describe and predict a number of sudden transitions between flight modes. These sudden transitions occur near singular points of the nonlinear equations and lead to multiple solution behavior (1:257). Numerical bifurcation analysis provides a modelling technique that predicts abrupt non-linear changes in state (due to control changes) such as transitions from equilibrium to periodic motions and jumps between rival equilibrium and periodic states. A systematic method of applying numerical bifurcation analysis to flight mechanics problems would result in a deeper understanding of high α phenomena and the underlying mechanisms leading to their occurence. A motivating example (which could be studied

1

upon extension of this work) follows. On 16 December 1985 an F15D fighter aircraft from Eglin Air Force Base took off for what was to be its last sortie. The objectives of the mission included an F-15 handling qualities demonstration. The first maneuver performed in the handling qualities phase was a straight ahead 1-G stall where about 35-40 units angle-of-attack was obtained with the airplane responding in characteristic mild wing rock. The second maneuver was another 1-G stall in excess of 45 units angle-of-attack with no adverse effects observed due to lateral control inputs. The third maneuver was to be an abrupt accelerated stall with a top rudder input. The intent of these manuevers was to demonstrate the benign handling qualities of the F-15 at high angles of attack.

The third maneuver was initiated at 31,500 feet in a slightly climbing left turn (approximately 60 to 70 degrees of bank). Full aft stick with no lateral deflection was applied to acheive an accelerated stall. As the aircraft began to dig in, the airspeed bled off to about 230 - 240 knots (0.39 M - 0.41 M). Full top (right) rudder was initiated while holding full aft stick. It was expected that the aircraft would yaw nose high and to the right describing an elliptical arc (Approximately 60 - 70 degrees nose high). The nose would then fall through the horizon putting the aircraft in a subsequent dive.

What happened instead was that once the top rudder

2

input was given the aircraft simultaneously rolled and yawed (sliced) to the right in a crescent arc (approximately 20 - 30 Degrees nose high). Upon commencement of the yaw or departure tone the top (right) rudder input was discontinued. By the time recovery procedures were initiated (controls neutralized) the F-15 had stabilized into a nose low, flat spin. The parameters of the spin were 15 degrees right bank, vertical velocity of 250 feet/sec, pitch was -34 degrees, and the yaw rate (q) was about 60 degrees/sec. The aircraft was never recovered from the flat spin and was destroyed in subsequent impact with the Gulf of Mexico.

The aircraft was equipped with Conformal Fuel Tanks (CFT's) which have been demonstrated to allow the F-15 to reach higher angles of attack. In addition there was an estimated 2100 to 2800 ft-lb asymmetry at the time of maneuver initiation.

The reason for the aircraft departing controlled flight and immediately entering a spin was never determined by the accident investigation board. The out-of-control recovery procedure failed to recover the aircraft even though simulations run with the accident parameters showed that the aircraft should have recovered. Hence a strong motivation for this thesis. In hindsight, solving the nonlinear equations of motion for stable equilibrium and periodic states at high angles-of-attack could possibly have been

3

used in the investigation to predict the consequences of the preceding maneuver as well as suggesting a recovery strategy. For the future a global, as opposed to a local, map of the F-15's stability could be used to reduce the possibility of repeat accidents. Warnings against such maneuvers might be included in the F-15-1 Flight Manual, and synthesis or modification of the control laws implemented by the Control Augmentation System (CAS) (6:7) might be possible.

This investigation is limited to the study of the high angle-of-attack (α) behavior of the F-15B since this aircraft was modelled previously by Barth and his model serves as a basis for comparison; also data are available. Previous investigations of the dynamic behavior and stability of the F-15 using Bifurcation Analysis include papers by Planeaux and Barth (9), Barth (12) and Hawkins(3). In addition, the model developed using this technique need only be slightly modified to be applied to the F-15D example mentioned above. Once the effects are fully understood for the basic F-15B then the differences in stability between it and the F-15D can be isolated to those caused by the Conformal Fuel Tanks (CFT's), the asymmetrical weight distribution and any other differences.

Objective

The objective of this investigation was to formulate a realistic and complete non-linear 8 state model of the F-

4

15B in order to study high angle-of-attack phenomena such as flat spins and be able to predict such behavior.

Method

As implied by earlier arguments bifurcation analysis lends itself to extracting important information without having to find many time-dependent solutions of non-linear differential equations. For this project the F-15B aerodynamic forces and moments were represented as polynomial functions of angle-of-attack, sideslip angle, aileron, rudder and stabilator deflection angles. These forces and moments as well as those due to thrust were then used to construct the non-linear differential equations of motion which constituted the aircraft 8 state vector $\bar{u} = (\alpha, \beta, p, q, r, \theta, \phi, V)^T$.

The aerodynamic coefficients for forces and moments were modeled for the full angle-of-attack range (-20 degrees to 90 degrees), sideslip angles between -30 degrees to 30 degrees, as well as for the entire range of control surface deflections. The airspeed and altitude chosen for investigation were 0.6 Mach and 20,000 feet due to the fact that the F-15B has reduced directional stability and spin resistance in this flight regime (3:3).

Numerical bifurcation analysis is used to study the aircraft dynamics. This methodology can be classified as a continuation method that calculates whole solution surfaces rather than specific equilibrium and periodic solutions. As

5

such it can be used to systematically investigate global as opposed to local or linear behavior. An advantage of this method is that once a single solution has been calculated on a "branch" the rest of the solutions that lie on that branch can be calculated in a sequential manner.

The aircraft model once formed was solved by hand for a set of equilibrium conditions that made the equations easy to work with. Once the equations were solved for that particular condition the solution was used as the starting point for a bifurcation software package AUTO (23). AUTO then calculated the rest of the equilibrium solutions for that branch. AUTO was also capable of switching onto and computing bifurcating branches of equilibrium and periodic solutions, but this was not the focus of this study.

It should be pointed out that bifurcation analysis does not give transient behavior, only long-term behavior. This contrasts with classical approaches with some advantages and disadvantages. The derivation of the equations of motion provide an excellent point of departure to compare how bifurcation analysis differs from classical aircraft control analysis and by doing so shows how the technique of bifurcation analysis can be used as a supplemental analytical tool by pointing out its following merits;

1) simplification of the non-linear equations of motion is not necessary

2) the range of application of results is wider

3) gives more of a big picture view (global versus local) of aircraft behavior, as such it is a more concise summary

4) A more straight forward and direct measure of the aircraft states. Less interpretation is required than for a root locus diagram, etc.

Although bifurcation analysis retains the above advantages over classical control analysis it does have its limitations and because of these limitations it should not be used to completely replace classical control theory. The biggest shortcoming of this technique is that it does not give the speed or rate at which the aircraft states go to equilibrium, which classical control theory does.

II. Bifurcation Theory

Bifurcation theory is best described as the study of qualitative as opposed to quantitative change. This notion is illustrated by the following verb associations (10:1);

    bend-break
    incline-tip over
    stretch-tear
    inflate-burst

The verbs on the left side can be thought of as a measure of a state that is stable under small changes. The verbs on the right hand side can be thought of as a drastic and irreversible change that occurs at some clearly defined point as certain critical values of underlying parameters are varied.

In the study of dynamic systems such as those found in flight mechanics problems a more appropriate class of verb associations would be the following;

    stable - unstable
    symmetric - asymmetric
    stationary - periodic (regular) motion
    equilibrium state - oscillatory motion
    regular - irregular
    order - chaos

The qualitative change caused by the variation of an underlying parameter can be thought of as a branching behavior, hence the term "bifurcation".

Bifurcation theory encompasses many areas of mathematics such as topology, qualitative theory of differential equations, differential geometry, structural

8

stability and catastrophe theory (1:529). Due to the large
amount of work done in this area, this discussion is not
meant to be an exhaustive treatise on bifurcation theory in
that there are several contemporary texts on the subject
(10,14,15,16). An excellent straight forward text on the
subject that is highly recommended is the text by Seydel
(10). This discussion is directed more toward being a brief
overview of the topic as it pertains to this research. For
the sake of brevity the examples that follow will be among
the simpler problems that one would encounter in this field.
These examples should more than adequately illustrate the
concepts.

Equilibrium Solutions

Bifurcations

A simple scalar example is the following; Consider the
equilibrium solution to the following differential equation

$$\mathring{y} = \lambda y - y^3 \tag{2.1}$$

For $\lambda > 0$ there are two nontrivial equilibria or zero
solutions, $y = \pm \sqrt{\lambda}$. Another term used in the literature
for equilibria is stationary. The transition of stability
is illustrated by what is known as a "bifurcation" or
"branching" diagram as shown in Figure 2-1. The trivial
branch $y = 0$ loses stability at the bifurcation point (y, λ)

9

= (0,0). The stable branches known as sinks are indicated
by heavy lines (10:46). The unstable branches known as
sources are indicated by dashed lines with the arrows
signifying domains of attraction. Stable equilibrium
solutions (heavy lines) attract while unstable equilibrium
solutions (dashed lines) repel. Stable solutions or more
correctly stable equilibrium solutions are physically
realizable while unstable equilibrium solutions are not.
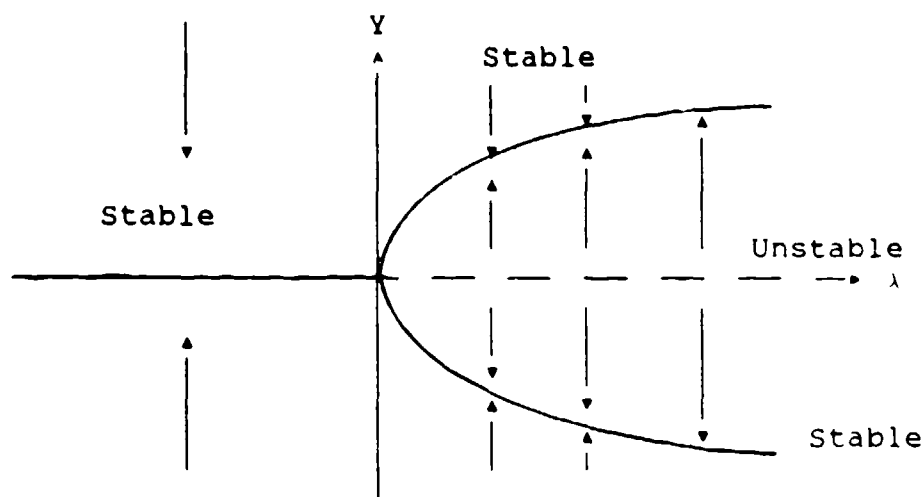
Figure 2-1 Bifurcation Diagram for $\dot{y} = \lambda y - y^3$

For the most part all "branching" or "simple"
bifurcations are a variation of the above. Some of the
possible configurations are surveyed below in Figure 2-2.
Figure 2-2a depicts a transcritical bifurcation while
figures b and c depict a supercritical pitchfork and
subcritical pitchfork, respectively. It should be noted

10

that a pitchfork is a transcritical bifurcation but a transcritical bifurcation is not a pitchfork bifurcation.
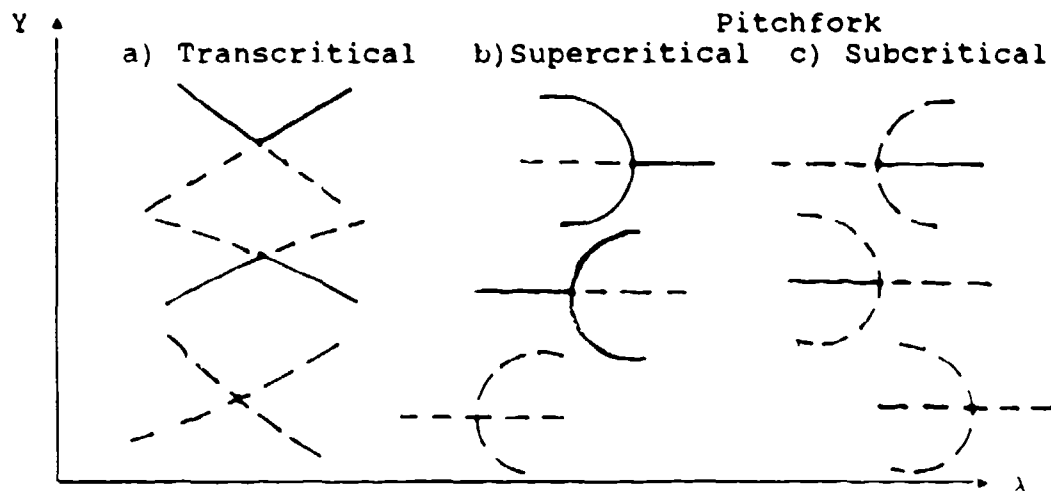

Figure 2-2   Simple Bifurcations

Limit Points

Another mathematical singularity that needs to be addressed is the limit point or as referred to in the literature saddle-nodes or noses and knees. They are neither hysteresis nor bifurcation but also are depicted on bifurcation diagrams. For the ordinary differential equation $\dot{y} = g(y, \lambda)$ (a scalar example) Golubitsky and Schaeffer (13:10) define this singularity by the following equations:

$$g = g_y = 0 \qquad g_{yy} \neq 0 \qquad g_\lambda \neq 0 \quad \text{at } (0,0) \qquad (2.2)$$

The behavior is shown in Figure 2-3.

11
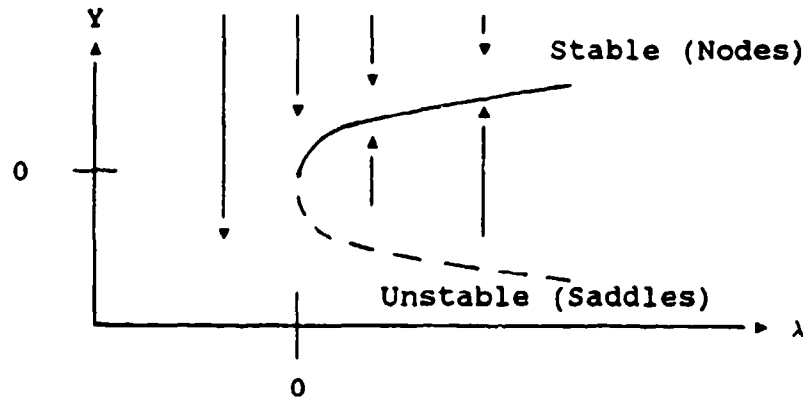
Figure 2-3 Diagram of Limit Point for $\dot{y} = \lambda - y^2$

Hysteresis Points

Another mathematical singularity that sometimes appears
in bifurcation diagrams is the hysteresis point. A
hysteresis point only appears when 2 parameters are fixed.
It is a transition from the kind of bifurcation diagram
shown at the top of Figure 2-4 to the bifurcation diagram
shown at the bottom of Figure 2-4 as λ_1 is varied. λ_1 has
the effect of horizontally compressing the equilibrium
curve. This is the simplest of several sources of "jump
phenomena" in that as the free or underlying parameter is
varied past one of the limit points the physical behavior of
the dynamic system changes drastically. The path of this
change is depicted by the vertical dotted lines.

Periodic Solutions

A mathematical singularity that is only defined for
multidimensional ($n \geq 2$) space and is frequently depicted on

12
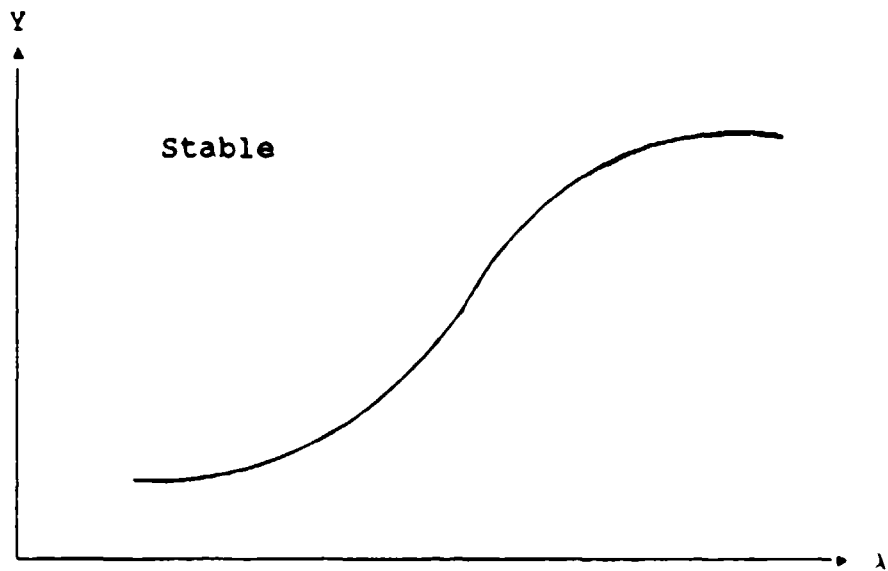
Equilibrium Curve $\lambda_1 < 0$
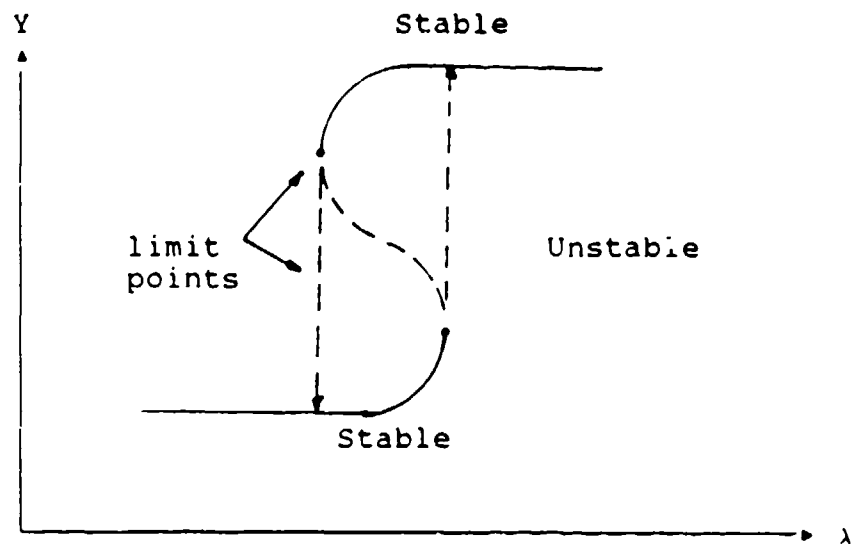
Equilibrium Curve $\lambda_1 > 0$

Figure 2-4   Bifurcation Diagrams near Hysteresis
Point as a second Parameter λ_1 is varied

bifurcation diagrams is the Hopf bifurcation point.   A Hopf

bifurcation point connects stationary solutions with

13

periodic solutions. If $\dot{y} = f(y, \lambda)$ defines the ordinary differential equation and y and f are vectors, then f_y is the Jacobian. More rigorously if we assume, as Seydel (10:63) does;

1) $f(y_0, \lambda_0) = 0$ (equilibrium solution)

2) $f_y (y_0, \lambda_0)$ has a simple pair of purely imaginary eigenvalues $\mu(\lambda_0) = \pm iB$ and no other eigenvalue with zero real part

3) $d(Re \, \mu(\lambda_0)) \, / \, d\lambda \neq 0$

Then there is a birth of limit cycles at (y_0, λ_0). The initial period (of the zero-amplitude oscillation) is

$$\rho = \frac{2\pi}{B} \qquad (2.3)$$

A simple example of a Hopf Bifurcation is illustrated for the following system;

$$\dot{y}_1 = -y_2 + y_1 (\lambda - y_1^2 - y_2^2) \qquad (2.4)$$
$$\dot{y}_2 = y_1 + y_2 (\lambda - y_1^2 - y_2^2) \qquad (2.5)$$

A quick calculation shows that $y_1 = y_2 = 0$ is the only equilibrium solution for all λ; there is no stationary bifurcation. The Jacobian matrix for equations 2.4 and 2.5 is depicted in the matrices on the next page and has eigenvalues $\lambda = \pm i$. The equilibrium solution is stable for $\lambda < 0$ and unstable for $\lambda > 0$. There is a loss of stability at $\lambda = 0$ but no new equilibrium is present for the

14

exchange of stability. A bifurcation occurs at $\lambda = 0$ which can be thought of geometrically as a line that meets a parabolic cone in π^3 as shown in Figure 2-6.

$$f^s{}_y = \frac{\partial f}{\partial y}(y^s)$$

$$= \begin{bmatrix} \dfrac{\partial f_1}{\partial y_1}(y_1^s, y_2^s) & \dfrac{\partial f_1}{\partial y_2}(y_1^s, y_2^s) \\[3em] \dfrac{\partial f_2}{\partial y_1}(y_1^s, y_2^s) & \dfrac{\partial f_2}{\partial y_2}(y_1^s, y_2^s) \end{bmatrix}$$

$$= \begin{bmatrix} \lambda & -1 \\[1em] 1 & \lambda \end{bmatrix}$$

Rewriting the preceeding equations in polar coordinates

$$\dot{r} = r(\lambda - r^2) \tag{2.6}$$

$$\dot{\theta} = 1 \tag{2.7}$$

one sees in Figure 2-5 that for $r = \sqrt{\lambda}$, $\dot{r} = 0$ and a closed orbit results ($\dot{\theta} \neq 0$). The amplitude of the orbit grows with the square root $\sqrt{\lambda}$. In this case the orbit is stable,

15

as seen from

$$\mathring{r} < 0 \quad \text{for } r > \sqrt{\lambda}$$
$$\mathring{r} > 0 \quad \text{for } r < \sqrt{\lambda}$$
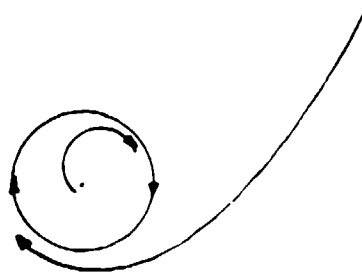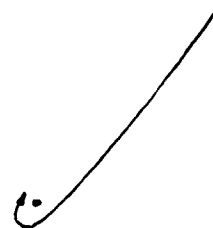
$\lambda > 0$ $\lambda < 0$

Figure 2-5   Limit Cycles
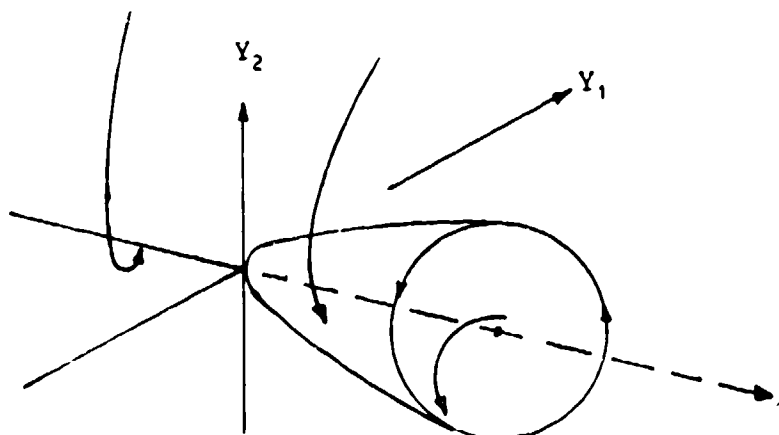
Figure   2-6   Hopf Bifurcation

In summary all the preceding concepts can be applied to

16

dynamic systems with multidimensional solution spaces (n>2). For such systems the stability of equilibria changes when one or more eigenvalues of the Jacobian crosses from the Left Half Plane (-) to the Right Half Plane (+) (19, 20, 21). At the point where this singularity occurs the solution trajectory or path bifurcates (branches). In an appropriate projection the geometry of bifurcation is always qualitatively similar to the simple diagrams of Figures 2-1, 2-2, 2-3, 2-4, 2-6. Numerical techniques for branch tracing and switching are based on this qualitative fact.

III. Description and Development of Aircraft Model

The aircraft mathematically modeled in this study was a McDonnell Douglas F-15B aircraft. The F-15B is high-performance two-place fighter aircraft currently in the USAF inventory. A brief description of the physical characteristics of the aircraft as well as a diagram and sign conventions for control surface deflections are provided in Appendix A. The following discussion is meant to be a brief summary of the model with the invitation to the reader to satisfy himself with a more detailed look at the model itself given in Appendix B.

The F-15B possesses four independent control surfaces: left and right ailerons, left and right rudder, left and right stabilators and speedbrake. The F-15B also possesses a Control Augmentation System (CAS) that uses as inputs all of the state variables in addition to aircraft altitude, Mach number, pilot inputs and control surface positions. The pilot has the option to manually override the CAS since the F-15B is a stable aircraft at moderate flight conditions even without the CAS on (12). In addition to the CAS the F-15B has an Aileron Rudder Interconnect (ARI). Since the primary emphasis of this study was on the aerodynamic forces and moments due to the control surface deflections and not the control laws that govern them, the CAS was not implemented in this model. It is realized that the CAS

merits study by itself and it is hoped that this basic research could be of some utility in the design and/or modification of it.

The following aircraft control surfaces were taken into account in the six degree-of-freedom model (X,Y,Z forces and L,M,N moments)- rudders, ailerons and stabilators. The aerodynamic effects of the speedbrake were not modeled due to the fact that the speedbrake is automatically retracted at angles-of-attack (α) greater than 15 degrees and the primary emphasis of this study is on high angle-of-attack ($\alpha > 40$ degrees) phenomena. In addition to the conventional effect of the ailerons the horizontal stabilators are deflected differentially to assist rolling the aircraft about its longitudinal axis. The differential stabilator deflection is fixed by the manufacturer to be a linear function of the aileron deflection ($\delta_{\Delta e} = 0.3 * \delta_a$) for the chosen altitude and airspeed, 20,000 feet and 0.6 Mach respectively.

In addition the following simplifications were made in the construction of the model: gear up, flaps up, and no stores carriage. A thrust setting of 8,300 lbs (military power) was chosen because it is the thrust setting for trim conditions (steady, level flight) at 0.6 Mach and 20,000 feet. Asymmetric thrust was not modeled, however asymmetric aerodynamic behavior was modeled. The asymmetric aerodynamic behavior manifested itself as an increment to

19

the side force and yawing moment stability derivatives at
high angles-of-attack ($\alpha > 30$ degrees) possibly due in part
to asymmetric vortex bursting on the F-15B's nose.
Flexibility effects were also taken into account via
correction factors multiplied by the appropriate
coefficients. For the F-15 in cruise configuration these
simplifications still allowed a realistic model for the
purposes of this study.

Force and Moment Equations

The following equations provide a summary of the force
and moment coefficients as well as the dependence of the
basic coefficients and stability derivatives upon their
respective aerodynamic parameters. These parameters were
the independent variables used in the curve fitting process
to be discussed later. The equations are:

$$C_x = C_L(\alpha, \delta_e) \sin(\alpha) - C_D(\alpha, \delta_e) \cos(\alpha) + T/\bar{q}S \quad (3.1)$$

$$C_y = Cy(\alpha, |\beta|, \delta_e) + Cy_{\delta_a}(\alpha)\delta_a + Cy_{\delta_r}(\alpha)\delta_r$$

$$+ \left(\frac{b}{2\,V}\right) \left[Cy_r(\alpha)r + Cy_p(\alpha)p \right] + \Delta Cy_{\beta^*}(\alpha, \beta)$$

$$+ Cy_{\delta_{\Delta e}}(\alpha, \delta_e)\delta_{\Delta e} \quad (3.2)$$

20

$$C_z = -\left[C_L(\alpha, \delta_e) \cos(\alpha) + C_D(\alpha, \delta_e) \sin(\alpha) \right] \quad (3.3)$$

$$C_l = C_{l\beta}(\alpha, |\beta|)\beta + C_{l\delta_a}(\alpha, \delta_e)\delta_a + C_{l\delta_r}(\alpha, |\delta_r|)\delta_r$$

$$+ \left[\frac{b}{2\,V}\right]\left[C_{lp}(\alpha)p + C_{lr}(\alpha)r \right] + C_{l\delta_{\Delta e}}(\alpha, \delta_e)\delta_{\Delta e}$$

$$+ \Delta C_{l\beta}(\alpha, \beta) \quad (3.4)$$

$$C_m = C_m(\alpha, \delta_e) + \left[\frac{\bar{c}}{2\,V}\right] C_{mq}(\alpha) + T\left[\Delta z_{offset}\right] / (\bar{q}S\bar{c}) \quad (3.5)$$

$$C_n = C_{n\beta}(\alpha, \beta, \delta_e)\beta + C_{n\delta_a}(\alpha)\delta_a + C_{n\beta}(\alpha, \beta)$$

$$+ C_{n\delta_r}(\alpha, \beta, \delta_r, \delta_e)\delta_r + \left[\frac{\bar{c}}{2\,V}\right]\left[Cn_p(\alpha)p + Cn_r(\alpha)r \right]$$

$$+ Cn_{\delta_{\Delta e}}(\alpha, \delta_{\Delta e})\delta_{\Delta e} + \Delta C_{n\beta}(\alpha, \beta) + \Delta C_{n\beta^*}(\alpha, \beta) \quad (3.6)$$

Two parameters not listed in the force and moment
coefficient expressions are Mach number and altitude, which
were fixed at 0.6 and 20,000 feet respectively. Flight at
Mach 0.6 can be assumed to be in the incompressible flow
region. $\Delta C_{l\beta}$, and $\Delta C_{n\beta}$, are the aerodynamic increments
(symmetric) due to a two place canopy. $\Delta C y_{\beta^*}$ and $\Delta C n_{\beta^*}$ are
the asymmetric aerodynamic effects mentioned previously.
For a more detailed investigation of the force and moment
equations see Appendix B. The principal source of the data
used in compiling the preceding aircraft aerodynamic force

21

and moment coefficients was the F-15 1988 Aerobase which was obtained from the F-15 Systems Program Office (SPO) at Wright-Patterson AFB, Ohio.

Due to the fact that the bifurcation analysis package AUTO works much better with functions with a continuous first derivative the data from the F15 Aerobase was curve fitted with polynomial functions. Due to the erratic or noisy behavior of the data several types of curve fits were considered and discarded - logarithmic, sinusoidal, etc. The process of converting the aerodynamic coefficient data from look-up tables to polynomial functions, although lengthy, was extremely useful in that it provided some insight as to how the coefficients varied due to angle-of-attack and sideslip angles.

Several curve fitting approaches were considered such as use of available software Grapher, Surfer and SAS. An important consideration and deciding factor was whether the curve fitting package could handle a function of 4 variables. For overall capabilities SAS was chosen.

SAS was an excellent curve fitting tool in that it possessed the following desirable features;

1) Able to handle a large number of independent variables.

2) Allowed the individual to choose the particular model beforehand, which allowed for a more efficient search for successful curve fits.

3) Graphically displayed the generated polynomial curve

22

fit functions versus up to 2 independent variables.

4) Provided statistical measures of how accurate the curve fit was.

5) Provided a direct measurement of the difference between the raw data and the polynomial curve fit.

The SAS analysis package has quite a large and diverse number of statistical techniques available to the user. For this investigation the Proc GLM procedure was used (4). The GLM procedure uses the method of least squares to fit general linear models (e.g. models which are linear combinations of monomials).

Because of the large number of data points for most coefficients it was found necessary to break up the data into 2 or more sections. The individual sections of the data were then represented by polynomial functions that were joined by cubic splines. This was done in order to keep the highest order power of the polynomial function to 9 or less for computational efficiency. The cubic splines were only needed on the stability derivatives that were a function of one variable, usually angle-of-attack (α) and were computed using an algorithm in (25:124). This resulted in a mathematical smoothing of the data which ensured continuous first derivatives required by AUTO as well as providing an elegant and systematic way of representing the data.

Figure 3-1 gives an example of the graphics capability of SAS for the stability derivative Cy_{δ_a} which is a function

23

of one variable (α). The jovial name for $Cy_{\delta a}$ is CYDAD and it's 1988 F-15 Aerobase name is ATAB75. For a more thorough explanation of jovial and F-15 Aerobase names see **Appendix B.** Figure 3-1 specifically shows the raw data plotted against the actual curve fit that SAS provides. What is not shown however is the tabular statistical measurements that accompany the plot. These following statistical measurements were used in conjunction with the curve fit plots for stability derivatives and aerodynamic coefficients that were a function of up to two independent variables. These measurements were also the primary means of evaluating the stability derivatives that were functions of 3 or more independent variables. Among the statistical measurements available in GLM are regression, analysis of variance, analysis of covariance, multivariate analysis of variance, and partial correlation. PROC GLM analyzes data within the framework of General Linear Models, hence the name GLM. GLM handles classification variables, which have discrete levels, as well as continuous variables, which measure quantities. For the purposes of this study Polynomial regression was used. The primary statistical measurements relied on for the quality of the curve fit were R-square, coefficient of variation, Root Mean Square Error, F Value and Residuals. R-square or coefficient of determination is a measure between 0 and 1 that indicates the portion of the total (corrected) variation that is attributed to the fit

24

rather than left to residual error (4:690). The coefficient of variation is 100 times Root MSE divided by the dependent variables mean. Root Mean Square Error is self explanatory. F Value is the quotient of the Mean Square of the model divided by the mean square of the error. Functions with R-Square or coefficient of determination greater than 0.9 where chosen to represent the raw data. The remaining statistical measurements were relied on in decreasing importance.

The function depicted in Figure 3-1 is represented up to 0.55851 radians ($\approx$ 32°) by the polynomial expression given by

```
CYDAD=-0.00020812+(0.00062122*RAL)+(0.00260729*RAL*RAL)
    ++(0.00745739*(RAL**3))-(0.0365611*(RAL**4))
    +-(0.04532683*(RAL**5))+(0.20674845*(RAL**6))
    +-(0.13264434*(RAL**7))-(0.00193383*(RAL**8))        (3.7)
```

where RAL is the angle-of-attack (α) in radians. For the rest of the angle-of-attack range the aerodynamic coefficient Cy_{δ_a} is represented by another polynomial which is connected to the curve in Figure 3-1 by a cubic spline.

8TH ORDER
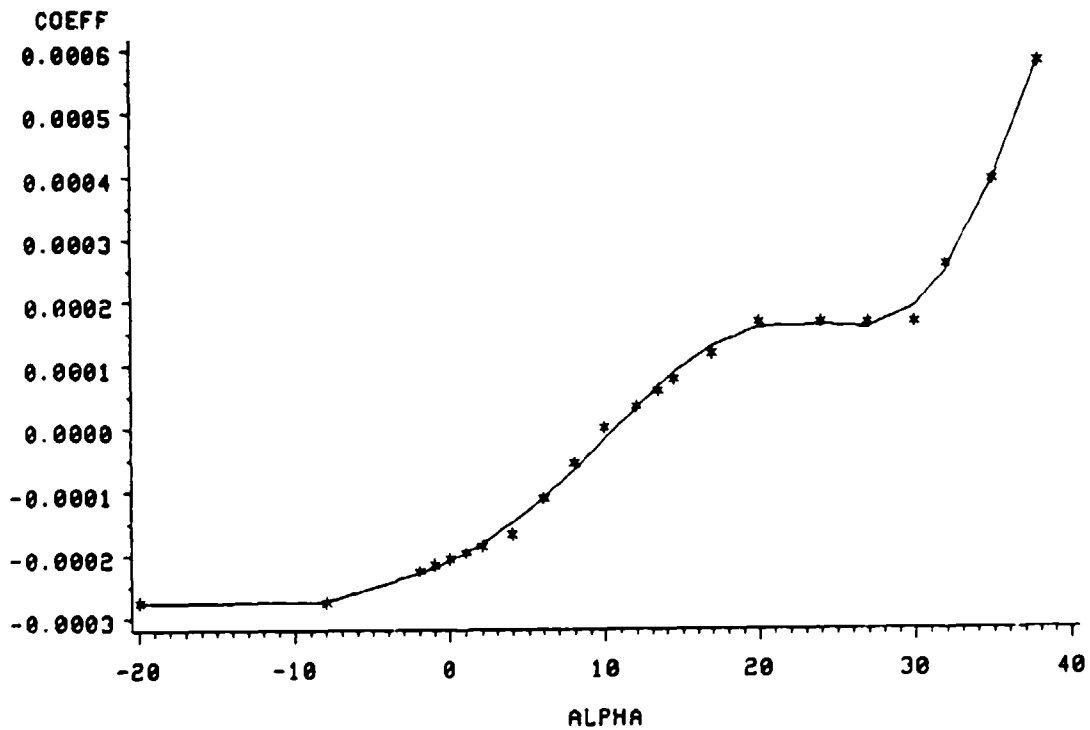
Figure 3-1   CYDAD (Cy_{δ_a})

Figure 3-2 provides an example of the graphical output from SAS for the aerodynamic coefficient $Cy_{\delta_{\Delta e}}$ which is a function of two independent variables. The aerodynamic coefficient $Cy_{\delta_{\Delta e}}$, also known as CYDTD or ATAB72A, is

SAS

Raw Data

g3d856

Curve Fit

Figure 3-2   CYDTD ($CY_{\delta a e}$)

27
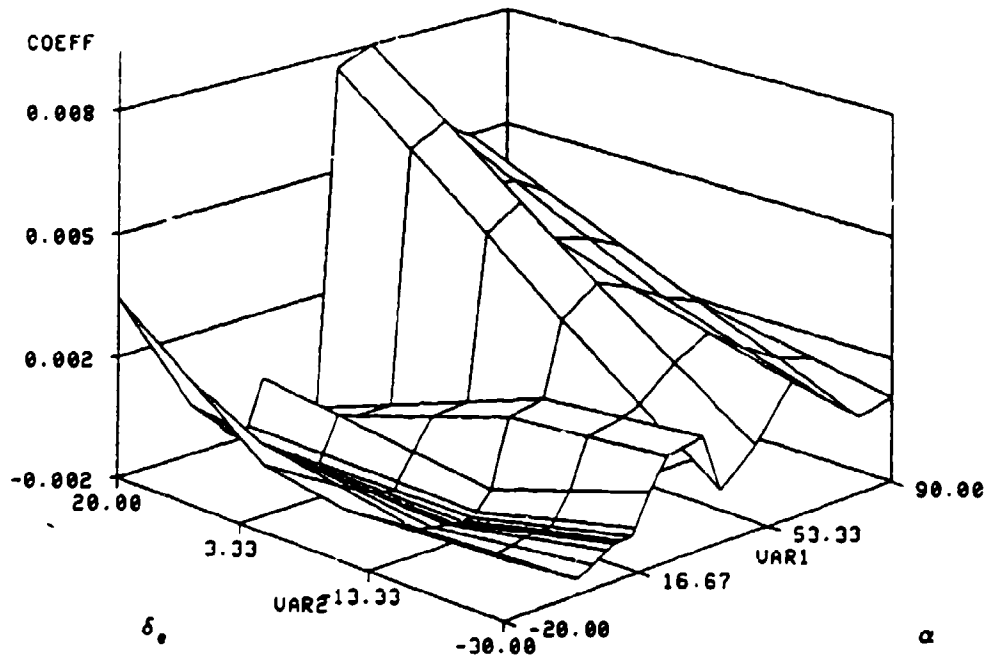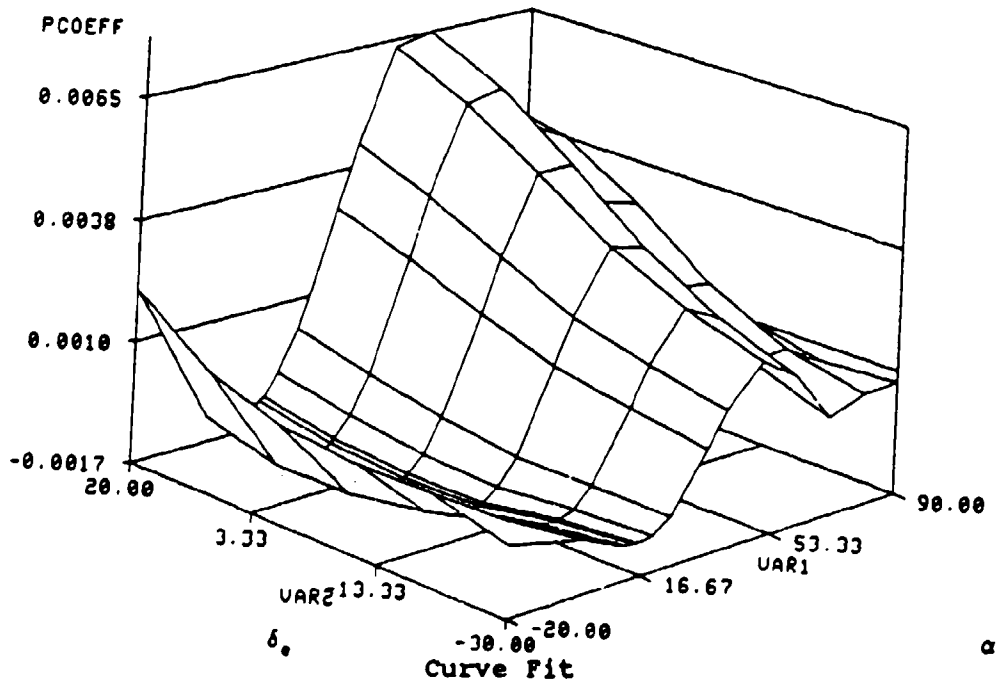
represented by a polynomial function given by

```
CYDTD=-0.00157745-(0.0020881*RAL)+(0.00557239*RAL*RAL)
    +-(0.00139886*(RAL**3))+(0.04956247*(RAL* 4))
    +-(0.0135353*(RAL**5))-(0.11552397*(RAL** ))
    ++(0.11443452*(RAL**7))-(0.03072189*(RAL* 8))
    +-(0.01061113*+(RAL**3)*DELESR)
    +-(0.00010529*RAL*RAL*DELESR*DELESR)
    +-(0.00572463*RAL*DELESR*DELESR)
    ++(0.01885361*RAL*RAL*DELESR)
    +-(0.01412258*RAL*(DELESR**3))
    +-(0.00081776*DELESR)+(0.00404354*(DELESR**2))-
    +(0.00212189*(DELESR**3))+(0.00655063*(DELESR**4))
    ++(0.03341584*(DELESR**5))                    (3.8)
```

where DELESR is the symmetrical stabilator deflection (δ_e)
in radians.

The asymmetric side force $\Delta Cy_{\beta*}$ and yawing moment $\Delta Cn_{\beta*}$
were unusual in that they were zero over most of the (α, β)
range. In order to ensure that these coefficients were
modelled with continuous functions with continuous first
derivatives, they were curve fitted differently than the
preceeding coefficients. Instead of using a polynomial
function generated by SAS, a rough approximation was used to
generate a "hat" function that had the same magnitude and
location as the peak magnitude of the raw data of the
coefficient. The domain for these functions was defined by
limits of the variables angle-of-attack (α) and sideslip
angle (β). The resulting polynomial functions had a
magnitude of zero and a first derivative equal to zero along
the border of these domains. For a more detailed
description of the algorithm used see Appendix B.

Another interesting curve fitting technique was used to

28

build the CFX aerodynamic coefficient. The CFX aerodynamic coefficient has two different data tables in the F-15 Aerobase dependent on whether or not α is greater than $\alpha_{Max\ Trim}$. These two data tables were individually curve fitted using SAS and the resulting polynomial functions were joined in the following manner: The polynomial representing CFX at the lower α's was used up to 20 degrees. From 20 degrees to 30 degrees the polynomial for the lower α's was multiplied by a ramp function that was 1 at 20 degrees and 0 at 30 degrees. This was added to the polynomial representing CFX at the higher α's, multiplied by another ramp function that was 0 at 20 degrees and 1 at 30 degrees. The polynomial representing CFX at the higher α's was used above 30 degrees. This ensured a smooth blend of the data from the two different tables.

Equations of Motion

The force and moment coefficients due to aerodynamics and thrust were used to construct the following autonomous (time independent) equations of motion:

$$
\dot{\alpha} = q + \left[- \left(\frac{\bar{q}\ S}{m\ V} C_x - \frac{g}{V} \sin \theta + r \sin \beta \right) \sin \alpha \right.
$$

$$
\left. + \left(\frac{\bar{q}\ S}{m\ V} C_z + \frac{g}{V} \cos \theta \cos \phi - p \sin \beta \right) \cos \alpha \right] \sec \beta
$$

$$(3.9)$$

$$\dot{\beta} = - \left[\left(\frac{\bar{q}\,S}{m\,V} C_x - \frac{g}{V} \sin \theta \right) \sin \beta + r \right] \cos \alpha$$

$$+ \left(\frac{\bar{q}\,S}{m\,V} C_y + \frac{g}{V} \cos \theta \sin \phi \right) \cos \beta$$

$$- \left[\left(\frac{q\,S}{m\,V} C_z + \frac{g}{V} \cos \theta \cos \phi \right) \sin \beta - p \right] \sin \alpha \qquad (3.10)$$

$$\dot{p} = \left[-\left(\frac{I_z - I_y}{I_x} + \frac{I_{xz}^2}{I_x I_z} \right) qr + \left(1 - \frac{I_y - I_x}{I_z} \right) \frac{I_{xz}}{I_x} pq \right.$$

$$\left. + \frac{\bar{q}\,S\,b}{I_x} \left(C_l + \frac{I_{xz}}{I_z} C_n \right) \right] \Bigg/ \left[1 - \frac{I_{xz}^2}{I_x I_z} \right] \qquad (3.11)$$

$$\dot{q} = \frac{\bar{q}\,S\,\bar{c}}{I_y} C_m + \frac{I_z - I_x}{I_y} pr + \frac{I_{xz}}{I_y} (r^2 - p^2) \qquad (3.12)$$

$$\dot{r} = \left[\left(\frac{I_{xz}^2}{I_x I_z} - \frac{I_z - I_x}{I_x} \right) pq - \left(1 + \frac{I_z - I_y}{I_x} \right) \frac{I_{xz}}{I_z} qr \right.$$

$$\left. + \frac{\bar{q}\,S\,b}{I_z} \left(\frac{I_{xz}}{I_x} C_l + C_n \right) \right] \Bigg/ \left[1 - \frac{I_{xz}^2}{I_x I_y} \right] \qquad (3.13)$$

$$\left(\frac{\dot{V}}{V} \right) = \left(\frac{\bar{q}\,S}{m\,V} C_x - \frac{g}{V} \sin \theta \right) \cos \alpha \cos \beta +$$

$$+ \left(\frac{\bar{q}\,S}{m\,V} C_y + \frac{g}{V} \cos \theta \sin \phi \right) \sin \beta$$

$$+ \left(\frac{\bar{q}\,S}{m\,V} C_z + \frac{g}{V} \cos \theta \cos \phi \right) \sin \alpha \cos \beta \qquad (3.14)$$

$$\dot{\theta} = q \cos \phi - r \sin \phi \qquad (2.15)$$

$$\dot{\phi} = p + q \tan \theta \sin \phi + r \tan \theta \cos \phi \qquad (3.16)$$

30

$$\dot{\psi} = q \sin \phi \sec \theta + r \cos \phi \sec \theta \qquad (3.17)$$

Equations 3.9 through 3.17 are written in a body axis set which differs from the principal axis set in that I_{xz} is not identically zero. The inertia values for the F-15B used in the above equations can be found in Appendix A. The equations of motion for the aircraft model are standard, see e.g. Carroll and Mehra (1:530). Equation 3.17 was eliminated since equations 3.9 to 3.16 do not depend on ψ. These equations can also be readily derived from the kinematic equations presented in Chapter 4 of McCruer and Ashkenas (11:233).

IV. Numerical Application of Bifurcation Theory

This chapter presents the practical implementation of the theory of bifurcation analysis as discussed in the three previous chapters. It outlines the three necessary components (Starting Point, Driver Program and AUTO) that make up the "tool" that actually calculates the equilibrium and periodic solutions.

Starting Point

Before the technique of numerical continuation can be implemented, a preparatory step is necessary in that the method requires that a solution to the problem be already known. With the equations of motion and the underlying constituent force and moment coefficients given in the preceding section and Appendix B all that remained to be done was to solve the equations for a starting point. This demonstrates one of the more desirable advantages of this technique in that one is free to reduce the number and difficulty of the equations of motion that the equilibrium conditions are subject to. Since numerical bifurcation analysis is by nature a continuation process the flight dynamicist need only solve for one equilibrium solution point, the method then enables the subsequent location of all the equilibrium solutions that lie on that "branch". This in and of itself becomes a built in check that allows

32

one to compare the results of this technique with those given by more classical techniques which require linearization of the equations of motion. It should be pointed out that the method does require the linearization of the Jacobian, as such it contains and expands on the previously mentioned "classical techniques". Naturally one chooses the starting conditions so as to reduce the number of equations to solve by hand, and lets the algorithm solve for the more difficult conditions (specifically, laterally asymmetric solutions).

The starting point of course has to be an equilibrium or stationary point. This point is mathematically represented by setting the left hand side of equations (3.9 - 3.16) to zero. The aircraft states chosen for a starting point of this investigation would represent symmetric, non turning, non accelerated flight. The starting point differs from trim condition in that it may or may not describe level flight. For these conditions the following aircraft states were set to 0 in equations 3.9 - 3.16: (β ,p, q, r, ϕ), as well as the following control surface deflections (δ_a, $\delta_{:e}$, δ_r). The problem was now reduced to determining the aircraft states (α, Θ, V) and control surface deflection (δ_e) analytically. This was done by picking α and solving for δ_e. Θ and V were then found as a function of (α, δ_e). It should be pointed out that one may choose trim conditions as a starting point. Trim conditions can be found by

33

setting γ to 0, where γ is the flight path angle defined as $\gamma = \Theta - \alpha$. The trim point for the Flight Dynamics Laboratory F-15B simulator, which used the F-15 1977 Aerobase, according to Barth (12:25) was $(\alpha, \Theta, \delta_e) = (4.38, 4.38, 0.245)$ with the same weight, inertia and thrust characteristics as used in the aircraft model. For this study the starting point turned out to be that of a steady straight ahead climb $(\alpha, \Theta, \delta_e) = (5.0, 12.02, -1.39)$.

Driver Program

To use AUTO, user must supply a driver program giving the nonlinear functions and Jacobian. The majority of the computer code for the driver program (D2ICCV28) pertains to the setup of equations 3.9 - 3.16 and the calculation of the force and moment coefficients (C_x, C_y, C_z, C_l, C_m, C_n) which have been previously discussed in Chapter 3. The discussion that follows pertains to the additional code that AUTO requires with respect to derivatives of the equations of motion. Since numerical bifurcation is a continuation process the derivative is required to determine the "direction" of the solution path or branch.

A simple central-difference algorithm was used to calculate the required derivatives numerically based on the following equation:

$$\frac{\partial \vec{F}}{\partial x} = \frac{\vec{F}(x + dx) - \vec{F}(x - dx)}{2dx} + O(dx)^2 \quad (4.1)$$

34

where x is a state variable, and dx is a very small number
($\approx 10^{-9}$). The aerodynamic coefficients were carefully
formulated to be not only continuous, which ensured equation
4.1 was alright, but also differentiable. This was done in
order to avoid jumps in eigenvalues which make finding
bifurcation points difficult.

The previous difference algorithm was used to calculate
the Jacobian $\partial \vec{F}/\partial \vec{u}$ shown in Figure 4-1 and the matrix $\partial \vec{F}/\partial \vec{\lambda}$
which is shown in Figure 4-2 where $\vec{F} = (\dot{\alpha}, \dot{\beta}, \dot{p}, \dot{q}, \dot{r}, \dot{\theta}, \dot{\phi}, \dot{V})^{\mathsf{T}}$
which is the right hand side of equations 3.9 - 3.16, and
$\vec{u} = (\alpha, \beta, p, q, r, \theta, \phi, V)^{\mathsf{T}}$ and $\vec{\lambda} = (\delta_a, \delta_e, \delta_r)$. $\delta_{\Delta e}$ does not show
up in the control or free parameter vector in that it was
not treated as an independent control surface and was
strictly a linear function of aileron deflection
($\delta_{\Delta e} = 0.3 * \delta_a$).

AUTO

This section provides a brief description of what AUTO
does and how it does it. The discussion that follows can be
investigated at greater length in references 5 and 12.

AUTO is a subroutine package for the bifurcation
analysis of autonomous systems of ordinary differential
equations written in 1979 by Eusebius Doedel of Concordia
University. It is a Fortran program written to do numerical
bifurcation analysis and continuation of the initial value

$$\partial \bar{F}/\partial \bar{u} =$$

$$
\begin{bmatrix}
\dfrac{\partial \dot{\alpha}}{\partial \alpha} & \dfrac{\partial \dot{\alpha}}{\partial \beta} & \dfrac{\partial \dot{\alpha}}{\partial p} & \dfrac{\partial \dot{\alpha}}{\partial q} & \dfrac{\partial \dot{\alpha}}{\partial r} & \dfrac{\partial \dot{\alpha}}{\partial \Theta} & \dfrac{\partial \dot{\alpha}}{\partial \phi} & \dfrac{\partial \dot{\alpha}}{\partial V} \\[2.5ex]
\dfrac{\partial \dot{\beta}}{\partial \alpha} & \dfrac{\partial \dot{\beta}}{\partial \beta} & \dfrac{\partial \dot{\beta}}{\partial p} & \dfrac{\partial \dot{\beta}}{\partial q} & \dfrac{\partial \dot{\beta}}{\partial r} & \dfrac{\partial \dot{\beta}}{\partial \Theta} & \dfrac{\partial \dot{\beta}}{\partial \phi} & \dfrac{\partial \dot{\beta}}{\partial V} \\[2.5ex]
\dfrac{\partial \dot{p}}{\partial \alpha} & \dfrac{\partial \dot{p}}{\partial \beta} & \dfrac{\partial \dot{p}}{\partial p} & \dfrac{\partial \dot{p}}{\partial q} & \dfrac{\partial \dot{p}}{\partial r} & \dfrac{\partial \dot{p}}{\partial \Theta} & \dfrac{\partial \dot{p}}{\partial \phi} & \dfrac{\partial \dot{p}}{\partial V} \\[2.5ex]
\dfrac{\partial \dot{q}}{\partial \alpha} & \dfrac{\partial \dot{q}}{\partial \beta} & \dfrac{\partial \dot{q}}{\partial p} & \dfrac{\partial \dot{q}}{\partial q} & \dfrac{\partial \dot{q}}{\partial r} & \dfrac{\partial \dot{q}}{\partial \Theta} & \dfrac{\partial \dot{q}}{\partial \phi} & \dfrac{\partial \dot{q}}{\partial V} \\[2.5ex]
\dfrac{\partial \dot{r}}{\partial \alpha} & \dfrac{\partial \dot{r}}{\partial \beta} & \dfrac{\partial \dot{r}}{\partial p} & \dfrac{\partial \dot{r}}{\partial q} & \dfrac{\partial \dot{r}}{\partial r} & \dfrac{\partial \dot{r}}{\partial \Theta} & \dfrac{\partial \dot{r}}{\partial \phi} & \dfrac{\partial \dot{r}}{\partial V} \\[2.5ex]
\dfrac{\partial \dot{\Theta}}{\partial \alpha} & \dfrac{\partial \dot{\Theta}}{\partial \beta} & \dfrac{\partial \dot{\Theta}}{\partial p} & \dfrac{\partial \dot{\Theta}}{\partial q} & \dfrac{\partial \dot{\Theta}}{\partial r} & \dfrac{\partial \dot{\Theta}}{\partial \Theta} & \dfrac{\partial \dot{\Theta}}{\partial \phi} & \dfrac{\partial \dot{\Theta}}{\partial V} \\[2.5ex]
\dfrac{\partial \dot{\phi}}{\partial \alpha} & \dfrac{\partial \dot{\phi}}{\partial \beta} & \dfrac{\partial \dot{\phi}}{\partial p} & \dfrac{\partial \dot{\phi}}{\partial q} & \dfrac{\partial \dot{\phi}}{\partial r} & \dfrac{\partial \dot{\phi}}{\partial \Theta} & \dfrac{\partial \dot{\phi}}{\partial \phi} & \dfrac{\partial \dot{\phi}}{\partial V} \\[2.5ex]
\dfrac{\partial \dot{V}}{\partial \alpha} & \dfrac{\partial \dot{V}}{\partial \beta} & \dfrac{\partial \dot{V}}{\partial p} & \dfrac{\partial \dot{V}}{\partial q} & \dfrac{\partial \dot{V}}{\partial r} & \dfrac{\partial \dot{V}}{\partial \Theta} & \dfrac{\partial \dot{V}}{\partial \phi} & \dfrac{\partial \dot{V}}{\partial V}
\end{bmatrix}
$$

Figure 4-1 $\partial \bar{F}/\partial \bar{u}$ Matrix

$$\partial \vec{F} / \partial \vec{\lambda} \;=\;
\begin{bmatrix}
\dfrac{\partial \dot{\alpha}}{\partial \delta_a} & \dfrac{\partial \dot{\alpha}}{\partial \delta_e} & \dfrac{\partial \dot{\alpha}}{\partial \delta_r} \\[2ex]
\dfrac{\partial \dot{\beta}}{\partial \delta_a} & \dfrac{\partial \dot{\beta}}{\partial \delta_e} & \dfrac{\partial \dot{\beta}}{\partial \delta_r} \\[2ex]
\dfrac{\partial \dot{p}}{\partial \delta_a} & \dfrac{\partial \dot{p}}{\partial \delta_e} & \dfrac{\partial \dot{p}}{\partial \delta_r} \\[2ex]
\dfrac{\partial \dot{q}}{\partial \delta_a} & \dfrac{\partial \dot{q}}{\partial \delta_e} & \dfrac{\partial \dot{q}}{\partial \delta_r} \\[2ex]
\dfrac{\partial \dot{r}}{\partial \delta_a} & \dfrac{\partial \dot{r}}{\partial \delta_e} & \dfrac{\partial \dot{r}}{\partial \delta_r} \\[2ex]
\dfrac{\partial \dot{\theta}}{\partial \delta_a} & \dfrac{\partial \dot{\theta}}{\partial \delta_e} & \dfrac{\partial \dot{\theta}}{\partial \delta_r} \\[2ex]
\dfrac{\partial \dot{\phi}}{\partial \delta_a} & \dfrac{\partial \dot{\phi}}{\partial \delta_e} & \dfrac{\partial \dot{\phi}}{\partial \delta_r} \\[2ex]
\dfrac{\partial \dot{V}}{\partial \delta_a} & \dfrac{\partial \dot{V}}{\partial \delta_e} & \dfrac{\partial \dot{V}}{\partial \delta_r}
\end{bmatrix}$$

Figure 4-2 $\partial \vec{F} / \partial \vec{\lambda}$ Matrix

problem

$$\bar{u}'(t) = \bar{F}(\bar{u}(t), \lambda)$$ (4.2)

where λ is a free parameter, $\bar{u}(t)$ is a vector of states and F is a vector function of same dimension.

AUTO (23) has the following capabilities that were utilized in this study;

1) Trace out branches of equilibrium solutions and compute the eigenvalues of the Jacobian along these branches.

2) Locate equilibrium bifurcation points

3) Switch automatically onto bifurcating equilibrium states

4) Locate Hopf bifurcation points

5) Switch automatically onto branches of periodic solutions and compute the Floquet multipliers along these branches.

6) Locate points on branches of periodic solutions where a single Floquet multiplier or a complex pair of multipliers enters or leaves the unit circle.

7) Compute past limit points on branches of equilibrium solutions and on branches of periodic solutions

8) Compute asymptotically stable as well as asymptotically unstable solutions.

9) Restart automatically at selected points along a branch of periodic and/or equilibrium solutions.

10) Continue Hopf bifurcation points and steady state limit points in two parameters.

Implementation of AUTO is done through the following

method; a driver program containing the model to be analyzed, in this study D2ICCV28, calls AUTO with a user-supplied starting point (equilibrium solution) $\bar{u}$ = $(\alpha, \beta, p, q, r, \theta, \phi, V)^{\mathsf{T}}$. The starting point is stored in its own separate data file so that it may be changed without having to recompile the rest of the driver program. AUTO also requires the standard Fortran IMSL subroutine EIGRF. Another data file containing software controls for AUTO completes the package necessary for running the program.

AUTO produces output to the following data files for post processing which can be retrieved at a later date:

Fort.7 : primarily gives the state vector

$\bar{u} = (\alpha, \beta, p, q, r, \theta, \phi, V)^{\mathsf{T}}$ for the equilibrium or stationary points at each parameter value during continuation. This file in conjunction with Fort.8 was used by a graphics program TXPLT to plot the results.

Fort.8 : contains restart information and used for plotting. Contains limit cycles if appropriate.

Fort.9 : contained the stability information. For the stationary or equilibrium branches this file provided the eigenvalues of the Jacobian matrix which were used as the primary indication whether the equilibrium solutions were stable or not. For periodic branches this file provided Floquet Multipliers which are analogous to eigenvalues. A

stable periodic solution is one where the Floquet
multipliers are all inside the unit circle with
one multiplier very nearly equal to +1 (2:221).
The closeness of the one Floquet multiplier to +1
gives a measure of the accuracy to which the
multipliers are computed. When one or more
multipliers move out of the unit circle the
solution becomes unstable.

This is how AUTO works to find equation solutions. To
continue the solution $\vec{u}(s)$, $\lambda(s)$ of $\vec{F} = 0$, AUTO starts from
a known solution $\vec{u}_0$, λ_0. Writing the nonlinear system of
equations in compact form

$$\vec{F}(\vec{u}, \lambda) = 0, \qquad \lambda \in \Re \qquad\qquad (4.3)$$

where s denotes some parameterization. The direction
$(\vec{u}'_0, \lambda'_0)$ of the branch at the starting or any known point
coincides with a null vector of the n by n+1 dimensional
matrix $(\vec{F}_u(\vec{u}_0, \lambda_0) \mid \vec{F}_\lambda(\vec{u}_0, \lambda_0))$ as is seen by differentation of
the relation $\vec{F}(\vec{u}(s), \lambda(s)) = 0$ with respect to s. With the
assumption that the null space is one dimensional the null
vector can be computed effectively by Gaussian Elimination.
The direction of the solution branch to equation 4.3 can be
defined as shown in Figure 4-3.

$$\begin{bmatrix} \bar{F}_u(\bar{u},\lambda) & \bar{F}_\lambda(\overline{\bar{u},\lambda}) \\ \bar{u'}_0^{\mathsf{T}} & \lambda'_0 \end{bmatrix} \begin{bmatrix} \bar{u}' \\ \dot{\lambda}' \end{bmatrix} = \begin{bmatrix} 0 \\ 1 \end{bmatrix}$$

Figure 4-3   Expanded Auto Matrix

From the starting point the branch is traced out in stepwise manner using a pseudo arclength continuation technique.   Once $(\bar{u}_{j-1}, \lambda_{j-1})$ and $(\bar{u'}_{j-1}, \lambda'_{j-1})$ have been computed, the next solution $(\bar{u}_j, \lambda_j)$ is determined by solving the equations

$$\bar{F}(\bar{u}_j, \lambda_j) = 0 \tag{4.4}$$

$$\theta_u^2 \, (\bar{u}_j - \bar{u}_{j-1})^{\mathsf{T}} \, \bar{u'}_{j-1} + \theta_\lambda^2 \, (\lambda_j - \lambda_{j-1}) \lambda'_{j-1} - \Delta s = 0 \tag{4.5}$$

where Δs is the stepsize along the branch and θ is a scaling factor.   The direction vector $(\bar{u'}_{j-1}, \lambda'_{j-1})$ is computed approximately by $\bar{u'}_{j-1} \approx (1/\Delta s)(\bar{u}_{j-1} - \bar{u}_{j-2})$ and similarly for λ'_{j-1}.   This vector is used to get an initial quess to the next solution, then Newton's method is used to solve.

AUTO possesses the capabilities of letting Δs be fixed or be adaptive as well as selection of convergence criteria. If Newton's method converges rapidly, then the stepsize is increased.   If the Newton iteration converges slowly or if it fails to converge at all, the stepsize is halved.   A maximum stepsize can be preselected so that the program can signal nonconvergence.

The determinant of the Jacobian of equations 4.4 and 4.5 is monitored along the solution branch.   Points where

41

the determinant vanishes are located accurately by the
following scheme; If $q(s)$ is the determinant of the Jacobian
of equations 4.4 and 4.5 along the solution branch
$(\bar{u}(s), \lambda(s))$ and its sign changes then the zero of the
Jacobian is approximated by the secant iteration

$$s^{i+1} = s^i - \frac{s^i - s^{i-1}}{q(s^i) - q(s^{i-1})} q(s^i) \qquad (4.6)$$

where i is the iteration index. The solution points where
the determinant of the Jacobian of equations 4.4 and 4.5
goes to zero are potential bifurcation points. AUTO then
checks eigenvalue real parts for zero or imaginary pair to
determine accurate location of bifurcation points.

Hopf bifurcation points along a branch of stationary
(equilibrium) solutions $(\bar{u}(s), \lambda(s))$ of equation 4.3 are
detected as points where a simple complex conjugate pair of
eigenvalues crosses the imaginary axis at a non-vertical
angle. This version of AUTO uses the standard Fortran IMSL
subroutine EIGRF to compute the eigenvalues of $\bar{F}_u(\bar{u}(s), \lambda(s))$
along the stationary (equilibrium) solution branches. AUTO
detects Hopf points by monitoring the number of eigenvalues
in the left-half plane together with the real part of the
eigenvalue closest to the imaginary axis. The precise
location of a crossing is determined by secant iteration on
the real part of the critical conjugate pair of eigenvalues.

42

The success of this procedure depends on the stepsize being sufficiently small and on the Hopf bifurcations being non-degenerate. If the stepsize was too large Hopf bifurcation points could be missed, so recomputation with smaller a stepsize was sometimes necessary. Since the main thrust of this investigation was stable equilibrium solutions the discussion of the computation of periodic solutions is omitted with the invitation to the reader to satisfy himself with discussion given in reference 5.

43

V. Results

The basis of this investigation was the hope that the process of continuation would lead to high - α periodic and equilibrium solutions. The main thrust of this investigation was to locate and describe spin behavior in the F-15B, however as a byproduct of the numerical bifurcation method many other aspects of the nonlinear flight dynamics of the F-15B were surveyed. A few of these aspects will be discussed first.

Low α Basic Solutions

One of the first pieces of information produced naturally was a data base of equilibrium (stationary) conditions at low α generated by a basic stabilator sweep which preserves zero lateral states. These equilibrium conditions differ from trim conditions in that they may or may not describe level flight. They may describe an unaccelerated climb or dive such as the computed starting point for example. The bifurcation diagrams that depict stable as well as unstable low α equilibrium solutions are graphically displayed in Appendix C. In addition the stable equilibria or physically realizable solutions are tabulated. Only equilibrium flight as a function of stabilator deflection is tabulated, however the process has the capability of calculating equilibrium solutions for other

44

types of equilibrium flight conditions as a function of stabilator, aileron and rudder deflections or any combination thereof so long as only one control is varied.

An interesting discovery that corroborates well with the work of Barth (12:59) is the detection of a Hopf bifurcation to periodic motion at 19° angle of attack. This is significant in that the model used in Barth's study is not the model used in this study. This implies that the phenomena is actually present in the aerobase data and provides a good cross check of the validity of the results produced by the model used in this study.

High α Solutions

The remainder of this section pertains specifically to the survey of high angle-of-attack phenomena such as flat spins with the analysis organized by the order of discovery. That is the discussion is meant to follow the chronological sequence of phenomena discovered and by this order hopefully delineate the pattern of inquiry that generated these results.

A little background on spin entry should help the reader follow the discussion of results better and is therefore presented. A spin entry maneuver involves the transition from a normally stabilized flight condition to another stable attitude characterized by $\alpha > \alpha_{Max\ trim}$ with a large sustained yaw rate (8:3.1). For Mach 0.6 and 20,000 feet $\alpha_{Max\ trim}$ is 29.46 degrees while stabilator deflection

45

angle corresponding to $\alpha_{max\ trim}$ is -27.5 degrees (24). The entry maneuver is divided into two phases to simplify analysis. The initial phase concerns the increase of angle of attack and yaw rate to a spin attitude. The second involves the stabilization into a spin mode once a spin attitude is attained, generally referred to as the incipient spin phase (8:3.1).

In order to optimize the utility of this research for future work an efficient scheme was necessary for the search of the physical behavior sought. The first and most obvious strategy was to apply physical intuition and insight to the problem. How is spin behavior initiated in the real world? From a pilots perspective this is done intentionally thru control inputs in the following manner; The stick is brought full aft and held in order to ensure stall. Full pro spin rudder is introduced to elicit a yaw rate. The control surface responses of the stabilator and rudder to the above control inputs are of course determined by the Control Augmentation System (CAS) and Aileron Rudder Interconnect (ARI) which were not implemented in this model. The effects of the CAS and ARI can be neglected since we are changing δ_e and δ_r deflections directly.

For the purpose of this study a simplifying assumption was made that full control input deflection would yield full control surface deflection. This is not intended to trivialize the effects of the CAS and ARI but is offered as

46

a rationale for trying to set the stabilator to its limit of -30 degrees and doing a rudder sweep. It should be pointed out that we are only mimicking a "maneuver" because only quasistatic variations are allowed. In addition at high angles-of-attack the range of control surface deflections are diminished on the F-15 (22:28).

Initial Rudder Sweep

So for δ_e near limit, a rudder sweep will be attempted. Hopefully continuation will take us to the high α region that the δ_e sweep in Appendix C did not. This approach provided an excellent place to start looking but is hueristic in that once the algorithm begins tracing equilibrium branches there is no control as to where those branches may lead. It is interesting to note that on the first attempt to locate flat spin behavior AUTO traced out a branch on the rudder sweep past 60 degrees before it returned back to the domain of physically realizable independent control surface deflections ($-20° \leq \delta_a \leq 20°$, $-30° \leq \delta_e \leq 20°$, $-30° \leq \delta_r \leq +30°$). What is even more important and especially encouraging about this technique is that *states describing a stable flat spin were found on the very first attempt to reach the 70° to 80° α range*.

Figure 5.1 is a bifurcation diagram of the equilibrium and periodic solution branches showing angle-of-attack vs. rudder deflection. It was started from a $\delta_r = 0°$ point on the stabilator deflection vs. angle-of-attack branch shown

47

in Figure C-1 of Appendix C. The origin of the branches is defined by 0 degree rudder deflection and an angle-of-attack of 30.70 degrees on the diagram. The stabilator deflection is -29.78 degrees with both the aileron and differential stabilator deflections set equal to 0 degrees at that point and for the rest of the branch. The short spurs emanating from the branches are periodic solutions which begin at Hopf bifurcations. The short spurs only represent the maximum amplitude of the limit cycles. It should be noted when viewing this plot that this is only a 2 dimensional projection of 8 dimensional space. The equilibrium or stationary branches from this perspective look like they intersect but in fact do not. This is clearly evident from the states (α, β, p, q, r, θ, ϕ, V) tabulated in the computer printout fort.7 which is not shown. The equilibrium states are distinct for each branch at the point that they appear to cross. Since the origin for these branches was unstable the branches are unstable except for small portions in the vicinity of Hopf Bifurcations found at angles-of-attack around 70 to 80 degrees angle-of-attack. AUTO has the capability to do extensive periodic solution continuation from Hopf bifurcations, however this is not shown in this plot except as short spurs in order to emphasize the equilibrium or stationary solutions. It should also be pointed out the richness and variety of behavior - limit points, Hopf bifurcations, etc. which

48

correspond to changes in flight stability.

Since the physical limits of rudder deflection are ± 30° the stability derivatives and therefore the aerodynamic coefficients are only accurately curve fitted for this region. Based on this limitation, stable

RUDDER SWEEP FOR STAB DEFLECTION = -29
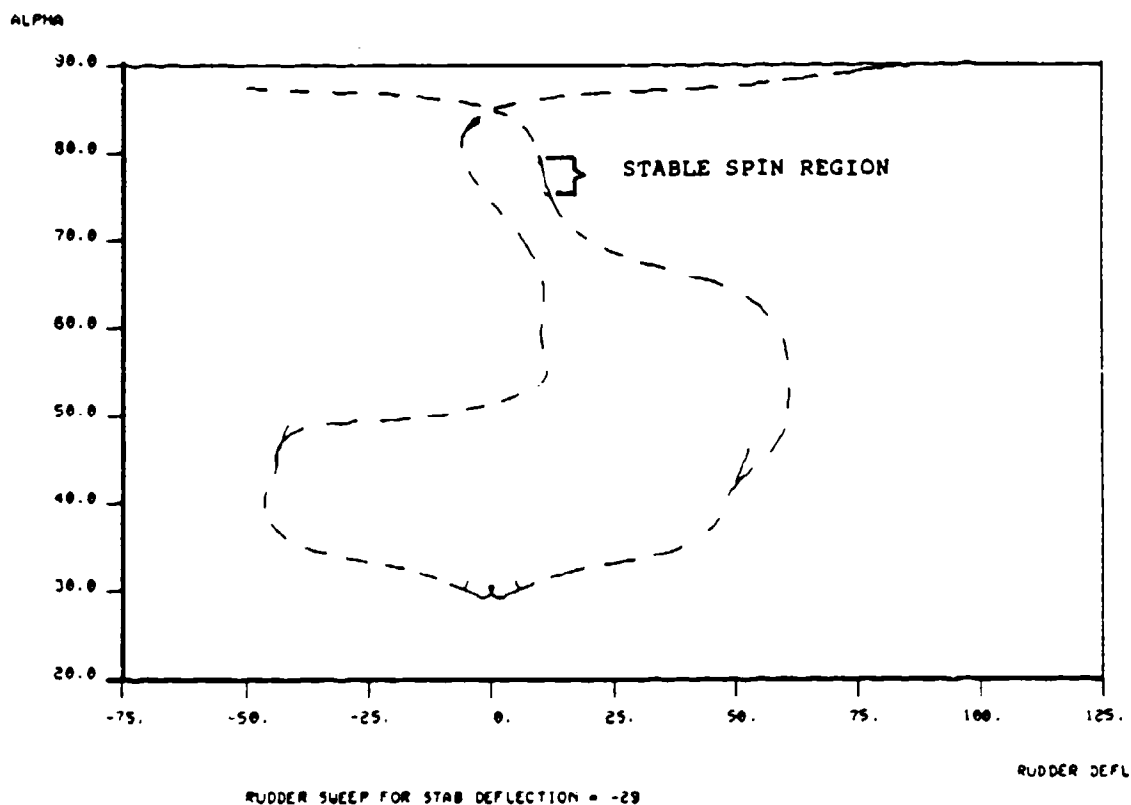
Figure 5-1   Rudder Sweep Solution Branches
$\delta_e = -29.73°$, $\delta_{\Delta e} = \delta_a = 0°$

49

equilibria found outside of this region (-30 degrees > rudder deflection > 30 degrees) would not correspond to any physically realizable state and should be discounted.

Effects of Asymmetry

One of the questions that became apparent during the gathering of results phase of this project was what if any effect do the asymmetric side force ($\Delta Cy_{\beta*}$) and yawing moment ($\Delta Cn_{\beta*}$) increments have on the equilibrium states of a flat spin especially since these asymmetries were also present during the F-15D accident mentioned in the introduction. This was investigated by removing those terms from the force and moment coefficients. The equilibrium branches were recalculated and plotted to see if equilibrium spin conditions could be attained. The equilibrium rudder sweep was computed with the same stabilator and aileron deflection angles which were -29.73 degrees and 0 degrees, respectively. It was discovered that the omitted terms shifted the actual values of the spin equilibrium states but did not identify themselves as the primal cause of them. This agrees qualitatively with MDC A0503 which states:

> The asymmetric yawing moment, $Cn_{\beta*}$, will generally cause the aircraft to spin more readily in one direction than another. Its magnitude decreases significantly above $\alpha = 75°$, so that it has a minor affect on the fast, flat spins. (8:5.2)

See Tables I and II on pages 55 and 56 for how these values compare. The actual plot of the solution branches

50

with the asymmetric terms omitted is shown in Figure 5-2.

ALPHA

STABLE SPIN REGION   STABLE SPIN REGION

ANGLE OF ATTACK US RUDDER DEFLECTION

RUDDER DEFL
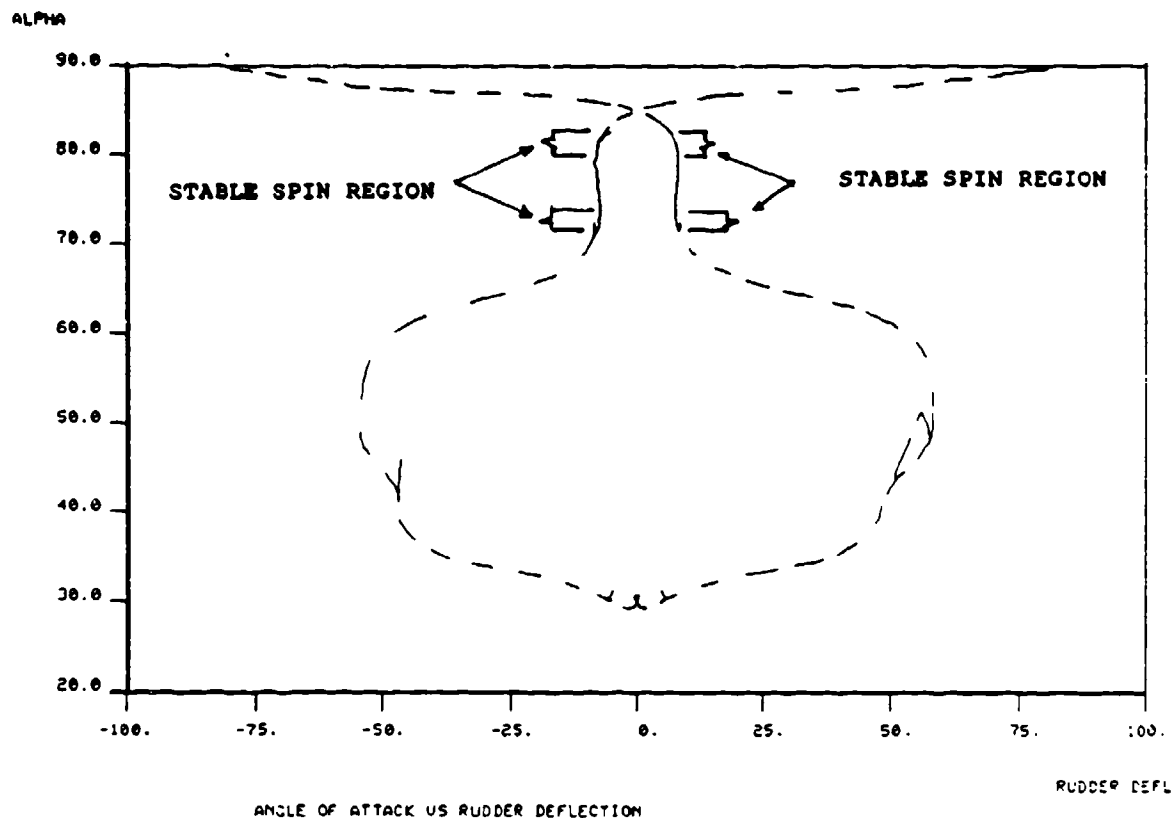
Figure 5-2   Rudder Sweep Solution Branches (without asymmetries)

$$\delta_e = -29.73^\circ, \quad \delta_{\Delta e} = \delta_a = 0^\circ$$

Analysis of Equilibrium States

Tables I and II are presented to clearly show that the stable equilibrium states correspond to flat spin behavior and also for comparison with actual flight test data and results generated by other analysis methods.

A quick check of the plausibility of the values given

51

in the tables is given by the definition of the flight path angle, $\gamma = \theta - \alpha$. Upon substituting the appropriate values of θ and α into the preceeding relationship, one sees that the flight path angle is approximately -90°, or straight down, for all entries. This agrees with common flight test and operational experience in that during a flat spin forward velocity is almost negligble and the spin aircraft is essentially falling. One of the more interesting aspects that tends to be obscured by the large number of details involved in this analysis and should be pointed out is that this *analysis seems to present a paradox of no forward velocity for a thrust of 8300 lbs (Mil Power)*. In reality this is not as incongruous as it first seems and can again be substantiated by flight test and operational experience. Stating the obvious, whether the spin is entered intentionally or inadvertently the engine is usually "on" and therefore producing thrust.

The velocity in both Tables I and II is in the range of 227 to 234 ft/sec and roughly in the ballpark with the vertical velocity of 250 ft/sec mentioned in the accident in the introduction. It should be noted that the accident aircraft was an F-15D while the model used in this study was an F-15B and that there are some significant differences in aerodynamic forces and moments as well as moments of inertia which could account for the difference in the rate of descent. The most obvious cause of the difference in the

rate of descent would be the aerodynamic forces and moments generated by the conformal fuel tanks.

Sideslip angle, β, ranges from -0.9° to -2.74° which agrees qualitatively with the prediction by MDC A0503 (8:5.2) that β would be small for a flat spin which is what the rest of the states would suggest.

Another source for comparison of the values in Tables I and II is actual flight test data given in reference 22, F-15A Approach-to-Stall / Stall / Post-Stall Evaluation. The primary differences in the aerodynamic forces and moments between the F-15A and F-15B are the increments in the rolling and yawing moments due to the two place canopy. In addition there are some differences in moments of inertia and weight between the two aircraft. Some of the test runs were also made with varying asymmetric lateral weight distributions. Even with these differences a good qualitative comparison can be made. The report states;

Two erect spin modes were identified. These were highly oscillatory and smooth spins. (22:27)

The smooth spin mode with symmetric loadings exhibited average AOA's from 60 to 75 degrees with average yaw rates of 75 to 133 degrees per second. (22:28)

The smooth spin mode was often very steady with no oscillations apparent to the pilot; (22:28)

Comparison of predicted flat spin equilibrium states was made with the smooth spin mode flight test data since it was the most closely matched by definition. The yaw rate of

53

1.9 to 2.48 radians per sec (108 to 142 degrees / sec) shown in Tables I and II agrees very well with the smooth spin mode flight test data. The angle-of-attack predicted in Tables I and II tended to be on the high side compared to the flight test data but still within reason. Bank angle (ϕ) for most of the smooth spin test runs tended to be close to 0° which agrees the values predicted in Tables I and II. Vertical velocity for most of the flight test runs tended to average around 250 ft/sec once the aircraft settled into the spin which compares favorably with the velocity predicted in Tables I and II. What is also interesting to point out about the smooth spin flight test runs is that the calibrated airspeed was 0 knots once the aircraft had settled into the spin which corroborates previous statements.

A final source for comparison of the values in Tables I and II is the F-15 Flight Manual which states;

> Steady spins have been encountered with both symmetric and asymmetric wing fuel. The flat spin is characterized by very high yaw rate and very little pitch or roll oscillation. Angles of attack greater than 80 degrees and yaw rates above 140 degrees/sec have been encountered (18:6-3).

54

Point	Rudder Deflection δ_r Degrees	Angle of Attack α Degrees	Sideslip Angle β Degrees	Roll Rate p Rad/sec
1	1.240774E+01	7.421302E+01	-9.536E-01	5.964E-01
2	1.199602E+01	7.479017E+01	-9.687E-01	5.860E-01
3	1.164181E+01	7.538705E+01	-9.815E-01	5.750E-01
4	1.133825E+01	7.599825E+01	-9.914E-01	5.633E-01
5	1.107421E+01	7.661838E+01	-9.984E-01	5.511E-01
6	1.083511E+01	7.724238E+01	-1.003E+00	5.383E-01
7	1.060392E+01	7.786564E+01	-1.007E+00	5.251E-01
8	1.036238E+01	7.848363E+01	-1.011E+00	5.114E-01
9	1.009310E+01	7.909171E+01	-1.018E+00	4.973E-01
10	9.780498E+00	7.968473E+01	-1.028E+00	4.829E-01
11	9.411933E+00	8.025693E+01	-1.044E+00	4.682E-01
12	9.396617E+00	8.027829E+01	-1.044E+00	4.676E-01

Point	Pitch Rate q Rad/sec	Yaw Rate r Rad/sec	Pitch Angle θ Degrees	Bank Angle ϕ Degrees	True Velocity V Ft/sec
1	? .?E-02	1.947E+00	-1.703E+01	1.063E+00	2.316E-01
2	3.295E-02	1.986E+00	-1.644E+01	9.505E-01	2.311E-01
3	2.975E-02	2.028E+00	-1.583E+01	8.403E-01	2.307E-01
4	2.657E-02	2.073E+00	-1.520E+01	7.343E-01	2.303E-01
5	2.343E-02	2.121E+00	-1.457E+01	6.331E-01	2.298E-01
6	2.034E-02	2.171E+00	-1.393E+01	5.367E-01	2.294E-01
7	1.725E-02	2.225E+00	-1.328E+01	4.442E-01	2.290E-01
8	1.411E-02	2.282E+00	-1.263E+01	3.543E-01	2.285E-01
9	1.086E-02	2.342E+00	-1.199E+01	2.656E-01	2.281E-01
10	7.425E-03	2.406E+00	-1.135E+01	1.768E-01	2.277E-01
11	3.764E-03	2.472E+00	-1.072E+01	8.722E-02	2.273E-01
12	3.619E-03	2.475E+00	-1.070E+01	8.377E-02	2.272E-01

$\star = (\star 1000)$

Table I. Stable Flat Spin Equilibrium States
for $\delta_e = -29°$, $\delta_{\Delta e} = \delta_a = 0°$

Point	Rudder Deflection δ_r Degrees	Angle of Attack α Degrees	Sideslip Angle β Degrees	Roll Rate p Rad/sec
1	8.660942E+00	7.072649E+01	-2.745E+00	6.216E-01
2	8.243752E+00	7.131086E+01	-2.679E+00	6.131E-01
3	7.936594E+00	7.193219E+01	-2.603E+00	6.039E-01
4	7.742710E+00	7.257995E+01	-2.518E+00	5.943E-01
5	7.653853E+00	7.324258E+01	-2.425E+00	5.843E-01
6	8.370946E+00	7.866498E+01	-1.605E+00	4.927E-01
7	8.331027E+00	7.931127E+01	-1.529E+00	4.792E-01
8	8.200088E+00	7.994443E+01	-1.467E+00	4.652E-01
9	7.963855E+00	8.055516E+01	-1.420E+00	4.507E-01

Point	Pitch Rate q Rad/sec	Yaw Rate r Rad/sec	Pitch Angle θ Degrees	Bank Angle ϕ Degrees	True Velocity V Ft/sec*
1	-5.605E-03	1.706E+00	-2.002E+01	-1.883E-01	2.347E-01
2	-6.930E-03	1.738E+00	-1.943E+01	-2.285E-01	2.342E-01
3	-8.092E-03	1.772E+00	-1.882E+01	-2.616E-01	2.337E-01
4	-9.035E-03	1.810E+00	-1.818E+01	-2.861E-01	2.332E-01
5	-9.725E-03	1.849E+00	-1.754E+01	-3.014E-01	2.326E-01
6	-1.049E-02	2.262E+00	-1.229E+01	-2.658E-01	2.286E-01
7	-1.118E-02	2.330E+00	-1.162E+01	-2.749E-01	2.261E-01
8	-1.234E-02	2.403E+00	-1.096E+01	-2.943E-01	2.276E-01
9	-1.408E-02	2.480E+00	-1.030E+01	-3.254E-01	2.272E-01

$* = (*1000)$

Table II. Stable Flat Spin Equilibrium States for $\delta_e = -29°$ without Asymmetric Side Force and Yawing Moment

Additional Rudder Sweeps

The next area of investigation was to decrease the stabilator deflection and do other rudder sweeps to see what effects if any stabilator deflection had on determining equilibrium spin conditions. A stabilator deflection of -25 degrees was chosen with no aileron deflection (0 degrees) in order to limit the number of possible causal variables. The origin from which the solution branches are "grown from" is 0 degrees rudder deflection and 25 degrees angle-of-attack (Bottom center of Figure 5-3). The starting point was an unstable equilibrium solution which translates to a physically unrealizable state and can be thought of in terms of domains of attraction as a source that repels. What becomes quickly apparent is the symmetry of the branches below 30 degrees angle-of-attack and the asymmetrical behavior above 30 degrees angle-of-attack. This is directly attributable to the asymmetric side force and yawing moments which are only available above 32 degrees and 38 degrees angle-of-attack respectively. Once again equilibrium spin conditions were found at angles-of-attack of 80 to 81 degrees (very small range). This correlates very well to actual flight data mentioned previously. Figure 5-3 depicts the equilibrium and periodic branches for the above configuration ($\delta_e = -25°$, $\delta_a = \delta_{\Delta e} = 0°$). Table III tabulates the stable equilibrium spin states.
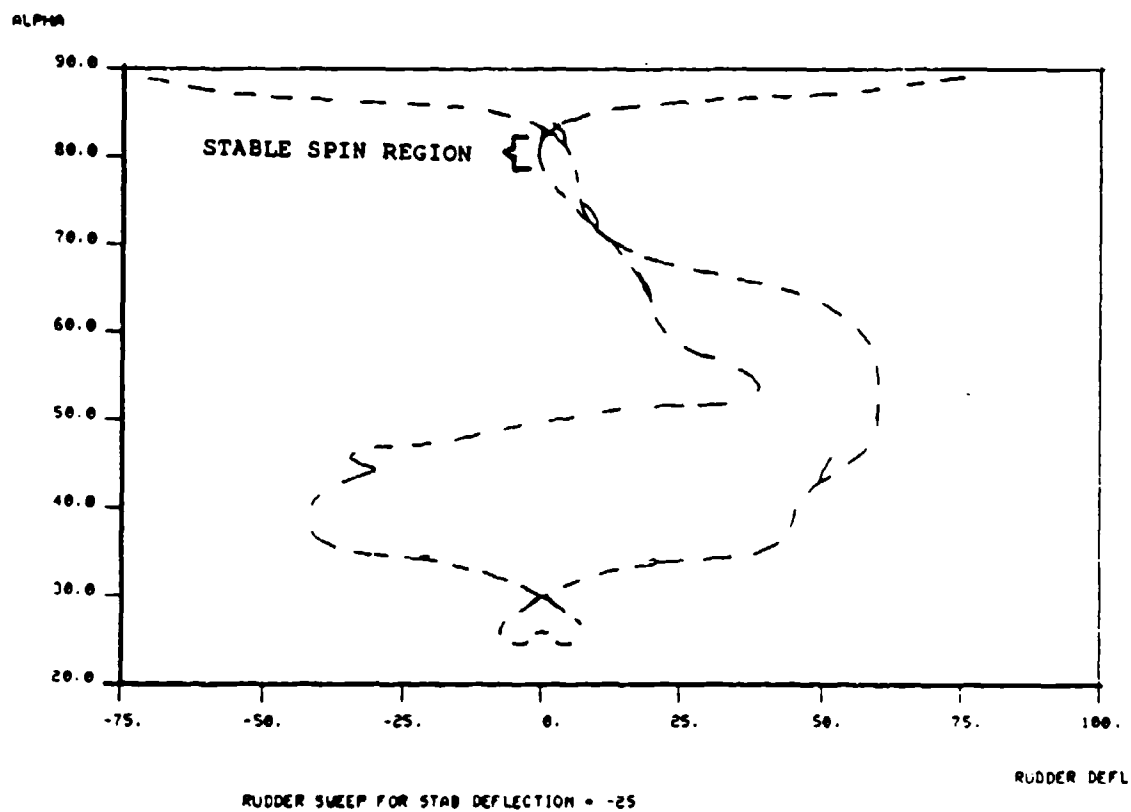
Figure 5-3 Equilibrium and Periodic Solutions
for $\delta_e = -25°$, $\delta_{\Delta e} = \delta_a = 0°$

Point	Rudder Deflection δ_r Degrees	Angle of Attack α Degrees	Sideslip Angle β Degrees	Roll Rate p Rad/sec
1	-9.808289E-01	8.015831E+01	3.788E+00	-4.136E-01
2	-8.070490E-01	8.094665E+01	3.606E+00	-3.960E-01
3	-5.972175E-01	8.130716E+01	3.540E+00	-3.872E-01

Point	Pitch Rate q Rad/sec	Yaw Rate r Rad/sec	Pitch Angle θ Degrees	Bank Angle ϕ Degrees	True Velocity V Ft/sec*
1	-1.066E-01	-2.329E+00	-1.006E+01	2.620E+00	2.275E-01
2	-1.075E-01	-2.429E+00	-9.249E+00	2.533E+00	2.269E-01
3	-1.087E-01	-2.480E+00	-8.865E+00	2.510E+00	2.266E-01

$* = (*1000)$

Table III.   Stable Flat Spin Equilibrium States
for $\delta_e = -25°$, $\delta_{\Delta e} = \delta_a = 0$

The next area of investigation was to pick a lower
starting point on the main stabilator deflection branch plotted
in Appendix C and do a rudder sweep. Figure 5-4 plots the
solution branches (rudder sweep) for a stabilator deflection of -
19.72 degrees and no aileron deflection. Table IV gives the
corresponding stable equilibrium conditions for the spins
encountered. What are also offered, but are too lengthy to list
here, are the equilibium states for the stable part of the lower
branch, these are given in Appendix D. What is interesting to
note is that the stable equilibrium solutions depicted here could
lead to jump phenomena (6). The possibility exists that by
holding stabilator and aileron fixed at -19.73 degrees and 0

59

degrees respectively, the equilibrium states describing the F-15B's dynamic behavior could jump, at Hopf bifurcation points which bound the stable region, from those describing a stable flat spin on the upper branch to those of cruise configuration, by varying the rudder. The stable equilibrium states that the F-15B could possibly recover to are given in Appendix D. The origin once again from which these branches were grown is the bottom center of the plot (0 degree rudder deflection and 21 degrees angle of attack). The lower part of the branches are stable from $\delta_r = 0°$ to $\delta_r = -13.43°$ and $\delta_r = +13.43°$ where Hopf bifurcations (not shown) are encountered. Upon the exchange of stability the branches become unstable and remain that way until about 70 - 80 degrees angle-of-attack where stable spin conditions are encountered. The symmetry below 32 degrees angle of attack contrasts sharply with the asymmetry above 32 degrees angle-of-attack.

Figure 5-5 is an enlargement of the stable equilibrium spin region in Figure 5-4 and clearly shows the two Hopf bifurcations bounding the region. The Hopf bifurcations are stable for a short distance from the main branch which suggests that there could be a transition from a stable equilibrium to stable oscillatory spin motion before finally "jumping" to stable low α equilibrium states. The lower periodic branch is stable for 7 steps while the upper periodic branch is stable for 20 steps.

60
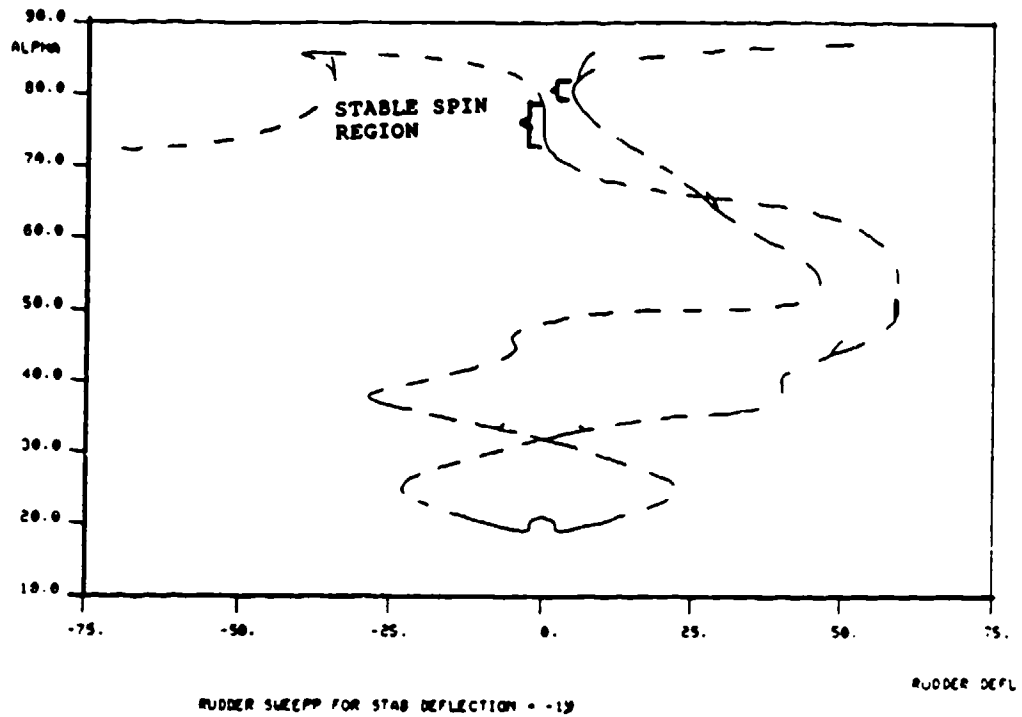
Figure 5-4 Periodic and Equilibium Solution Branches
$\delta_e = -19°$, $\delta_{\Delta e} = \delta_a = 0°$
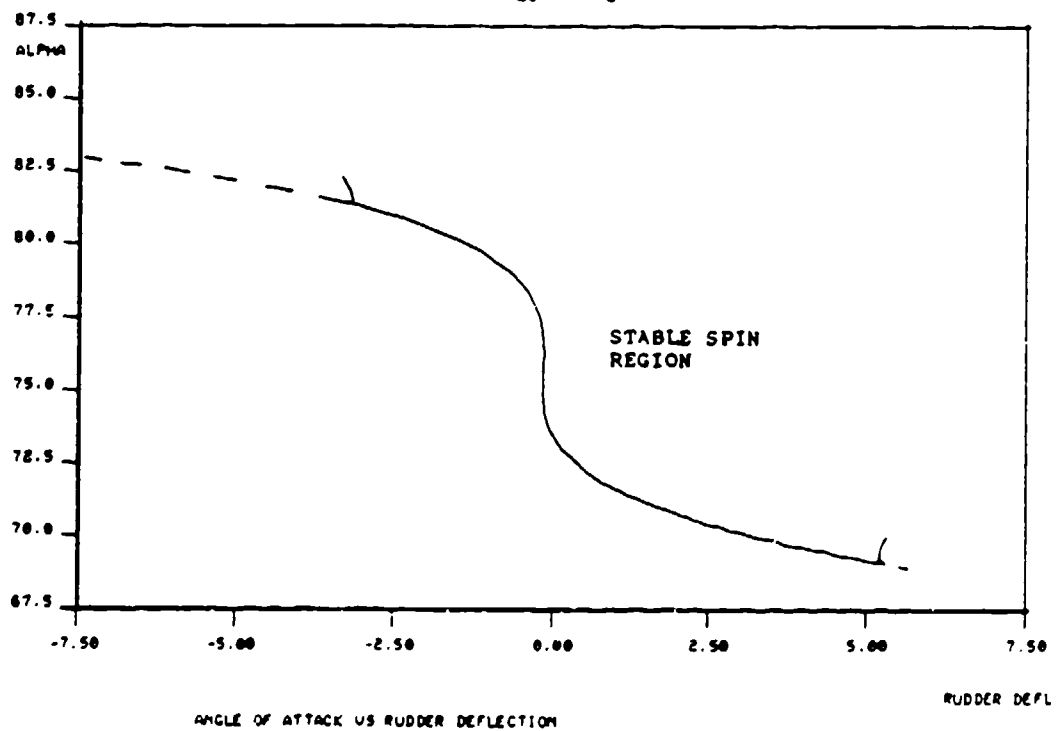
Figure 5-5 Stable Equilibrium Spin Region Enlargement
$\delta_e = -19°$, $\delta_a = \delta_{\Delta e} = 0°$

61

Point	Rudder Deflection δ_r Degrees	Angle of Attack α Degrees	Sideslip Angle β Degrees	Roll Rate p Rad/sec
	4.573708E+00	7.986353E+01	5.813E+00	-3.819E-01
1	4.889537E+00	8.087819E+01	5.586E+00	-3.578E-01
2	5.014476E+00	6.913565E+01	-4.173E+00	6.729E-01
3	4.235099E+00	6.946161E+01	-4.225E+00	6.657E-01
4	3.483146E+00	6.981571E+01	-4.279E+00	6.577E-01
5	2.766480E+00	7.020241E+01	-4.334E+00	6.489E-01
6	2.095887E+00	7.062678E+01	-4.390E+00	6.393E-01
7	1.485794E+00	7.109398E+01	-4.446E+00	6.286E-01
8	9.541467E-01	7.160783E+01	-4.499E+00	6.168E-01
9	5.199236E-01	7.216853E+01	-4.546E+00	6.039E-01
10	1.969605E-01	7.277046E+01	-4.585E+00	5.900E-01
11	-1.369470E-02	7.340273E+01	-4.612E+00	5.754E-01
12	-1.265108E-01	7.405311E+01	-4.628E+00	5.603E-01
13	-1.677815E-01	7.471214E+01	-4.634E+00	5.450E-01
14	-1.567384E-01	7.621992E+01	-4.624E+00	5.090E-01
15	-1.745491E-01	7.688125E+01	-4.616E+00	4.927E-01
16	-2.454737E-01	7.753748E+01	-4.611E+00	4.761E-01
17	-3.938092E-01	7.818228E+01	-4.613E+00	4.591E-01
18	-6.381852E-01	7.880620E+01	-4.624E+00	4.421E-01
19	-9.879613E-01	7.939817E+01	-4.645E+00	4.252E-01
20	-1.441491E+00	7.994833E+01	-4.678E+00	4.088E-01
21	-1.988095E+00	8.045063E+01	-4.721E+00	3.931E-01
22	-2.612532E+00	8.090361E+01	-4.773E+00	3.783E-01
23	-3.188041E+00	8.124872E+01	-4.823E+00	3.666E-01

Table IV.   Stable Flat Spin Equilibrium States
for $\delta_e = -19°$, $\delta_a = \delta_{\Delta e} = 0°$

Point	Pitch Rate q Rad/sec	Yaw Rate r Rad/sec	Pitch Angle θ Degrees	Bank Angle ϕ Degrees	True Velocity V Ft/sec
1	-1.764E-01	-2.213E+00	-9.758E+00	4.556E+00	2.261E-01
2	-1.805E-01	-2.322E+00	-8.734E+00	4.446E+00	2.253E-01
3	-4.468E-02	1.735E+00	-2.119E+01	-1.475E+00	2.364E-01
4	-4.853E-02	1.750E+00	-2.082E+01	-1.589E+00	2.360E-01
5	-5.265E-02	1.766E+00	-2.042E+01	-1.708E+00	2.356E-01
6	-5.704E-02	1.783E+00	-1.999E+01	-1.832E+00	2.352E-01
7	-6.171E-02	1.803E+00	-1.952E+01	-1.961E+00	2.348E-01
8	-6.666E-02	1.823E+00	-1.901E+01	-2.094E+00	2.343E-01
9	-7.182E-02	1.846E+00	-1.846E+01	-2.228E+00	2.338E-01
10	-7.712E-02	1.871E+00	-1.787E+01	-2.360E+00	2.332E-01
11	-8.240E-02	1.898E+00	-1.725E+01	-2.485E+00	2.327E-01
12	-8.753E-02	1.927E+00	-1.661E+01	-2.601E+00	2.322E-01
13	-9.241E-02	1.957E+00	-1.596E+01	-2.703E+00	2.317E-01
14	-9.705E-02	1.989E+00	-1.531E+01	-2.794E+00	2.312E-01
15	-1.071E-01	2.065E+00	-1.383E+01	-2.969E+00	2.301E-01
16	-1.116E-01	2.102E+00	-1.318E+01	-3.039E+00	2.297E-01
17	-1.163E-01	2.140E+00	-1.252E+01	-3.111E+00	2.292E-01
18	-1.214E-01	2.181E+00	-1.187E+01	-3.186E+00	2.287E-01
19	-1.269E-01	2.223E+00	-1.123E+01	-3.268E+00	2.282E-01
20	-1.329E-01	2.267E+00	-1.061E+01	-3.356E+00	2.277E-01
21	-1.393E-01	2.310E+00	-1.002E+01	-3.450E+00	2.272E-01
22	-1.460E-01	2.354E+00	-9.464E+00	-3.549E+00	2.267E-01
23	-1.529E-01	2.396E+00	-8.955E+00	-3.652E+00	2.262E-01
	-1.589E-01	2.431E+00	-8.559E+00	-3.740E+00	2.258E-01

Table IV. Flat Spin Equilibrium States
for $\delta_e = -19°$, $\delta_a = \delta_{\Delta e} = 0°$
(Continued)

Based on the similiarities of the general shape of the preceding curves a comparison was felt necessary. Figure 5-6 shows the preceding curves on the same plot. It looks like "All roads lead to Rome" in that spin phenomena were found in the same region for all solution curves.

RUDDER SWEEPS FOR STAB DEFL = -19, 25,29

RUDDER DEFL
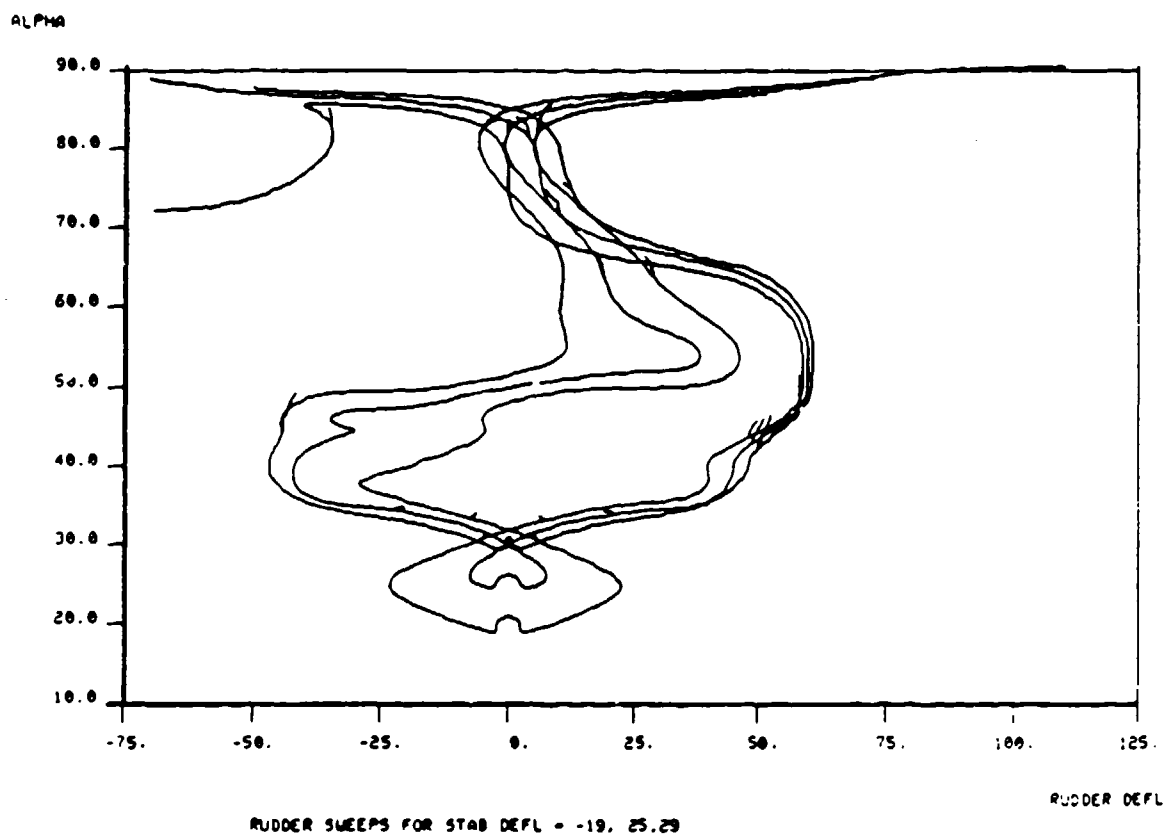
Figure 5-5 Equilibrium and Periodic Solutions
δ_e = -19, -25, -29 degrees

Based on this observation it was logical to ask the question
"Do the equilibrium spin conditions look the same for all
stabilator deflections?" It was decided to see if this was
true by growing branches from a much lower stabilator
deflection of -5 degrees. Figure 5-7 shows a plot of the
equilibrium and periodic solution curves for a stabilator
deflection of -5 degrees. Only three stable equilibrium
spin conditions were observed at 79° to 81° α and δ_r = 12°

64

to 14°. The states for the stable spin conditions are given in Table V.

AUTO as mentioned before has the capability to do a two parameter continuation which would have had the effect of expediting the preceeding survey process. In particular, only the Hopf bifurcation points bounding regions of stable spin would be computed, result being a "spin domain" δ_r vs δ_e. This, however, was not able to be taken advantage of during this research due to computation difficulties encountered at high angles of attack (60° to 80°). Two parameter continuation (not shown) was successful at low angles-of-attack. Two parameter continuation would have provided a concise summary and enabled the accurate mapping of the spin stability boundary as a function of control surface deflections (δ_a, δ_e, $\delta_{\Delta e}$, δ_r) or at least (δ_e, δ_r).
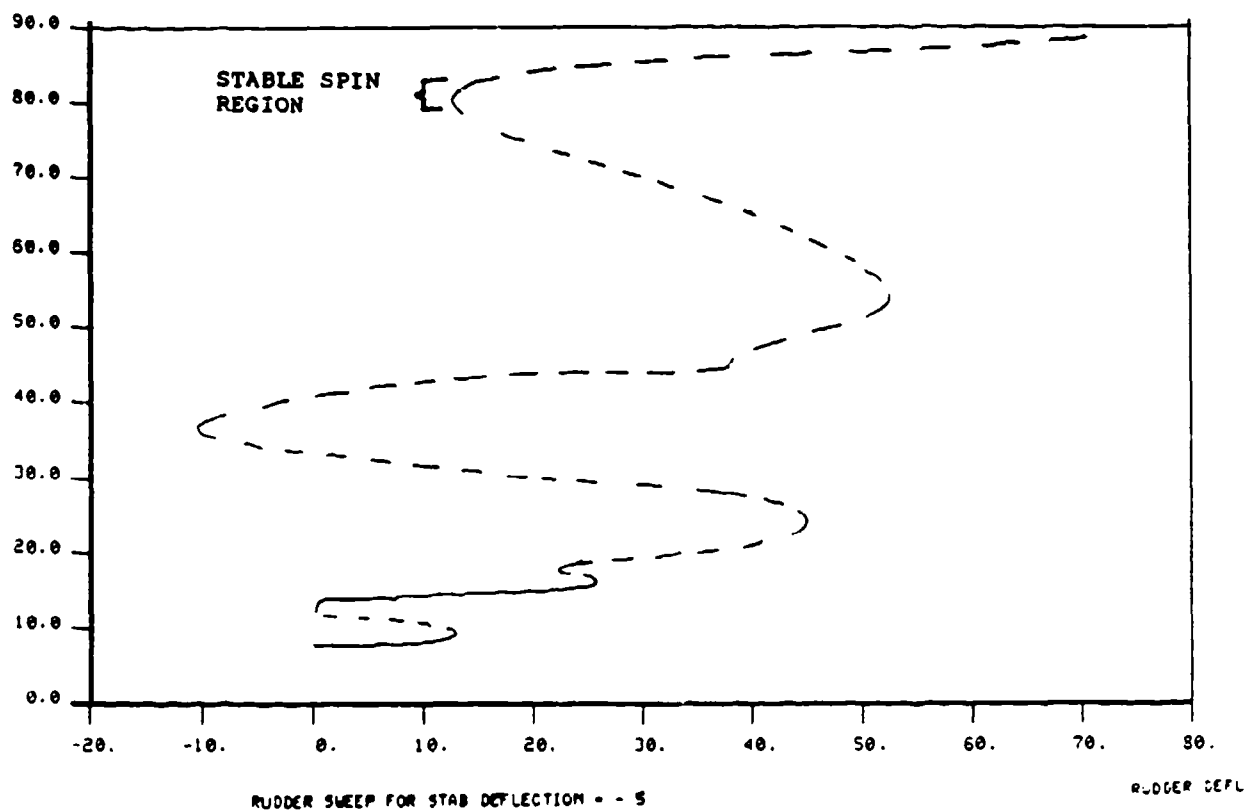
Figure 5-7   Equilibrium and Periodic Solutions
$\delta_e = -5°$, $\delta_{\Delta e} = \delta_a = 0°$

Point	Rudder Deflection δ_r Degrees	Angle of Attack α Degrees	Sideslip Angle β Degrees	Roll Rate p Rad/sec
1	1.280650E+01	7.950540E+01	9.048E+00	-3.273E-01
2	1.318868E+01	8.056331E+01	8.897E+00	-2.994E-01
3	1.414824E+01	8.139728E+01	8.843E+00	-2.752E-01

Point	Pitch Rate q Rad/sec	Yaw Rate r Rad/sec	Pitch Angle θ Degrees	Bank Angle ϕ Degrees	True Velocity V Ft/sec
1	-2.671E-01	-2.018E+00	-9.134E+00	7.540E+00	2.202E-01
2	-2.750E-01	-2.089E+00	-8.088E+00	7.501E+00	2.194E-01
3	-2.852E-01	-2.155E+00	-7.214E+00	7.538E+00	2.185E-01

Table V. Stable Flat Spin Equilibrium States
for $\delta_e = -5°$, $\delta_a = \delta_{\Delta e} \approx 0°$

VI. Conclusions and Recommendations

This simple straight forward procedure gives results
that correlate well with empirical flight test data, despite
using the constraints and approximations that the F-15B
model was formulated with. It is offered with the intent
that this research be primarily used to understand F15 high
angle-of-attack stability which is the underlying cause of
non-linear dynamic behavior and as a basis for further study
into the high angle-of-attack flight regime. It is not
intended nor implied to be a complete definitive survey of
the F-15B's high α stability but is an important step toward
that goal. In short, the qualitative behavior found is
stressed over quantitative behavior given.

One conclusion made on the high α results that can be
given with certainty is that stable equilbrium spin
conditions (based on the non-linear equations of motion used
in this study) exist and can be predicted. The results
given should be used as a rough estimation of the conditions
of a flat spin and are offered as comparative information.

This procedure (bifurcation analysis) has shown its
efficacy in surveying non-linear global dynamic aircraft
behavior and agrees well with previous research done by
Barth at lower angles of attack (12). As an expansion of
this previous work this technique has demonstrated itself to
be well suited to locating and cataloging equilibrium

solutions at higher angles-of-attack (> 60°).

In order to increase the practical application of bifurcation analysis of flight mechanics problems the following recommendations for further study in this area are offered:

1) Make AUTO run with look up tables for the stability derivatives and aerodynamic coefficients. It is realized that discontinuities in the data may be present and a suggested possible solution to this problem would be to smooth the data with some sort of clamped cubic spline scheme.

2) Modify the aerodynamic model to include conformal fuel tanks and lateral asymmetry to study the F-15D spin susceptibility of the accident mentioned in the introduction.

3) Do multi-parameter continuation of the equilibrium spin entry boundary (Hopf bifurcation) to get a map of the spin region as a function of control surface deflections $(\delta_a, \delta_e, \delta_r)$.

4) Since thrust was held fixed in this study, investigate effects of variable thrust settings or thrust/weight ratios on stable equilibrium spin states. Also along this line of inquiry, investigate the possibility of using thrust vectoring to escape flat spins.

5) One area though that was not investigated thoroughly due to time constraints and meriting further investigation

69

is the cataloging of high α stable periodic behavior
such as oscillatory spins, wing rock, etc.. The
cataloging of stable high angle-of-attack oscillatory
phenomena shows great promise and will really exhibit
the utility of this procedure.

6) This study was focused primarily on the prediction of
stable high α equilibrium conditions, however, the
future success of this technique (bifurcation analysis)
lies in the ability of the flight dynamicist to utilize
this information in the design and synthesis of feedback
and control laws. An application of this research is in
developing an effective recovery strategy from or
avoidance of stable spin equilibrium states. The next
step of toward this goal is the investigation of the
presence or lack of control authority to avoid spins or
enable recovery from them.

Appendix A: F-15 Weight and Balance Data

Table 1 lists the weight and balance data as well as the physical dimensions of the F-15B.   These values were primarily obtained from Barth (12) but were verified wherever possible (7).

The take-off gross weight and mass inertia values are for a clean aircraft configuration and were the same used in the F-15B baseline flight simulator at the Flight Dynamics Laboratory (12).

The force and moment sign conventions for the aircraft are as follows; Axial force is positive forward, normal force is positive downward, and side force is positive to the right.   Rolling moment is positive for right wing moving down, pitching moment is positive when tne nose of the aircraft moves upward, and positive yawing moment is when the nose of the aircraft moves to the right.

The sign conventions for the control surfaces are as follows; Rudders have positive deflection when the trailing edge is to the left of the chord line.   The ailerons are positively deflected when the right aileron's trailing edge is below the chord line.   Horizontal stabilator surfaces are positively deflected when the leading edges are up (trailing edges are therefore down.)

71

Table VI. Physical Characteristics of the F-15B Aircraft

Takeoff gross weight (clean config.)	38400 lbs
I_{xx}	33400 slug-ft
I_{yy}	172800 slug-ft
I_{zz}	192000 slug-ft
I_{xz}	-105 slug-ft

Wing

Area (reference)	608.00 sq ft
Area (actual)	599.39 sq ft
Aspect Ratio	3.01
Taper Ratio	0.25
Sweep (leading edge)	45 degrees
Dihederal	-1 degree

Airfoil & Chord

Root (BL 0)	NACA 64A006.6	301.5 in actual
BL 77.0	NACA 64Ax05.9	226.0 in actual
BL 155.0	NACA 64Ax04.6	149.6 in actual
BL 224.73	NACA 64A203.5	94.0 in actual
Tip	NACA 64A203.0	68.3 in actual
Incidence		None
Twist		None
Modified Conical Camber		Cl/D=0.3
Aileron Area		26.48 sq ft
Aileron Travel		+30 degrees
Flaperon Area		35.84 sq ft
Flaperon Travel		0 to 30 deg do

Stabilator

Area (reference)	120.0 sq ft total
Area (actual)	111.36 sq ft total
Aspect Ratio	2.05
Taper Ratio	0.34
Sweep (leading edge)	50 degrees
Dihedral	0 degrees

Airfoil Chord

Root (Bl 0)	NACA 0005.5-64	137.2 in reference
BL 90.0	NACA 0003.5-64	117.9 in reference
Tip	NACA 0002.5-64	46.5 in reference
Stabilator Travel		+20 to -30 degrees

Table VI. <u>Physical Characteristics of the F-15B</u>
(Continued)

<u>Vertical Tails</u>
Effective Area	125.2 sq ft total
Aspect Ratio	1.7
Taper Ratio	0.27
Sweepback	34.57 degrees

<u>Airfoil & Chord</u>
Root	NACA 0005.0-64	115.0 in actual
Tip	NACA 0003.5-64	30.6 in actual
Rudder Area		19.94 sq ft total
Rudder Travel		+30 degrees

<u>Miscellaneous Data</u>
Aircraft Length (Static)	63.8 ft
Aircraft Height (Static)	18.6 ft

<u>Fuel Capacity</u>
Fuselage	944 Gal.
Wing	846 Gal.
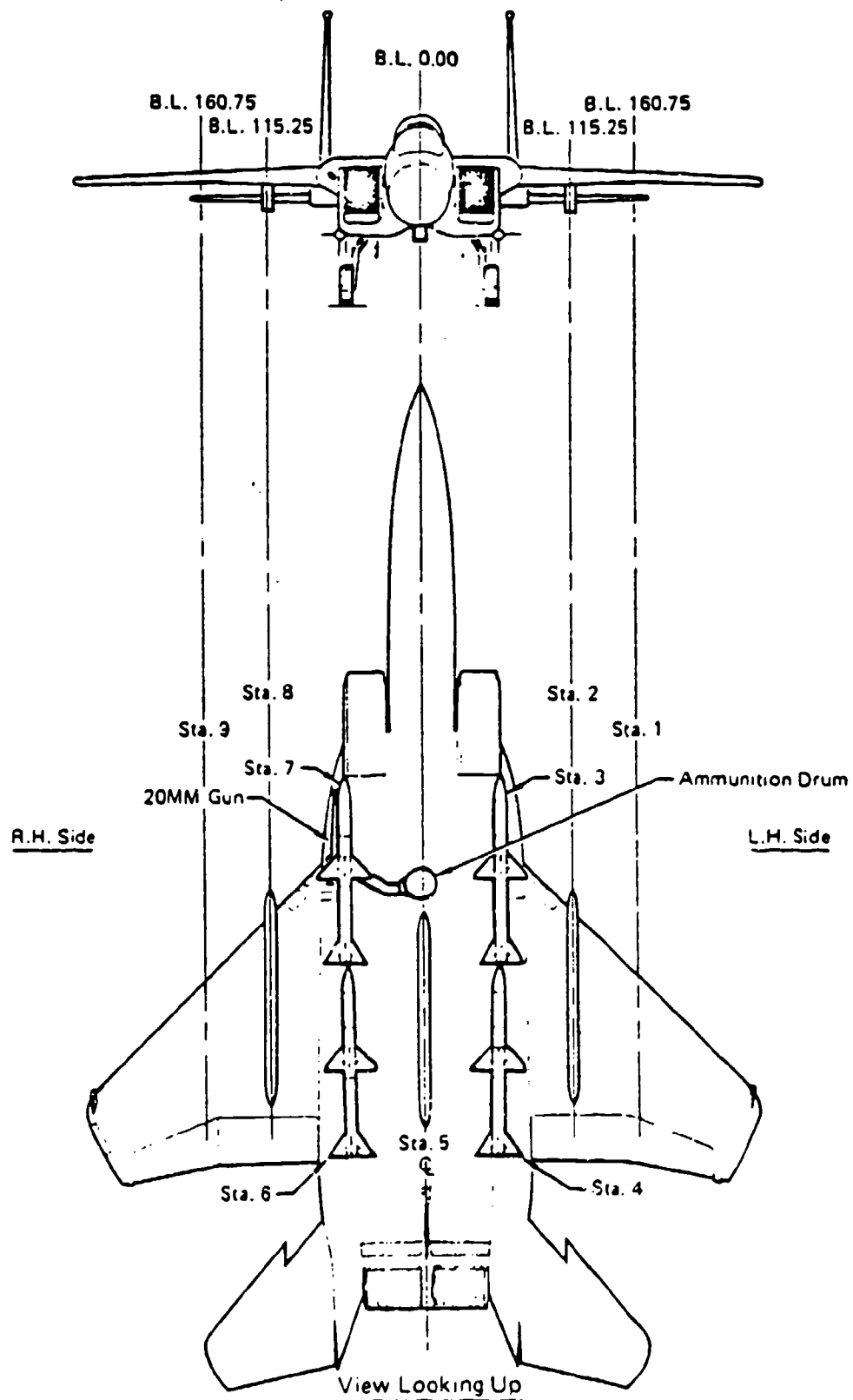
Figure A-1   F15 Diagram

```
      PROGRAM DRVR2
C
C     CAPTAIN DANIEL D. BAUMANN     AFIT GAE-89D
C     MASTERS THESIS
C
C     COMPUTER PROGRAM THAT SOLVES THE NONLINEAR DIFFERENTIAL
C     EQUATIONS OF MOTION FOR THE F-15B AIRCRAFT.  USED AS AN
C     ANALYTICAL TOOL IN THE SEARCH OF HIGH ANGLE OF ATTACK
C     PHENOMENA (I. E. FLAT SPINS).  BASED ON A COMPUTER
C     PROGRAM ORIGINALLY WRITTEN BY TOM BARTH.
C
C     LAST EDITED ON 17 OCTOBER 1989
C
      IMPLICIT DOUBLE PRECISION(A-H,O-Z)
      DIMENSION W(300000), IW(1000)
C
C
C     THIS WAS ADDED SO THAT AUTO CAN READ FROM UNIT
C     3 ON A RESTART
C
      OPEN(UNIT=3,FILE='fort.3')
      OPEN(UNIT=4,FILE='fort.4')
      OPEN(UNIT=7,FILE='fort.7')
      OPEN(UNIT=8,FILE='fort.8')
      OPEN(UNIT=9,FILE='fort.9')
C
      REWIND 7
      REWIND 8
      REWIND 9
      REWIND 3
      REWIND 4
      CALL AUTO(W,IW)
      STOP
      END
C
C
      SUBROUTINE FUNC(NDIM,NPAR,U,ICP,PAR,IJAC,F,DFDU,DFDP)
C     ---------- -------------------------------------------
C
      IMPLICIT DOUBLE PRECISION (A-H,O-Z)
      COMMON /KS/ K1,K5,K7,K8,K9,K10,K12,K13,K14,K15,K16,K17
      COMMON /ACDATA/ BWING,CWING,SREF,RHO,RMASS,THRUST
      DOUBLE PRECISION K1,K5,K7,K8,K9,K10,K12,K13,K14,K15,K16,K17
C     DOUBLE PRECISION K2,K3,K4,K6,K11,IX,IY,IZ,IXZ
      COMMON /SEIZE/ CX,CY,CZ,CLM,CMM,CNM
C
C
      DIMENSION DFDU(NDIM,NDIM),DFDP(NDIM,NPAR),DELF1(8),
```

75

```
    +                  DELF2(8),U(NDIM),PAR(10),F(NDIM),DX(8)
C
C        WRITE(6,*) 'ENTERED FUNC'
C
C
C     INITIALIZE SOME CONSTANTS THAT ARE PASSED THROUGH
C     THE COMMON BLOCK ACDATA
C
C     DATA IS FROM MCAIR REPORT# A4172 AND AFFTC-TR-75-32
C     F-15A APPROACH-TO-STALL/STALL/POST-STALL EVALUATION
C
C     BWING   - A/C WINGSPAN, FT
C     CWING   - A/C MEAN AERODYNAMIC CHORD, FT
C     SREF    - A/C WING REFERENCE AREA, SQ FT
C     RHO     - AIR DENSITY AT 20000 FT ALTITUDE, SLUG/FT^3
C     RMASS   - A/C MASS, SLUGS
C     THRUST  - TOTAL A/C THRUST, LBS
C
      BWING=42.8
      CWING=15.94
      SREF=608.
      RHO=.0012673
      RMASS=37000./32.174
      THRUST=8300.
C
C
C     DETERMINE CONSTANTS K1 THROUGH K17.  SOME ARE MADE COMMON AND
C     PASSED TO SUBROUTINE FUNX AND USED IN THE EQUATIONS
C     OF MOTION THERE
C
C     INERTIAS HAVE UNITS OF SLUG-FT^2
C
C     K1 HAS UNITS OF 1/FT
C
C     K6, K8, K11, K14, AND K17 HAVE UNITS OF 1/FT^2
C
C
C     IX=  25480.
C     IY=  166620.
C     IZ=  186930.
C     IXZ=  -1000.
C     K1=.5*RHO*SREF/RMASS
C     K2=(IZ-IY)/IX
C     K3=IXZ*IXZ/(IX*IZ)
C     K4=(IY-IX)/IZ
C     K5=IXZ/IX
C     K6=.5*RHO*BWING*SREF/IX
C     K7=IXZ/IZ
C     K8=.5*RHO*SREF*CWING/IY
C     K9=(IZ-IX)/IY
C     K10=IXZ/IY
C     K11=.5*RHO*SREF*BWING/IZ
```

76

```
C          K12=(K2+K3)/(1.-K3)
C          K13=(1.-K4)*K5/(1.-K3)
C          K14=K6/(1.-K3)
C          K15=(K3-K4)/(1.-K3)
C          K16=(1.+K2)*K7/(1.-K3)
C          K17=K11/(1.-K3)
C
C
           K1  = 3.350088890D-04
           K5  =-3.924646781D-02
           K7  =-5.349596105D-03
           K8  = 3.685650971D-05
           K9  = .96897131196
           K10 =-6.001680471D-03
           K12 = .79747314581
           K13 =-9.615755341D-03
           K14 = 6.472745847D-04
           K15 =-.754990553922
           K16 =  K13
           K17 = 8.822851558D-05
C
C
C
C          FIND THE VALUES OF F(1) THROUGH F(NDIM).  SUBROUTINES
C          COEFF AND FUNX ARE CALLED ONCE.
C
C
C          WRITE(6,*)'ALPHA,BETA,P,Q=',U(1),U(2),U(3),U(4)
C          WRITE(6,*)'R,THETA,PHI,VELOCITY=',U(5),U(6),U(7),U(8)
           CALL COEFF(U,PAR,NDIM)
C
           CALL FUNX(NDIM,U,F)
C
C          WRITE(6,*) 'F1,F2= ',F(1),F(2)
C          WRITE(11,*) 'F1,F2= ',F(1),F(2)
C          WRITE(6,*) 'F3,F4= ',F(3),F(4)
C          WRITE(11,*) 'F3,F4= ',F(3),F(4)
C          WRITE(6,*) 'F5,F6= ',F(5),F(6)
C          WRITE(11,*) 'F5,F6= ',F(5),F(6)
C          WRITE(6,*) 'F7,F8= ',F(7),F(8)
C          WRITE(11,*) 'F7,F8= ',F(7),F(8)
C
           IF(IJAC.EQ.0) RETURN
C
C     SET THE VALUES OF DX
C     MODIFIED TO SCALE DX ACCORDING TO VARIABLE
C     13 JUN 88
C
C          WRITE(6,*)' ENTER DX'
C          READ(5,*) DX0
C
           DX0=1.0D-9
```

```
          DX(1)=DX0*50.
          DX(2)=DX0*10.
          DX(3)=DX0*.5
          DX(4)=DX0*.25
          DX(5)=DX0*.5
          DX(6)=DX0*50.
          DX(7)=DX0*50.
          DX(8)=DX0*.5
C
C
C        NEXT THE PARTIAL OF F W.R.T. A GIVEN PARAMETER ARE FINITE
C        DIFFERENCED
C
         PTEMP=PAR(ICP)
         PAR(ICP)=PTEMP+DX(1)
C         WRITE (6,*) 'PAR PLUS DPAR=',PAR(ICP)
         CALL COEFF(U,PAR,NDIM)
         CALL FUNX(NDIM,U,DELF1)
C
         PAR(ICP)=PTEMP-DX(1)
C         WRITE(6,*) 'PAR MINUS DPAR=',PAR(ICP)
         CALL COEFF(U,PAR,NDIM)
         CALL FUNX(NDIM,U,DELF2)
C
            DO 13 I=1,NDIM
C               WRITE(6,*)'DPAR1(I),DPAR2(I)=   ',DELF1(I),DELF2(I)
C
               DFDP(I,ICP)=(DELF1(I)-DELF2(I))/(2.*DX(1))
C
C               WRITE(6,*) 'DFDP(I,ICP)=   ',DFDP(I,ICP)
C
   13       CONTINUE
         PAR(ICP)=PTEMP
C
C        THE NEXT DO LOOP CALCULATES THE PARTIAL DERIVATIVE OF F W.R.T.

C        TO U USING FINITE DIFFERENCES.
C
C        SET U(J) EQUAL TO U+DU, THEN CALL COEFF WITH THIS UPDATED
C        STATE VECTOR.  THIS IS DONE SIMILARLY WITH U-DU
C
         DO 20 J=1,NDIM
C
            UTEMP=U(J)
C
            U(J)=UTEMP+DX(J)
C            WRITE (6,*) 'U PLUS DU=',U(J)
            CALL COEFF(U,PAR,NDIM)
            CALL FUNX(NDIM,U,DELF1)
C            WRITE(6,*)'DELF1',DELF1(2),U(1),CX,CY,CZ
C
            U(J)=UTEMP-DX(J)
```

78

```
C              WRITE(6,*) 'U MINUS DU=',U(J)
           CALL COEFF(U,PAR,NDIM)
           CALL FUNX(NDIM,U,DELF2)
C           WRITE(6,*) 'DELF2',DELF2(2),U(1),CX,CY,CZ
C
C
           DO 16 I=1,NDIM
C
C              WRITE(6,*) 'DELF1(I),DELF2(I)=',DELF1(I),DELF2(I)
C
              DFDU(I,J)=(DELF1(I)-DELF2(I))/(2.*DX(J))
C
C              WRITE(6,*) 'DFDU=', DFDU(I,J)
C
   16         CONTINUE
C
           U(J)=UTEMP
C
   20  CONTINUE
C
C
C      WRITE(6,30) ((DFDU(I,J),J=1,NDIM),I=1,NDIM)
C   30  FORMAT(8(1X,E8.2)/)
C      WRITE(6,*) 'LEAVING FUNC'
C
       RETURN
       END

       SUBROUTINE FUNX(NDIM,U,F)
C      ---------- ---------------
C
C
C      SUBROUTINE FUNX EVALUATES THE NDIM EQUATIONS GIVEN THE
C      STATE VECTOR U.
C
C      NDIM- THE DIMENSION OF THE PROBLEM
C      U   - THE VECTOR OF STATES ALPHA, BETA, ... (INPUT)
C      F   - THE VECTOR RESULT OF FUNCTION EVALUATIONS (OUTPUT)
C
       IMPLICIT DOUBLE PRECISION (A-H,O-Z)
       COMMON /SEIZE/ CX,CY,CZ,CLM,CMM,CNM
       COMMON /KS/ K1,K5,K7,K8,K9,K10,K12,K13,K14,K15,K16,K17
       DOUBLE PRECISION K1,K5,K7,K8,K9,K10,K12,K13,K14,K15,K16,K17
       DIMENSION U(NDIM),F(NDIM)
C
C      SET TRIGONOMETRIC RELATIONSHIPS OF THE STATES ALPHA, BETA,
C      THETA, AND PHI AND THEN SET P, Q, R, AND VTRFPS
C
C      WRITE(6,*) 'ENTERED FUNX'
       IWRITE=1
C      IF(IWRITE.EQ.1)WRITE(6,*)' K1,5,7,8,9,10,12-17=',K1,K5,K7,K8,
C      +                                K9,K10,K12,K13,K14,K15,K16,K17
C      IF(IWRITE.EQ.1)WRITE(6,*)'FUNX U(1)-U(8)=',U(1),U(2),U(3),
```

79

```
C         +      U(4),U(5),U(6),U(7),U(8)
C
C
          DEGRAD=57.29577951
C
          CA=COS(U(1)/DEGRAD)
          SA=SIN(U(1)/DEGRAD)
          CB=COS(U(2)/DEGRAD)
          SB=SIN(U(2)/DEGRAD)
          CTHE=COS(U(6)/DEGRAD)
          STHE=SIN(U(6)/DEGRAD)
          CPHI=COS(U(7)/DEGRAD)
          SPHI=SIN(U(7)/DEGRAD)
C
          P=U(3)
          Q=U(4)
          R=U(5)
          VTRFPS=1000.*U(8)
C
C      SET THE GRAVITATIONAL CONSTANT, FT/SEC
C
          G=32.174
C
C      THE FOLLOWING SYSTEM OF NONLINEAR DIFFERENTIAL EQUATIONS
C      GOVERN AIRCRAFT MOTION
C
C      UPDATED FOR PROPER DEGREE-RADIAN UNITS AND PROPERLY
C      SCALED VELOCITY EQUATION:   7 JUN 88
C
C   F(1)=ALPHA-DOT
C
    1     F(1)=Q+(-(K1*VTRFPS*CX-G*STHE/VTRFPS+R*SB)*SA+(K1*VTRFPS
         +           *CZ+(G*CTHE*CPHI/VTRFPS)-P*SB)*CA)/CB
          F(1)=F(1)*DEGRAD
C
C
C   F(2)=BETA-DOT
C
    2     F(2)=-((K1*VTRFPS*CX-G*STHE/VTRFPS)*SB+R)*CA+(K1*VTRFPS*CY
         +    +G*CTHE*SPHI/VTRFPS)*CB-((K1*VTRFPS*CZ+G*CTHE*CPHI/VTRFPS)
         +    *SB-P)*SA
          F(2)=F(2)*DEGRAD
C
C         WRITE(6,*)'K1,CX,CY,CZ,F(2),G,SB,CB,CA,SA,SPHI,CPHI,CTHE,STHE',
C         +              K1,CX,CY,CZ,F(2),G,SB,CB,CA,SA,SPHI,CPHI,CTHE,STHE
C
C   F(3)=P-DOT
C
    3     F(3)=-K12*Q*R+K13*P*Q+K14*(CLM+K7*CNM)*VTRFPS*VTRFPS
C
C
```

80

```fortran
C     F(4)=Q-DOT
C
   4    F(4)=K8*VTRFPS*VTRFPS*CMM+K9*P*R+K10*(R*R-P*P)
C
C
C     F(5)=R-DOT
C
   5    F(5)=K15*P*Q-K16*Q*R+K17*VTRFPS*VTRFPS*(K5*CLM+CNM)
C
C
C     F(6)=THETA-DOT
C
   6    F(6)=Q*CPHI-R*SPHI
        F(6)=F(6)*DEGRAD
C
C
C     F(7)=PHI-DOT
C
   7    F(7)=P+Q*(STHE/CTHE)*SPHI+R*(STHE/CTHE)*CPHI
        F(7)=F(7)*DEGRAD
C
C
C     F(8)=VTRFPS-DOT   (SCALED BY A FACTOR OF 1000)
C
   8    F(8)=U(8)*((K1*VTRFPS*CX-G*STHE/VTRFPS)*CA*CB+(K1*VTRFPS*CY
     +  +G*CTHE*SPHI/VTRFPS)*SB
     +  +(K1*VTRFPS*CZ+G*CTHE*CPHI/VTRFPS)*SA*CB)
C
C
C       WRITE(6,*) 'LEAVING FUNX'
C       WRITE(6,*)'lv funx F=',F(1),F(2),F(3),F(4),F(5),F(6),F(7),F(8)

        RETURN
        END
C
        SUBROUTINE STPNT(NDIM,U,NPAR,ICP,PAR)
C       ----------  --------------------------
C
C
C       THIS SUBROUTINE SETS THE VALUES OF THE STATES AND PARAMETERS
C       AT THE START OF THE ANALYSIS.  THE STATES AND CONTROL SURFACE
C       SETTINGS REPRESENT AN EQUILIBRIUM STATE OF THE AIRCRAFT
C
        IMPLICIT DOUBLE PRECISION (A-H,O-Z)
C
        DIMENSION U(NDIM),PAR(10)
C
C        WRITE(6,*) 'ENTERED STPNT'
C
C       U(1) - ALPHA, DEG
C       U(2) - BETA, DEG
C       U(3) - P, RAD/SEC
C       U(4) - Q, RAD/SEC
```

81

```
C       U(5) - R, RAD/SEC
C       U(6) - THETA, DEG
C       U(7) - PHI, DEG
C       U(8) - TRUE VELOCITY, IN THOUSANDS OF FT/SEC
C
C       THE STARTING POINT (VECTOR) IS READ IN THIS WAY
C       SO THAT THE DATA FILE (UNIT 15) HAS A COLUMN OF
C       NUMBERS.  I BELIEVE THAT USING A COLUMN WILL MAKE IT
C       EASIER TO GET THE NUMBERS RIGHT THE FIRST TIME.
C
        OPEN(UNIT=15,FILE='fort.15')
        REWIND (15)
C
        READ(15,*) U(1)
        READ(15,*) U(2)
        READ(15,*) U(3)
        READ(15,*) U(4)
        READ(15,*) U(5)
        READ(15,*) U(6)
        READ(15,*) U(7)
        READ(15,*) VTRFPS
        U(8)=VTRFPS/1000.
C
C       PAR(1)=DELESD
C       PAR(2)=DRUDD        THE PARAMETERS, IN DEGREES
C       PAR(3)=DDA
C
        READ(15,*) PAR(1)
        READ(15,*) PAR(2)
        READ(15,*) PAR(3)
C
C
        RETURN
        END
C
C
        SUBROUTINE INIT
C       ---------- ----
C
        IMPLICIT DOUBLE PRECISION(A-H,O-Z)
C
        COMMON /BLCSS/ NDIM,ITMX,NPAR,ICP,IID,NMX,IPS,IRS
        COMMON /BLCPS/ NTST,NCOL,IANCH,NMXPS,IAD,NPR,NWTN,ISP,ISW1
        COMMON /BLDLS/ DS,DSMIN,DSMAX,IADS
        COMMON /BLLIM/ RL0,RL1,A0,A1,PAR(10)
        COMMON /BLOPT/ ITNW,MXBF,IPLT,ICP2,ILP
        COMMON /BLEPS/ EPSU,EPSL,EPSS,EPSR
C
C
C IN THIS SUBROUTINE THE USER SHOULD SET THOSE CONSTANTS
C THAT REQUIRE VALUES DIFFERENT FROM THE DEFAULT VALUES
C ASSIGNED IN THE LIBRARY SUBROUTINE DFINIT.  FOR A DESCRIPTION
```

82

```
C OF THESE CONSTANTS SEE THE DOCUMENTATION CONTAINED IN THE
C LIBRARY.  COMMON BLOCKS CORRESPONDING TO CONSTANTS THAT THE USER
C WANTS TO CHANGE MUST BE INSERTED ABOVE.  THESE COMMON BLOCKS
C SHOULD OF COURSE BE IDENTICAL TO THOSE IN DFINIT.
C
C
        DSMAX = 10.
        DSMIN = .0000001
        EPSU  = 1.0D-07
        EPSL  = 1.0D-07
        EPSS  = 1.0D-05
        EPSR  = 1.0D-07
        IAD   = 1
        ILP   = 1
        ITMX  = 40
        ITNW  = 20
        MXBF  = 5
        NDIM  = 8
        NPAR  = 3
C
        OPEN(UNIT=25,FILE='fort.25')
        REWIND (25)
C
        READ(25,*) RL0,RL1
        READ(25,*) A0,A1
        READ(25,*) DS
        READ(25,*) NMX
        READ(25,*) NTST,NCOL,NMXPS,NPR
        READ(25,*) ISP,IRS,ICP,ICP2,IPLT,IPS
        READ(25,*) ISW1
C
C   WRITE(6,*) 'LEAVING INIT'
C
        RETURN
        END
        SUBROUTINE BCND
C     ---------- ----
C
        RETURN
        END
C
        SUBROUTINE ICND
C     ---------- ----
C
        RETURN
        END
C
C
        SUBROUTINE COEFF(U,PAR,NDIM)
C
C
        IMPLICIT DOUBLE PRECISION (A-H,O-Z)
```

```
      COMMON /ACDATA/ BWING,CWING,SREF,RHO,RMASS,THRUST
      COMMON /SEIZE/ CX,CY,CZ,CLM,CMM,CNM
      DIMENSION U(NDIM),PAR(10)
C
C
C     THE PRIMARY SOURCE OF THESE COEFFICIENT EQUATIONS IS SUBROUTINE
C     ARO10 FROM MCAIR CODE USED IN THE F15 BASELINE SIMULATOR.
C
C     MOST OF THE COEFFICIENTS USED IN THE EQUATIONS WERE COMPUTED
C     USING SAS WITH RAW DATA FROM THE F15 SIMULATOR DATA TABLES.
C
C     THIS SUBROUTINE IS CALLED BY THE DRIVER PROGRAM FOR THE AUTO
C     SOFTWARE.  IT MERELY TAKES INPUTS ON THE A/C STATE AND CONTROL
C     SURFACE POSITIONS AND RETURNS THE APPROPRIATE AERO COEFFICIENTS
C     CX, CY, CZ, CL, CM, AND CM.
C
C     INPUTS TO THIS SUBROUTINE
C
C     AL       - ANGLE OF ATTACK, DEG
C     BETA     - SIDESLIP ANGLE, DEG
C     DDA      - AILERON DEFLECTION ANGLE, DEG
C     DELEDD   - DIFFERENTIAL TAIL DEFLECTION ANGLE, DEG
C     DELESD   - SYMMETRICAL TAIL DEFLECTION ANGLE, DEG
C     DRUDD    - RUDDER DEFLECTION, POSITIVE TRAILING EDGE LEFT, DEG
C     P        - ROLL RATE, RAD/SEC
C     Q        - PITCH RATE, RAD/SEC
C     R        - YAW RATE, RAD/SEC
C     THRUST   - TOTAL ENGINE THRUST, POUNDS
C     VTRFPS   - TRUE AIRSPEED, FT/SEC
C
C
C     INTERMEDIATE VARIABLES USED IN THIS SUBROUTINE
C
C     ABET     - ABSOLUTE VALUE OF BETA, DEG
C     ARUD     - ABSOLUTE VALUE OF RUDDER DEFLECTION, DEG
C     BWING    - WING SPAN, FEET
C     CA       - COSINE RAL (RAL IN RADIANS)
C     CD       - COEFFICIENT OF DRAG
C     CL       - B@SIC LIFT COEFFICIENT
C     CWING    - MEAN AERODYNAMIC CHORD, FEET
C     DAHD     - DIFFERENTIAL ELEVATOR DEFLECTION, DEG
C     DAHLD    - LEFT AILERON DEFLECTION, DEG
C     DAHRD    - RIGHT AILERON DELFECTION, DEG
C     DELEDR   - DIFFERENTIAL TAIL DEFLECTION ANGLE, RAD
C     DELESR   - SYMMETRIC TAIL DEFLECTION ANGLE, RAD
C     QBARS    - DYNAMIC PRESSURE TIMES WING REFERENCE AREA, LBF
C     RABET    - ABSOLUTE VALUE OF BETA, RADIANS
C     RAL      - ABSOLUTE VALUE OF ALPHA, RADIANS
C     RARUD    - ABSOLUTE VALUE OF RUDDER, RADIANS
C     SA       - SINE RAL (RAL IN RADIANS)
C
C
```

84

```
C
C      OUTPUTS FROM THIS SUBROUTINE
C
C      CX      - BASIC AXIAL FORCE COEFFICIENT, BODY AXIS, + FORWARD
C      CY      - BASIC SIDE FORCE COEFFICIENT, BODY AXIS, + RIGHT
C      CZ      - BASIC NORMAL FORCE COEFFICIENT, BODY AXIS, + DOWN
C      CLM     - BASIC ROLLING MOMENT COEFFICIENT, BODY AXIS, + R WING
C                DOWN
C      CMM     - BASIC PITCHING MOMENT COEFFICIENT, BODY AXIS, + NOSE UP
C      CNM     - BASIC YAWING MOMENT COEFFICIENT, BODY AXIS, + NOSE RIGHT
C
C       ANGLES USED IN CALCULATING CL, CLLDB, ..., ARE IN RADIANS. THIS
C       IS BECAUSE RADIANS WERE USED IN THE CURVE FITTING PROGRAM TO
C       OBTAIN THE COEFFICIENTS OF THE ALPHA, BETA, ..., TERMS IN THE
C       FOLLOWING EQUATIONS.
C
C
C      MOMENT REFERENCE CENTER WAS SET IN ARO10 PROGRAM AS:
C
C        DATA CMCGR /.2565/, CNCGR /.2565/
C
C      THE AERO STABILITY DATA WAS TAKEN REFERENCED TO THESE CG
C      LOCATIONS.  THE MOMENTS OF INERTIA AND OTHER AIRCRAFT DATA
C      ARE FOR A CLEAN CONFIGURATION TEST AIRCRAFT WITH A CG AT
C      THE SAME CG.  AS A RESULT, THERE IS NO 'CG OFFSET' TO BE
C      COMPUTED.
C
C
C        WRITE(6,*) 'ENTERED COEFF'
C
         IWRITE=0
C        IF(IWRITE.EQ.1)WRITE(6,*)' U(1)-U(8)= ',U(1),U(2),U(3),U(4),
C       +                U(5),U(6),U(7),U(8)
C
C        IF(IWRITE.EQ.1)WRITE(6,*)' PAR(1)-PAR(3)=',PAR(1),PAR(2),PAR(3)
C
C
         AL=U(1)
         BETA=U(2)
         P=U(3)
         Q=U(4)
         R=U(5)
         THETA=U(6)
         PHI=U(7)
         VTRFPS=U(8)*1000.
C
         DELESD=PAR(1)
         DRUDD=PAR(2)
         DDA=PAR(3)
C
         DEGRAD=57.29577951
         DELESR=DELESD/DEGRAD

                                  85
```

```
C
      QBARS=.5*RHO*VTRFPS*VTRFPS*SREF
      CO2V=CWING/(2.*VTRFPS)
      BO2V=BWING/(2.*VTRFPS)
      QSB=BWING'QBARS
      ARUD=ABS(LRUDD)
      RARUD=ARUD/DEGRAD
      RAL=AL/DEGRAD
      ABET=ABS(BETA)
      RABET=ABET/DEGRAD
C
C
C
C*******************************************************************
C
C
C
C     NEW SECTION OF CODE - 1) ALL THE AERODYNAMIC COEFFICIENTS IN
C                              THIS VERSION OF THE DRIVER PROGRAM
C                              ARE TAKEN DIRECTLY FROM THE 1908
C                              F15 AEROBASE (0.6 MACH, 20000 FEET)
C
C                           2) THIS SECTION SUMMARIZES THE
C                              AERODYNAMIC COEFFICIENTS AS TO WHAT
C                              THEY ARE AND HOW THEY ARE USED.
C                              THE FIRST ACCRONYM IS THE JOVIAL NAME
C                              OF THE AERODYNAMIC COEFFICIENT (CFX1,
C                              ETC), THE SECOND ACCRONYM IS THE
C                              F15 AEROBASE CODE OR CTAB NAME
C                              (ATAB15, ETC).  A BRIEF DEFINITION
C                              OF THE AERODYNAMIC COEFFICIENT IS ALSO
C                              PROVIDED.
C
C                           3) THERE IS ALSO A SECTION THAT PROVIDES
C                              A TABLE OF CONVERSIONS BETWEEN WHAT
C                              THE VARIABLE IS CALLED IN THE ORIGINAL
C                              SECTION OF THIS PROGRAM
C                              AND ITS NAME IN THE 1988 F15 AEROBASE.
C                              FOR THE SAKE OF CONTINUITY THE
C                              ORIGINAL PROGRAM NAME IS USED AND
C                              THE 1988 F15 AEROBASE NAME
C                              IS PROVIDED AS BOOK KEEPING
C                              INFORMATION.
C
C
C*******************************************************************
C
C
C
C  CFX = FORCE IN STABILITY AXIS X DIRECTION (CD IN BODY AXIS)
C        (FUNCTION OF CL OR CFZ1)
C  CFX = CFX1 + CXRB + STORE INCREMENTS + CXDSPD + DCXLG + DCD
```

86

```
C
C    CFX1 = ATAB15 = PERFORMANCE DRAG COEFFICIENT - CD
C    CXRB = ATAB22 = DELTA CD DUE TO CG (=0.0)
C    CXDSPD = ATAB27 = DELTA CD DUE TO SPEEDBRAKE (NORMALLY = 0.0436)
C                       SET TO 0 SINCE THIS STUDY IS CONCERNED
C                       WITH HIGH ANGLES
C                       OF ATTACK PHENOMENON (>40 DEGREES) AND BECAUSE
C                       THE SPEEDBRAKE WILL NOT DEPLOY AT ANGLES OF
C                       ATTACK GREATER THAN 15 DEGREES.
C    DCXLG = ATAB19 = DELTA CD DUE TO REYNOLD'S NUMBER  (=-0.0005)
C    DCD = BTAB03 = DELTA CD DUE TO 2-PLACE CANOPY (F15B) (=0.0005)
C          ****** NOTE THAT DCXLG AND DCD CANCEL EACH OTHER ******
C
C
C***********************************************************************
C
C
C
C    CFY = FORCE IN BODY AXIS Y DIRECTION
C    CFY = CFY1*EPA02 + CYDAD*DAILD + [CYDRD*DRUDD*DRFLX5]*EPA43
C          +[CYDTD*DTFLX5 + DTFLX6]*DTALD + CFYP*PB + CFYR*RB
C          +CYRB + STORE INCREMENTS + DCYB*BETA
C
C    CFY1 = ATAB16 = BASIC SIDE FORCE COEFFICIENT - CY(BETA)
C    EPA02 = ATAB21 = BETA MULTIPLIER TABLE
C    CYDAD = ATAB75 = SIDE FORCE COEFFICIENT DUE TO AILERON DEFLECTION
C    DAILD          = AILERON DEFLECTION (DEG)
C    CYDRD = ATAB69 = SIDE FORCE COEFFICIENT DUE TO RUDDER DEFLECTION
C    DRUDD          = RUDDER DEFLECTION   (DEG)
C    DRFLX5 = ATAB88 = FLEX MULTIPLIER ON CYDRD (=0.89)
C    EPA43 = ATAB30 = MULTIPLIER ON CNDR, CLDR, CYDR DUE TO SPEEDBRAKE
C                    (=1.0)
C    CYDTD = ATAB72 = SIDE FORCE COEFFICIENT DUE TO DIFFERENTIAL TAIL
C                    DEFLECTION - CYDDT
C    DTFLX5 = ATAB10 = FLEX MULTIPLIER ON CYDTD (=0.975)
C    DTFLX6 = ATAB77 = FLEX INCREMENT TO CYDTD (=0.0)
C    DTALD          = DIFFERENTIAL TAIL DEFLECTION (DEG) WHICH IS
C                    DIRECTLY PROPORTIONAL TO AILERON DEFLECTION AND
C                    IS PRIMARILY USED TO ASSIST IN ROLLING THE
C                    F-15B (DTALD=0.3*DAILD)
C    CFYP = ATAB13 = SIDE FORCE COEFFICIENT DUE TO ROLL RATE (CYP)
C    PB            = (PEOBB*SPAN)/(2*VILWF)
C                    PEOBB = ROLL RATE IN RAD/SEC = P
C                    SPAN = WING SPAN = 42.8 FEET = BWING
C                    VILWF = VELOCITY IN FT/SEC = VTRFPS
C    CFYR = ATAB07 = SIDE FORCE COEFFICIENT DUE TO YAW RATE (CYR)
C    RB            = (REOBB*SPAN)/(2*VILWF)
C                    REOBB = YAW RATE IN RAD/SEC = R
C    CYRB = ATAB93 = ASSYMETRIC CY AT HIGH ALPHA (ANGLE OF ATTACK)
C    DCYB          = 0.0  THERE IS NO INCREMENT DELTA CYB (SIDE FORCE)
C                    DUE TO A 2-PLACE CANOPY ON THE F15B.  THIS IS
C                    BECAUSE THE SAME CANOPY IS USED ON BOTH THE
```

87

```
C                       BASELINE F15A AND THE F15B.  THE SIDEFORCE IS THE
C                       SAME FOR BOTH VERSIONS OF THE F15 AND ALREADY
C                       INCLUDED IN THE BASIC SIDE FORCE (CFY1).  THE TWO
C                       PLACE CANOPY IS MOUNTED DIFFERENTLY HOWEVER, SO
C                       THERE IS A DIFFERENCE IN YAWING AND ROLLING MOMENT.
C                       (SEE DCNB AND DCLB)
C
C
C***********************************************************************
C
C
C
C   CFZ = FORCE IN STABILITY AXIS Z DIRECTION (CL IN BODY AXIS)
C   CFZ = CFZ1 + CZDSPD + STORE INCREMENTS + DCL*BETA
C
C
C   CFZ1 = ATAB17 = BASIC LIFT COEFFICIENT - CL
C   CZDSPD = ATAB26 = DELTA CL DUE TO SPEEDBRAKE
C                       SET TO 0 DUE TO THE REASONS GIVEN ABOVE IN CXDSPD
C   DCL = BTAB01 = DELTA CL DUE TO 2-PLACE CANOPY (F15B) (=0.0)
C
C
C***********************************************************************
C
C
C                     '
C   CML = TOTAL ROLLING MOMENT COEFFICIENT IN BODY AXIS
C   CML = CML1*EPA02 + CLDAD*DAILD + [CLDRD*DRUDD*DRFLX1]*EPA43 +
C         [CLDTD*DTFLX1 + DTFLX2]*DTALD + CMLP*PB + CMLR*RB +
C         STORE INCREMENTS + CLDSPD + DCLB*BETA
C
C
C   CML1 = ATAB01 = BASIC ROLLING MOMENT COEFFICIENT - CL(BETA)
C   EPA02 = ATAB21 = BETA MULTIPLIER TABLE
C   CLDAD = ATAB73 = ROLL MOMENT COEFFICIENT DUE TO AILERON DEFLECTION
C                       -(CLDA)
C   DAILD            = AILERON DEFLECTION (DEG)
C   CLDRD = ATAB67 = ROLLING MOMENT COEFFICIENT DUE TO RUDDER
C                       DEFLECTION  -(CLD)
C   DRUDD            = RUDDER DEFLECTION (DEG)
C   DRFLX1 = ATAB80 = FLEX MULTIPLIER ON CLDRD (=0.85)
C   EPA43 = ATAB30 = MULTIPLIER ON CNDR, CLDR, CYDR DUE TO SPEEDBRAKE
C                       (=1.0)
C   CLDTD = ATAB70 = ROLL MOMENT COEFFICIENT DUE TO DIFFERENTIAL TAIL
C                       DEFLECTION - CLDD
C   DTFLX1 = ATAB04 = FLEX MULTIPLIER ON CLDTD (=0.975)
C   DTFLX2 = ATAB84 = FLEX INCREMENT TO CLDTD (=0.0)
C   DTALD            = DIFFERENTIAL TAIL DEFLECTION (DEG) WHICH IS
C                       DIRECTLY PROPORTIONAL TO AILERON DEFLECTION AND
C                       IS PRIMARILY USED TO ASSIST IN ROLLING THE F-15B
C                       (DTALD = 0.3*DAILD)
C   CMLP = ATAB02 = ROLL DAMPING DERIVATIVE -CLP
```

```
C  PB              = (PEOBB*SPAN)/(2*VILWF)
C                     PEOBB = ROLL RATE IN RAD/SEC = P
C                     SPAN = WING SPAN = 42.8 FEET = BWING
C                     VILWF = VELOCITY IN FT/SEC = VTRFPS
C  CMLR = ATAB11 = ROLLING MOMENT COEFFICIENT DUE TO YAW RATE - CLR
C  RB              = (REOBB*SPAN)/(2*VILWF)
C                     REOBB = YAW RATE IN RAD/SEC = R
C  CLDSPD = ATAB29 = DELTA CL DUE TO SPEEDBRAKE
C                     SET TO 0 DUE TO THE REASONS GIVEN ABOVE IN CXDSPD
C  DCLB = BTAB04 = INCREMENT DELTA CLB (ROLLING MOMENT) DUE TO 2-PLACE
C                     CANOPY FROM PSWT 499
C
C
C*******************************************************************
C
C
C
C  CMM = TOTAL PITCHING MOMENT COEFFICIENT IN STABILITY AXIS
C          (BODY AXIS - AS WELL)
C  CMM = CMM1 + CMMQ*QB + STORE INCREMENTS + CMDSPD + DCM
C
C  CMM1 = ATAB03 = BASIC PITCHING MOMENT COEFFICIENT - CM
C  CMMQ = ATAB05 = PITCH DAMPING DERIVATIVE - CMQ
C  QB              = (QEOBB*MAC)/(2*VILWF)
C                     QEOBB = PITCH RATE IN RAD/SEC = Q
C                     MAC = MEAN AERODYNAMIC CHORD = 15.94 FEET = CWING
C                     VILWF = VELOCITY IN FT/SEC = VTRFPS
C  CMDSPD = ATAB25 = DELTA CM DUE TO SPEEDBRAKE
C                     SET TO 0 DUE THE REASONS GIVEN ABOVE IN CXDSPD
C  DCM = BTAB02 = DELTA CM DUE TO 2-PLACE CANOPY (F15B) (=0.0)
C
C
C*******************************************************************
C
C
C
C  CMN = TOTAL YAWING MOMENT COEFFICIENT IN BODY AXIS
C  CMN = CMN1*EPA02 + CNDAD*DAILD + [CNDRD*DRUDD*DRFLX3]*EPA43
C        +[CNDTD*DTLX3 + DTFLX4]*DTALD + CMNP*PB + CMNR*RB + CNRB
C        +DCNB2*EPA36 + STORE INCREMENTS + CNDSPD + DCNB*BETA
C
C
C  CMN1 = ATAB12 = BASIC YAWING MOMENT COEFFICIENT  - CN (BETA)
C  EPA02 = ATAB21 = BETA MULTIPLIER TABLE
C  CNDAD = ATAB74 = YAW MOMENT COEFFICIENT DUE TO AILERON
C                     DEFLECTION -CNDA
C  DAILD =        = AILERON DEFLECTION (DEG)
C  CNDRD = ATAB68 = YAWING MOMENT COEFFICIENT DUE TO RUDDER
C                     DEFLECTION -CNDR
C  DRUDD          = RUDDER DEFLECTION (DEG)
C  DRFLX3 = ATAB85 = FLEX MULTIPLIER ON CNDRD
C  EPA43 = ATAB30 =  MULTIPLIER ON CNDR, CLDR, CYDR DUE TO SPEEDBRAKE
```

89

```
C  CNDTD = ATAB71 = YAWING MOMENT COEFFICIENT DUE TO DIFFERENTIAL TAIL
C                   DEFLECTION - CNDDT
C  DTFLX3 = ATAB08 = FLEX MULTIPLIER ON CNDTD
C  DTFLX4 = ATAB09 = FLEX INCREMENT ON CNDTD  (=0.0)
C  DTALD =         = DIFFERENTIAL TAIL DEFLECTION (DEG) WHICH IS
C                   DIRECTLY PROPORTIONAL TO AILERON DEFLECTION
C                   AND IS PRIMARILY USED TO ASSIST IN ROLLING
C                   THE F-15B (DTALD = 0.3*DAILD)
C  CMNP = ATAB06 = YAWING MOMENT COEFFICIENT DUE TO ROLL RATE - CNP
C  PB           = (PEOBB*SPAN)/(2*VILWF)
C                 PEOBB=ROLL RATE IN RAD/SEC = P
C                 SPAN = WING SPAN = 42.8 FT = BWING
C                 VILWF = VELOCITY IN FT/SEC = VTRFPS
C  CMNR = ATAB14 = YAW DAMPING DERIVATIVE - CNR
C  RB           = (REOBB*SPAN)/(2*VILWF)
C                 REOBB = YAW RATE IN RAD/SEC = R
C  CNRB = ATAB86 = ASSYMETRIC CN AT HIGH ALPHA
C  DCNB2 = ATAB44 = DELTA CNB WITH STABILATOR EFFECT - DELCNB (=0.0)
C  EPA36 = ATAB94 = MULTIPLIER ON DCNB2  (=BETA)
C  CNDSPD = ATAB28 = DELTA CN DUE TO SPEEDBRAKE
C                   SET TO 0 DUE TO THE REASONS GIVEN ABOVE IN CXDSPD
C  DCNB = BTAB05 = INCREMENT DELTA CNB (YAWING MOMENT) DUE TO
C                   2-PLACE CANOPY (F15B)
C
C
C***************************************************************************
C
C
C
C  MISCELLANEOUS COEFFICIENTS AND NAME CONVERSION TABLE
C
C
C      1988 F15              ORIGINAL
C      AEROBASE NAME         PROGRAM NAME        DEFINITION
C      *************         ************        **********
C
C      AL77D                 AL                  ANGLE OF ATTACK
C                                                (DEG)
C      BE77D                 BETA                SIDESLIP ANGLE
C                                                (DEG)
C      BE77D                 RBETA               SIDESLIP ANGLE
C                                                (RAD)
C      BO77D                 ABET                ABSOLUTE VALUE OF
C                                                SIDESLIP ANGLE
C                                                (DEG)
C      DAILA                 DAILA               ABSOLUTE VALUE OF
C                                                AILERON DEFLEC-
C                                                TION (DEG)
C      DAILD                 DDA                 AILERON DEFLEC-
C                                                TION (DEG)
C      DRUABS                ARUD                ABSOLUTE VALUE OF
C                                                RUDDER DEFLEC-
```

90

```
C                                                       TION (DEG)
C       DRUABS                      RARUD               ABSOLUTE VALUE OF
C                                                       RUDDER DEFLEC-
C                                                       TION (RAD)
C       DRUDD                       DRUDD               RUDDER DEFLECTION
C                                                       (DEG)
C       DSTBD                       DELESD(R)           AVERAGE
C                                                       STABILATOR
C                                                       DEFLECTION
C                                                       DEG (RAD)
C       DTALD                       DELEDD(R)           DIFFERENTIAL TAIL
C                                                       DEFLECTION
C                                                       DEG (RAD)
C
        RBETA=BETA/DEGRAD
        DAILA=ABS(DDA)
C
C
C
C
        PB=(P*BWING)/(2*VTRFPS)
        QB=(Q*CWING)/(2*VTRFPS)
        RB=(R*BWING)/(2*VTRFPS)
C
C       THE F-15B AERO DATA TABLES DO NOT CONTAIN STABILITY COEFFICIENT
C       DATA FOR BETA AND RUDDER DEFLECTION ,DRUDD, LESS THAN 0
C       DEGREES.  THE ABSOLUTE VALUE OF BETA, ABET, AND THE ABSOLUTE
C       VALUE OF RUDDER DEFLECTION, ARUDD, ARE USED IN THE FOLLOWING
C       EQUATIONS.  IN RADIANS THESE PARAMETERS ARE RABET AND RARUD,
C       RESPECTIVELY.  IN SOME CASES THE COEFFICIENT IS MULTIPLIED BY A
C       -1 FOR PARAMETER VALUES LESS THAN ZERO.
C
C       EPA02 IS A MULTIPLIER THAT ADJUSTS THE PARTICULAR COEFFICIENT
C       IT IS WORKING ON (CFY1,CML1,CMN1) BY CHANGING THAT PARTICULAR
C       COEFFICIENTS SIGN (POSITIVE OR NEGATIVE) DEPENDENT ON THE SIGN
C       OF THE SIDESLIP ANGLE (BETA).  IF BETA IS NEGATIVE THEN
C       EPA02=-1.0.  IF BETA IS POSITIVE THEN EPA02=1.0.  SINCE THIS
C       FUNCTION IS DISCONTINUOUS AT THE ORIGIN A CUBIC SPLINE HAS
C       BEEN EMPLOYED TO REPRESENT THIS FUNCTION IN ORDER THAT
C       AUTO CAN RUN.
C
C
        IF (BETA .LT. -1.0) THEN
        EPA02S= -1.00
        ENDIF
C
        IF ((BETA .GE. -1.0) .AND. (BETA .LE. 1.0)) THEN
        EPA02S=-1.00+(1.5*((BETA+1.0)**2))-(0.5*((BETA+1.0)**3))
        ENDIF
C
        IF (BETA .GT. 1.0) THEN
```

91

```fortran
      EPA02S=1.00
      ENDIF
C
      IF (BETA .LT. -5.0) THEN
      EPA02L= -1.00
      ENDIF
C
      IF ((BETA .GE. -5.0) .AND. (BETA .LE. 5.0)) THEN
      EPA02L=-1.00+(0.06*((BETA+5.0)**2))-(0.004*((BETA+5.0)**3))
      ENDIF
C
      IF (BETA .GT. 5.0) THEN
      EPA02L=1.00
      ENDIF
C
C
C      DTALD=0.3*DAILD
      DELEDD=0.3*DDA
      DELEDR=0.3*(DDA/DEGRAD)
C
C
C
C*******************************************************************
C
C
C
C
      CFZ1=-0.00369376+(3.78028702*RAL)+(0.6921459*RAL*RAL)-(5.0005867
     +*(RAL**3))+(1.94478199*(RAL**4))+(0.40781955*DELESR)+(0.10114579
     +*(DELESR*DELESR))
C
      CFZ=CFZ1
C
C
C*******************************************************************
C
C
C
C
C
      CL=CFZ1/57.29578
C
C      THIS CONVERSION OF CFZ1 TO CL IS AN ARTIFACT FROM THE
C      CURVE FITTING PROCESS WHERE ALL THE INDEPENDENT VARIABLES
C      WERE ANGLES THAT WERE CONVERTED FROM DEGREES TO RADIANS.
C      IT JUST SO HAPPENED THAT FOR CFX1 ONE OF THE VARIABLES
C      WAS NOT AN ANGLE BUT A DIMENSIONLESS COEFFICIENT.
C
C
      CFX1=0.01806821+(0.01556573*CL)+(498.96208868*CL*CL)
     +-(14451.56518396*(CL**3))+(2132344.6184755*(CL**4))
C
```

92

```fortran
C        TRANSITIONING FROM LOW AOA DRAG TABLE TO HIGH AOA DRAG TABLE
C
      CFX2=0.0267297-(0.10646919*RAL)+(5.39836337*RAL*RAL)
     +-(5.0086893*(RAL**3))+(1.34148193*(RAL**4))+
     +(0.20978902*DELESR)+(0.30604211*(DELESR**2))+0.09833617
C
      A1=20.0/DEGRAD
      A2=30.0/DEGRAD
      A12=A1+A2
      BA=2.0/(-A1**3+3.*A1*A2*(A1-A2)+A2**3)
      BB=-3.*BA*(A1+A2)/2.
      BC=3.*BA*A1*A2
      BD=BA*A2**2*(A2-3.*A1)/2.
      F1=BA*RAL**3+BB*RAL**2+BC*RAL+BD
      F2=-BA*RAL**3+(3.*A12*BA+BB)*RAL**2-
     +    (BC+2.*A12*BB+3.*A12**2*BA)*RAL+
     +    BD+A12*BC+A12**2*BB+A12**3*BA
C
      IF (RAL .LT. A1) THEN
C
         CFX=CFX1
C
      ELSEIF (RAL .GT. A2) THEN
C
         CFX=CFX2
C
      ELSE
C
         CFX=CFX1*F1+CFX2*F2
C
      ENDIF
C
C
C*******************************************************************
C
C
      DTFLX5=0.975
      DRFLX5=0.89
C
      CFY1=-0.05060386-(0.12342073*RAL)+(1.04501136*RAL*RAL)
     +-(0.17239516*(RAL**3))-(2.90979277*(RAL**4))
     ++(3.06782935*(RAL**5))-(0.88422116*(RAL**6))
     +-(0.06578812*RAL*RABET)-(0.71521988*RABET)-(0.00000475273
     +*(RABET**2))-(0.04856168*RAL*DELESR)-(0.05943607*RABET*DELESR)+
     +(0.02018534*DELESR)
C
      IF (RAL .LT. .52359998) THEN
C
      CFYP=0.014606188+(2.52405055*RAL)-(5.02687473*(RAL**2))
     +-(106.43222962*(RAL**3))+(256.80215423*(RAL**4))
     ++(1256.39636248*(RAL**5))
     +-(3887.92878173*(RAL**6))-(2863.16083460*(RAL**7))+
```

93

```fortran
     +(17382.72226362*(RAL**8))-(13731.65408408*(RAL**9))
      ENDIF
C
      IF ((RAL .GE. .52359998) .AND. (RAL .LE. .610865)) THEN
C
      CFYP=0.00236511+(0.52044678*(RAL-0.52359998))-(12.8597002*(RAL-
     +0.52359998)**2)+(75.46138*(RAL-0.52359998)**3)
      ENDIF
C
      IF (RAL .GT. 0.610865) THEN
C
      CFYP=0.0
      ENDIF
C
      IF (RAL .LT. -0.06981) THEN
C
      CFYR=0.35
      ENDIF
C
      IF ((RAL .GE. -0.06981) .AND. (RAL .LT. 0.0)) THEN
C
      CFYR=0.34999999+(35.4012413*(RAL+0.06981)**2)-(493.33441162*
     +(RAL+0.06981)**3)
      ENDIF
C
      IF ((RAL .GE. 0.0) .AND. (RAL .LE. 0.523599)) THEN
C
      CFYR=0.35468605-(2.26998141*RAL)+(51.82178387*RAL*RAL)
     +-(718.55069823*(RAL**3))
     ++(4570.00492172*(RAL**4))-(14471.88028351*(RAL**5))+
     +(22026.58930662*(RAL**6))-(12795.99029404*(RAL**7))
      ENDIF
C
      IF ((RAL .GT. 0.523599) .AND. (RAL .LE. 0.61087)) THEN
C
      CFYR=0.00193787+(1.78332496*(RAL-0.52359903))-(41.63198853*(RAL-
     +0.52359903)**2)+(239.97909546*(RAL-0.52359903)**3)
      ENDIF
C
      IF (RAL .GT. 0.61087) THEN
C
      CFYR=0.0
      ENDIF
C
      IF (RAL .LT. 0.55851) THEN
C
      CYDAD=-0.00020812+(0.00062122*RAL)+(0.00260729*RAL*RAL)
     ++(0.00745739*(RAL**3))-(0.0365611*(RAL**4))
     +-(0.04532683*(RAL**5))+(0.20674845*(RAL**6))
     +-(0.13264434*(RAL**7))-(0.00193383*(RAL**8))
```

94

```
C     ENDIF
C
      IF ((RAL .GE. 0.55851) .AND. (RAL .LT. 0.61087)) THEN
C
      CYDAD=0.00023894+(0.00195121*(RAL-0.55851001))+(0.02459273
     +*(RAL-0.55851001)**2)-(0.1202244*((RAL-0.55851001)**3))
      ENDIF
C
      IF (RAL .GE. 0.61087) THEN
C
      CYDAD=0.27681285-(2.02305395*RAL)+(6.01180715*RAL*RAL)
     +-(9.24292188*(RAL**3))+(7.59857819*(RAL**4))
     +-(2.8565527*(RAL**5))+(0.25460503*(RAL**7))
     +-(0.01819815*(RAL**9))
      ENDIF
C
C
C     IF (RAL .LE. 0.0) THEN
C     EPA43=1.0
C     ENDIF
C     IF (RAL .GT. 0.0 AND .LE. 0.6283185) THEN
C     0.6283185 RADIANS = 36 DEGREES
C     EPA43=0.9584809+(4.13369452*RAL)-(18.31288396*RAL*RAL)+
C     +(19.5511466*(RAL**3))-(1.09295946*RAL*DSPBD)+(0.17441033*
C     +DSPBD*DSPBD)
C     ENDIF
C     IF (RAL .GT. 0.6283185) THEN
C     EPA43=1.0
C     ENDIF
C     **********************************************************
C     *   NOTE - THE PARAMETER EPA43 IS A MULTIPLIER ON RUDDER *
C     *   EFFECTIVENESS DUE TO SPEEDBRAKE.  THIS TABLE IS ALSO  *
C     *   LIMITED TO 36 DEG AOA.  HOWEVER, THERE IS NO AERODY   *
C     *   NAMIC EFFECT FOR ANGLES OF ATTACK LESS THAN 16 DEG,   *
C     *   AND THE SPEEDBRAKE IS AUTOMATICALLY RETRACTED AT AOA  *
C     *   GREATER THAN 15 DEG.  THEREFORE, THIS TABLE SHOULD    *
C     *   NOT BE NECESSARY FOR THE ORDINARY OPERATION OF THE    *
C     *   AIRCRAFT                                              *
C     **********************************************************
C
      CYDRD=0.00310199+(0.00119963*RAL)+(0.02806933*RAL*RAL)
     +-(0.12408447*(RAL**3))-(0.12032121*(RAL**4))
     ++(0.79150279*(RAL**5))-(0.86544347*(RAL**6))
     ++(0.27845115*(RAL**7))+(0.00122999*RAL*RARUD)+(0.00145943
     +*RARUD)-(0.01211427*RARUD*RARUD)+(0.00977937*(RARUD**3))
C
      CYDTD=-0.00157745-(0.0020881*RAL)+(0.00557239*RAL*RAL)
     +-(0.00139886*(RAL**3))+(0.04956247*(RAL**4))
     +-(0.0135353*(RAL**5))-(0.11552397*(RAL**6))
     ++(0.11443452*(RAL**7))-(0.03072189*(RAL**8))-(0.01061113*
     +(RAL**3)*DELESR)-(0.00010529*RAL*RAL*DELESR*DELESR)
     +-(0.00572463*RAL*DELESR*DELESR)
```

95

```
          ++(0.01885361*RAL*RAL*DELESR)-(0.01412258*RAL*(DELESR**3))
          +-(0.00081776*DELESR)+(0.00404354*(DELESR**2))-
          +(0.00212189*(DELESR**3))+(0.00655063*(DELESR**4))
          ++(0.03341584*(DELESR**5))
    C
          RALY1=0.6108652
          RALY2=90.0/DEGRAD
          RBETY1=-0.0872665
          RBETY2=0.1745329
    C
          AY=0.164
          ASTARY=0.95993
          BSTARY=0.087266
    C
          ZETAY=(2.0D0*ASTARY-(RALY1+RALY2))/(RALY2-RALY1)
          ETAY=(2.0D0*BSTARY-(RBETY1+RBETY2))/(RBETY2-RBETY1)
    C
          X=(2.0D0*RAL-(RALY1+RALY2))/(RALY2-RALY1)
          Y=(2.0D0*RBETA-(RBETY1+RBETY2))/(RBETY2-RBETY1)
    C
          FY=((5.0D0*(ZETAY**2))-(4.0D0*ZETAY*X)-1.0D0)*( (X**2)-1.0D0)
          +**2)*(1.0D0/(((ZETAY**2)-1.0D0)**3))
    C
          GY=((5.0D0*(ETAY**2))-(4.0D0*ETAY*Y)-1.0D0)*(((Y**2)-1.0D0)**2)
          +*(1.0D0/(((ETAY**2)-1.0D0)**3))
    C
          CYRB=AY*FY*GY
    C
          IF (RAL .LT. 0.6108652) THEN
    C
          CYRB=0.0
          GOTO 500
          ENDIF
    C
          IF ((RBETA .LT. -0.0872665) .OR. (RBETA .GT. 0.1745329)) THEN
    C
          CYRB=0.0
          GOTO 500
          ENDIF
    C
    500   CFY=(CFY1*EPA02L)+(CYDAD*DDA)+(CYDRD*DRUDD*DRFLX5*EPA43)+
          +((CYDTD*DTFLX5)*DELEDD)+(CFYP*PB)+(CFYR*RB)
          ++CYRB
    C
    C
    C*************************************************************************
    C
    C
    C
          DTFLX1=0.975
          DRFLX1=0.85
    C
```

96

```
      CML1=-0.00238235-(0.04616235*RAL)+(0.10553168*RAL*RAL)
     ++(0.10541585*(RAL**3))-(0.40254765*(RAL**4))
     ++(0.32530491*(RAL**5))-(0.08496121*(RAL**6))
     ++(0.00112288*(RAL**7))-(0.05940477*RABET*RAL)-
     +(0.07356236*RABET)-(0.00550119*RABET*RABET)+(0.00326191
     +*(RABET**3))
C
      IF (RAL .LT. 0.29671) THEN
C
      CMLP=-0.24963201-(0.03106297*RAL)+(0.12430631*RAL*RAL)
     +-(8.95274618*(RAL**3))+(100.33109929*(RAL**4))
     ++(275.70069578*(RAL**5))-(1178.83425699*(RAL**6))
     +-(2102.66811522*(RAL**7))+(2274.89785551*(RAL**8))
      ENDIF
C
      IF ((RAL .GE. 0.29671) .AND. (RAL .LT. 0.34907)) THEN
C
      CMLP=-0.1635261-(3.77847099*(RAL-0.29671001))+(147.47639465
     +*(RAL-0.29671001)**2)-(1295.94799805*(RAL-0.29671001)**3)
      ENDIF
C
      IF (RAL .GE. 0.34907) THEN
C
      CMLP=-1.37120291+(7.06112181*RAL)-(13.57010422*RAL*RAL)
     ++(11.21323850*(RAL**3))
     +-(4.26789425*(RAL**4))+(0.6237381*(RAL**5))
      ENDIF
C
      IF (RAL .LT. 0.7854) THEN
C
      CMLR=0.03515391+(0.59296381*RAL)+(2.27456302*RAL*RAL)
     +-(3.8097803*(RAL**3))
     +-(45.83162842*(RAL**4))+(55.31669213*(RAL**5))+
     +(194.29237485*(RAL**6))-(393.22969953*(RAL**7))+(192.20860739*
     +(RAL**8))
      ENDIF
C
      IF ((RAL .GE. 0.7854) .AND. (RAL .LE. 0.87266)) THEN
C
      CMLR=0.0925579071-(0.6000000238*(RAL-0.7853999734))
     ++(1.3515939713*((RAL-0.7853999734)**2))
     ++(29.0733299255*((RAL-0.7853999734)**3))
      ENDIF
C
      IF (RAL .GT. 0.87266) THEN
C
      CMLR=-311.126041+(1457.23391042*RAL)-(2680.19461944*RAL*RAL)+
     +(2361.44914738*(RAL**3))-(893.83567263*(RAL**4))+(68.23501924*
     +(RAL**6))-(1.72572994*(RAL**9))
      ENDIF
C
      CLDAD=0.00057626+(0.00038479*RAL)-(0.00502091*RAL*RAL)
```

97

```fortran
      ++(0.00161407*(RAL**3))+(0.02268829*(RAL**4))
      +-(0.03935269*(RAL**5))+(0.02472827*(RAL**6))
      +-(0.00543345*(RAL**7))+(0.0000007520348*DELESR*RAL)+
      +(0.000000390773*DELESR)
C

      CLDRD=0.00013713-(0.00035439*RAL)-(0.00227912*RAL*RAL)
      ++(0.00742636*(RAL**3))+(0.00991839*(RAL**4))
      +-(0.04711846*(RAL**5))+(0.046124*(RAL**6))
      +-(0.01379021*(RAL**7))+(0.00003678685*RARUD*RAL)+
      +(0.00001043751*RARUD)-(0.00015866*RARUD*RARUD)+(0.00016133
      +*(RARUD**3))
C

      CLDTD=0.00066663+(0.00074174*RAL)+(0.00285735*RAL*RAL)
      +-(0.02030692*(RAL**3))-(0.00352997*(RAL**4))
      ++(0.0997962*(RAL**5))-(0.14591227*
      +(RAL**6))+(0.08282004*(RAL**7))
      +-(0.0168667*(RAL**8))+(0.00306142*(RAL**3)*DELESR)
      +-(0.00110266*RAL*RAL*(DELESR**2))+(0.00088031*RAL*
      +(DELESR**2))-(0.00432594*RAL*RAL*DELESR)-
      +(0.00720141*RAL*(DELESR**3))
      +-(0.00034325*DELESR)+(0.00033433*(DELESR**2))+(0.00800183
      +*(DELESR**3))-(0.00555986*(DELESR**4))-(0.01841172*(DELESR**5))
C
      IF (RAL .LT. 0.0) THEN
C
      DCLB=-0.00006
      ENDIF
C
      IF ((RAL .GE. 0.0) .AND. (RAL .LE. 0.209434)) THEN
C
      DCLB=-0.00006+(0.0041035078*RAL*RAL)-(0.0130618699*(RAL**3))
      ENDIF
C
      IF (RAL .GT. 0.209434) THEN
C
      DCLB=0.0
      ENDIF
C
C
      CML=(CML1*EPA02S)+(CLDAD*DDA)+(CLDRD*DRUDD*DRFLX1*EPA43)+
      +((CLDTD*DTFLX1)*DELEDD)+(CMLP*PB)+(CMLR*RB)+(DCLB*BETA)
C
C
C*********************************************************************
C
C
C
      CMM1=0.00501496-(0.08004901*RAL)-(1.03486675*RAL*RAL)
      +-(0.68580677*(RAL**3))+(6.46858488*(RAL**4))
      +-(10.15574108*(RAL**5))+
      +(6.44350808*(RAL**6))-(1.46175188*(RAL**7))
      ++(0.24050902*RAL*DELESR)
```

98

```
      +-(0.42629958*DELESR)-(0.03337449*DELESR*DELESR)
      +-(0.53951733*(DELESR**3))
C
       IF (RAL .LE. 0.25307) THEN
C
       CMMQ=-3.8386262+(13.54661297*RAL)+(402.53011559*RAL*RAL)
      +-(6660.95327122*(RAL**3))-(62257.89908743*(RAL**4))
      ++(261526.10242329*(RAL**5))
      ++(2177190.33155227*(RAL**6))-(703575.13709062*(RAL**7))-
      +(20725000.34643054*(RAL**8))-(27829700.53333649*(RAL**9))
       ENDIF
C
       IF ((RAL .GT. 0.25307) .AND. (RAL .LT. 0.29671)) THEN
C
       CMMQ=-8.4926528931-(2705.3000488281*(RAL-0.2530699968))
      ++(123801.5*(RAL-0.2530699968)**2)
      +-(1414377*(RAL-0.2530699968)**3)
       ENDIF
C
       IF (RAL .GE. .29671) THEN
C
       CMMQ=47.24676075-(709.60757056*RAL)+(3359.08807193*RAL*RAL)-
      +(7565.32017266*(RAL**3))+(8695.1858091*(RAL**4))
      +-(4891.77183313*(RAL**5))+(1061.55915089*(RAL**6))
       ENDIF
C
       CMM=CMM1+(CMMQ*QB)
C
C
C****************************************************************
C
C
C
       DTFLX3=0.975
       DRFLX3=0.89
C
C
       CMN1=0.01441512+(0.02242944*RAL)-(0.30472558*(RAL**2))
      ++(0.14475549*(RAL**3))
      ++(0.93140112*(RAL**4))-(1.52168677*(RAL**5))+
      +(0.90743413*(RAL**6))-(0.16510989*(RAL**7))
      +-(0.0461968*(RAL**8))
      ++(0.01754292*(RAL**9))-(0.17553807*RAL*RABET)+
      +(0.15415649*RAL*RABET*DELESR)
      ++(0.14829547*(RAL**2)*(RABET**2))
      +-(0.11605031*(RAL**2)*RABET*DELESR)
      +-(0.06290678*(RAL**2)*(DELESR**2))
      +-(0.01404857*(RAL**2)*(DELESR**2))
      ++(0.07225609*RABET)-(0.08567087*(RABET**2))
      ++(0.01184674*(RABET**3))
      +-(0.00519152*RAL*DELESR)+(0.03865177*RABET*DELESR)
      ++(0.00062918*DELESR)
```

99

```fortran
C
      CNDRD=-0.00153402+(0.00184982*RAL)-(0.0068693*RAL*RAL)
     ++(0.01772037*(RAL**3))
     ++(0.03263787*(RAL**4))-(0.15157163*(RAL**5))+(0.18562888
     +*(RAL**6))-(0.0966163*(RAL**7))+(0.01859168*(RAL**8))+(0.0002587
     +*RAL*DELESR)-(0.00018546*RAL*DELESR*RBETA)-(0.00000517304*RBETA)
     +-(0.00102718*RAL*RBETA)-(0.0000689379*RBETA*DELESR)-(0.00040536
     +*RBETA*RARUD)-(0.00000480484*DELESR*RARUD)
     +-(0.00041786*RAL*RARUD)
     ++(0.0000461872*RBETA)+(0.00434094*(RBETA**2))
     +-(0.00490777*(RBETA**3))
     ++(0.000005157867*RARUD)+(0.00225169*RARUD*RARUD)-(0.00208072
     +*(RARUD**3))
C
      IF (RAL .LT. 0.55851) THEN
C
      CMNP=-0.00635409-(1.14153932*RAL)+(2.82119027*(RAL**2))+
     +(54.4739579*(RAL**3))-(140.89527667*(RAL**4))-(676.73746128*
     +(RAL**5))+(2059.18263976*(RAL**6))+(1579.41664748*(RAL**7))
     +-(8933.08535712*(RAL**8))+(6806.54761267*(RAL**9))
      ENDIF
C
      IF ((RAL .GE. 0.55851001) .AND. (RAL .LE. 0.61087)) THEN
C
      CMNP=-.07023239+(1.085815*(RAL -0.55851))
     ++(8.852651*((RAL-.55851)**2))-(192.6093*((RAL-0.55851)**3))
      ENDIF
C
      IF (RAL .GT. 0.61087) THEN
C
      CMNP=-71.03693533+(491.32506715*RAL)
     +-(1388.11177979*(RAL**2))+
     +(2033.48621905*(RAL**3))
     +-(1590.91322362*(RAL**4))+(567.38432316*(RAL**5))
     +-(44.97702536*(RAL**7))+(2.8140669*(RAL**9))
      ENDIF
C
C
C
      IF (RAL .LE. -.069813) THEN
C
      CMNR= -0.2805
      ENDIF
C
      IF ((RAL .GT. -.069813) .AND. (RAL .LT. 0.0)) THEN
C
      CMNR=-0.2804999948+(35.9903717041*(RAL+.0698129982)**2)
     +-(516.1574707031*(RAL+.0698129982)**3)
      ENDIF
C
      IF ((RAL .GE. 0.0) .AND. (RAL .LE. 0.78539801)) THEN
C
```

```fortran
      CMNR=-.28071511-(2.52183924*RAL)+(68.90860031*(RAL**2))
     +-(573.23100511*(RAL**3))+(2009.08725005*(RAL**4))
     +-(3385.15675307*(RAL**5))
     ++(2730.49473149*(RAL**6))-(848.12322034*(RAL**7))
      ENDIF
C
      IF ((RAL .GT. 0.78539801) .AND. (RAL .LT. 0.95993102)) THEN
C
      CMNR=-0.1096954+(0.52893072*(RAL-0.78539801))-(6.09109497*(RAL-
     +0.78539801)**2)+(17.47834015*(RAL-0.78539801)**3)
      ENDIF
C
      IF (RAL .GE. 0.95993102) THEN
C
      CMNR=-0.11
      ENDIF
C
      CNDTD=0.00058286+(0.0007341*RAL)-(0.00746113*RAL*RAL)
     +-(0.00685223*(RAL**3))
     ++(0.03277271*(RAL**4))-(0.02791456*(RAL**5))
     ++(0.00732915*(RAL**6))
     ++(0.00120456*RAL*DELESR)-(0.00168102*DELESR)+'0.0006462*
     +DELESR*DELESR)
C
      CNDAD=0.00008228887-(0.00014015*RAL)-(0.0013493*RAL*RAL)+
     +(0.00020487*(RAL**3))+(0.00561241*(RAL**4))
     +-(0.00634392*(RAL**5))
     ++(0.00193323*(RAL**6))-(2.05815E-17*(RAL*DAILA))+(3.794816E-17*
     +(DAILA**3))
C
      DCNB=-2.500E-4
C
      RALN1=0.69813
      RALN2=90.0/DEGRAD
      RBETN1=-0.174532
      RBETN2=0.34906
C
      AN=0.034
      ASTARN=1.0472
      BSTARN=0.087266
C
      ZETAN=(2.0D0*ASTARN-(RALN1+RALN2))/(RALN2-RALN1)
      ETAN=(2.0D0*BSTARN-(RBETN1+RBETN2))/(RBETN2-RBETN1)
C
      XN=(2.0D0*RAL-(RALN1+RALN2))/(RALN2-RALN1)
      YN=(2.0D0*RBETA-(RBETN1+RBETN2))/(RBETN2-RBETN1)
C
      FN=((5.0D0*(ZETAN**2))-(4.0D0*ZETAN*XN)-1.0D0)*
     +(((XN**2)-1.0D0)**2)/(((ZETAN**2)-1.0D0)**3)
C
      GN=((5.0D0*(ETAN**2))-(4.0D0*ETAN*YN)-1.0D0)*
```

101

```fortran
      +(((YN**2)-1.0D0)**2)/(((ETAN**2)-1.0D0)**3)
C
       CNRB=AN*FN*GN
C
       IF (RAL .LT. 0.69813) THEN
C
       CNRB=0.0
       GOTO 1000
       ENDIF
C
       IF ((RBETA .LT. -0.174532) .OR. (RBETA .GT. 0.34906)) THEN
C
       CNRB=0.0
       GOTO 1000
       ENDIF
C
C
C
 1000 CMN=(CMN1*EPA02S)+(CNDAD*DDA)+((CNDRD*DRUDD*DRFLX3)*EPA43)+
      +((CNDTD*DTFLX3)*DELEDD)+(CMNP*PB)+(CMNR*RB)+(DCNB*BETA)
      ++CNRB
C
C
C*****************************************************************
C
C
C
       CX=CFZ*SIN(RAL)-CFX*COS(RAL)+THRUST/QBARS
       CY=CFY
       CZ=-(CFZ*COS(RAL)+CFX*SIN(RAL))
       CLM=CML
       CMM=CMM+THRUST*(0.25/12.0)/(QBARS*CWING)
C
C      THE (0.25/12.0) IS THE OFFSET OF THE THRUST VECTOR FROM THE CG
C
       CNM=CMN
C
C     RETURN CX, CY, CZ, CLM, CMM, CNM TO CALLING PROGRAM.
C
C
C
C       IWRITE=0
C       IF(IWRITE.EQ.1) WRITE(6,*)' CX,CY,CZ,CLM,CMM,CNM=',
C       +                         CX,CY,CZ,CLM,CMM,CNM
C
C       WRITE(6,*) ' END OF SUB COEFF U(1,2,3)=',U(1),U(2),U(3)
C       WRITE(6,*)'LEAVING COEFF'
       RETURN
       END
C
```

102

Appendix C: <u>Low Angle-of-Attack Equilibrium Conditions</u>

The bifurcation diagrams below depict both stable and unstable equilibrium solutions as a function of stabilator deflection (δ_e). The reader is reminded that the physical limits of the stabilator are -30 degrees to +20 degrees and that the equilibrium branches that lie outside this domain are not physically attainable. For all the plots in Appendix C $\delta_a = \delta_{\Delta e} = \delta_r = 0°$. It should be pointed out that these plots are only a two dimensional projection of an 8 dimensional space. The plots taken as a group can be thought of as pictures taken from different perspectives of the same branch. The branch loses its stability at -19.73° through a Hopf bifurcation and is unstable for δ_e < -19.73°. The bifurcation that originates at δ_e = -10° and lies above the hysteresis depicted in Figure C-1 really has another symmetrical branch behind it which is shown clearly in Figures C-2 and C-7. Both branches are stable. Figure C-1 also shows the origins of δ_e = -5°, -19°, -25° and -29° branches. Figure C-4 depicts pitch rate vs stabilator deflection and shows a sensitivity of pitch rate around 0° stabilator deflection. Figure C-6 shows an interesting phenomena around 0° where the states are highly sensitive to small perturbations. Figure C-8 clearly illustrates the sensitivity of the equilibrium velocity to small changes in stabilator deflection. Mach 0.6 at 20,000 ft is equivalent

103

to 622.14 ft/sec. Velocities much higher than that are in the compressible flow region and invalidate the assumptions made in deriving the model, as such they are discounted. Table VII omits these equilibrium solutions. Since the stable equilibrium solution for velocity at $\delta_e = 0°$ is greater than 1000 ft/sec and outside the range of compressible flow, it is discounted. Physically, the plots show a turn state (see Figure C-7) which is stable between about 0 and -10°; at about 0° there is a rapid transition from level to level inverted flight (see especially Figures C-6 and C-8). Figure C-9 shows the nonzero lateral branches started from the rudder sweep of Figure 5-3.

ANGLE OF ATTACK (ALPHA) US STAB DEFLECT
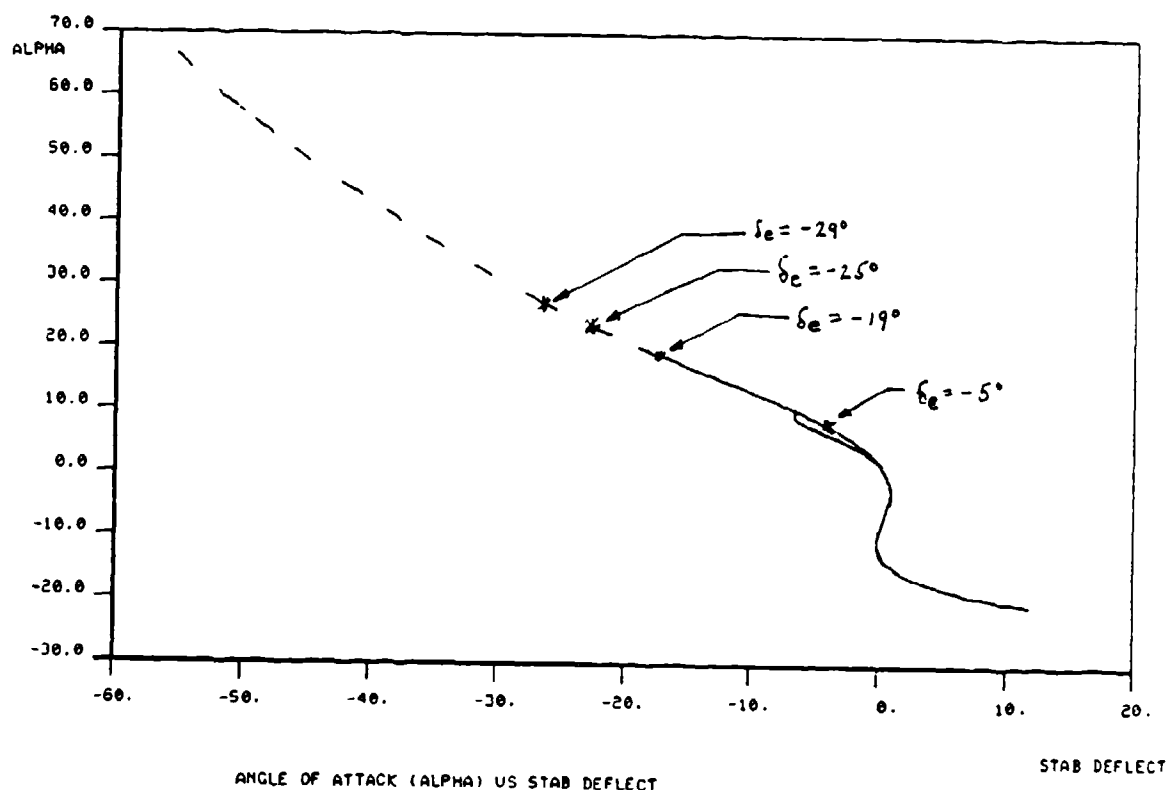
Figure C-1   Angle-of-Attack vs Stabilator Deflection
(δ_e vs α)

104
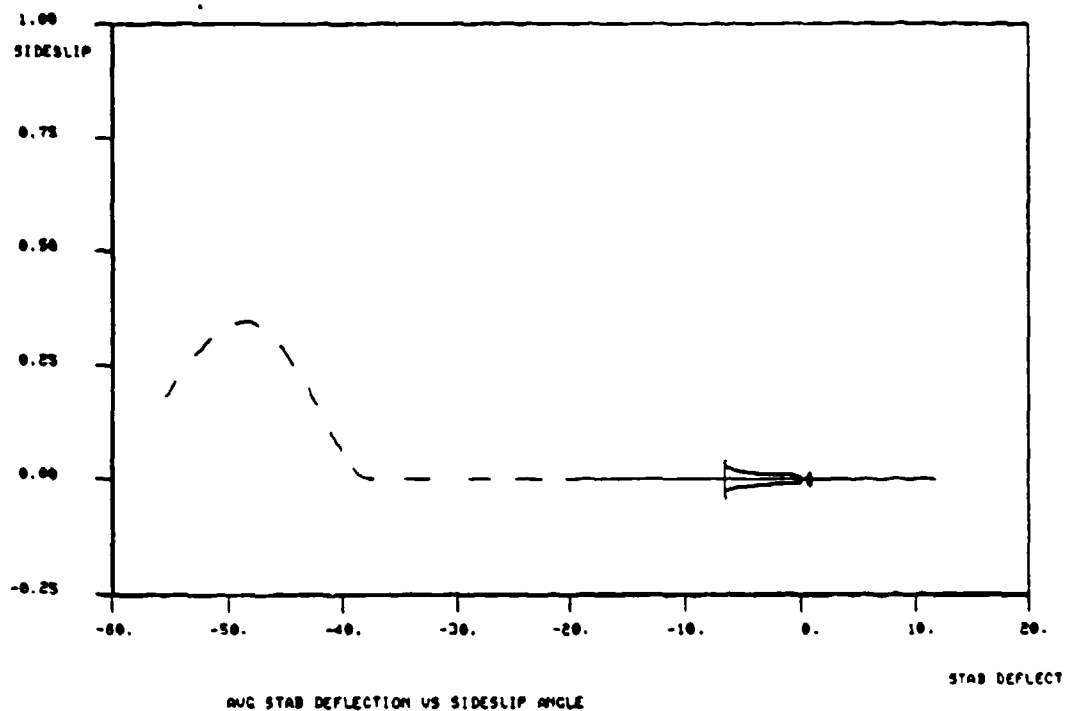
Figure C-2   Sideslip Angle vs Stabilator Deflection (β vs δ_e)
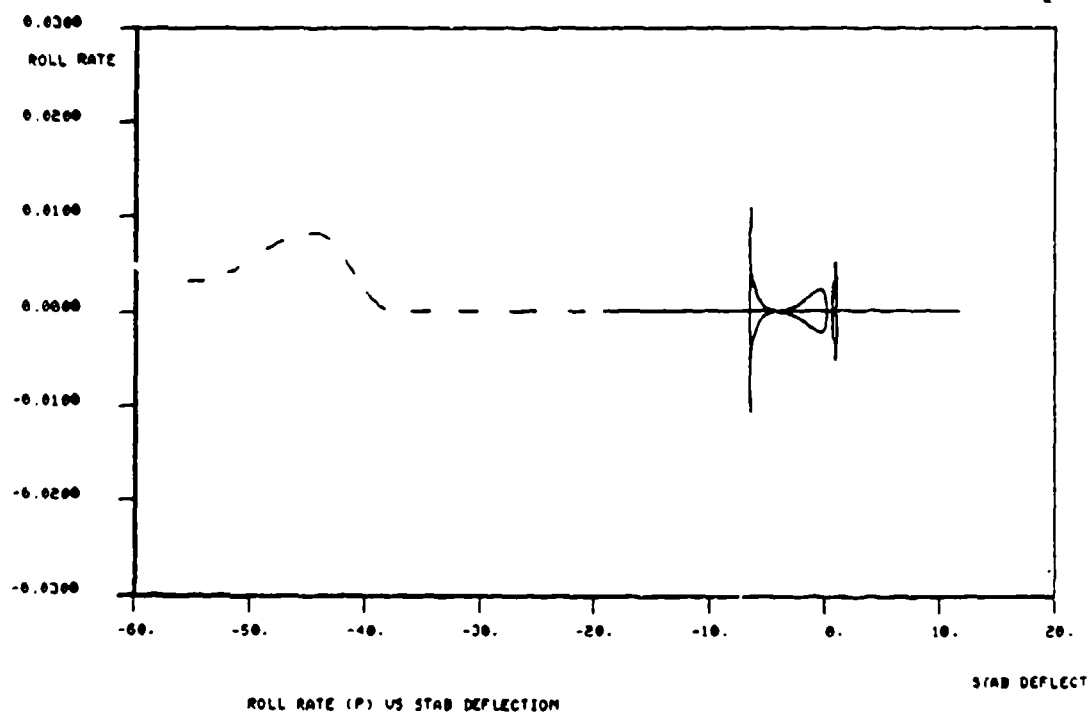
Figure C-3   Roll Rate vs Stabilator Deflection (p vs δ_e)

105

PITCH RATE (Q) VS STABILATOR DEFLECTION
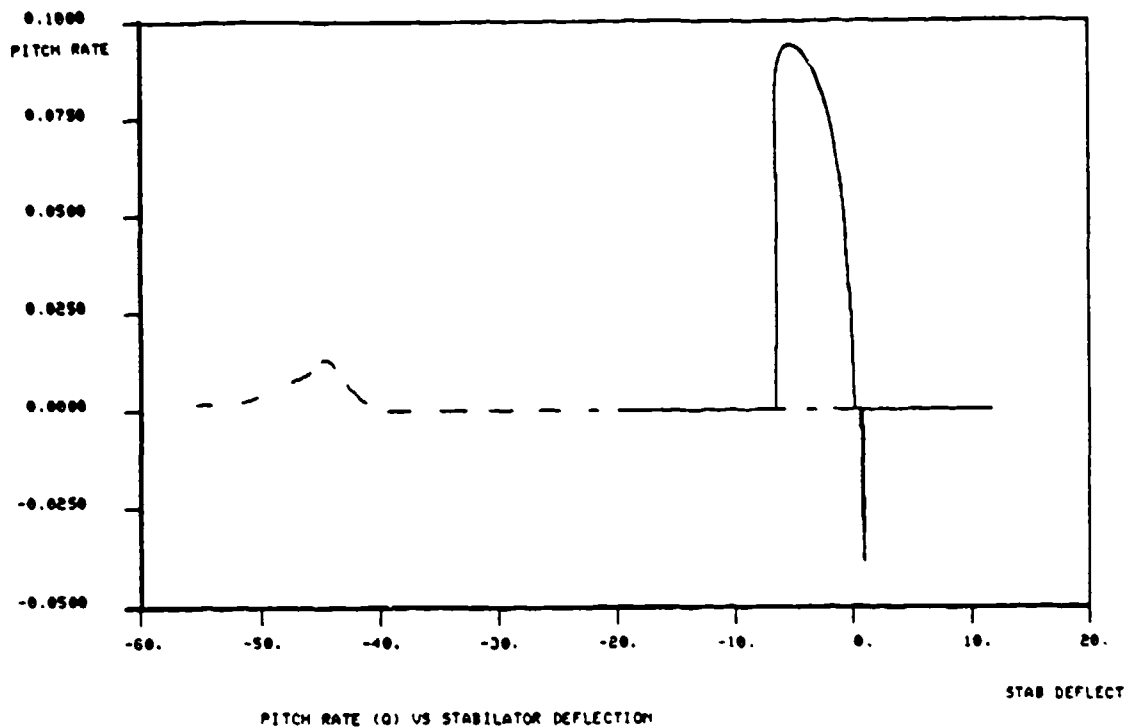
Figure C-4   Pitch Rate vs Stabilator Deflection (q vs δ_e)

YAW RATE (R) VS STABILATOR DEFLECTION
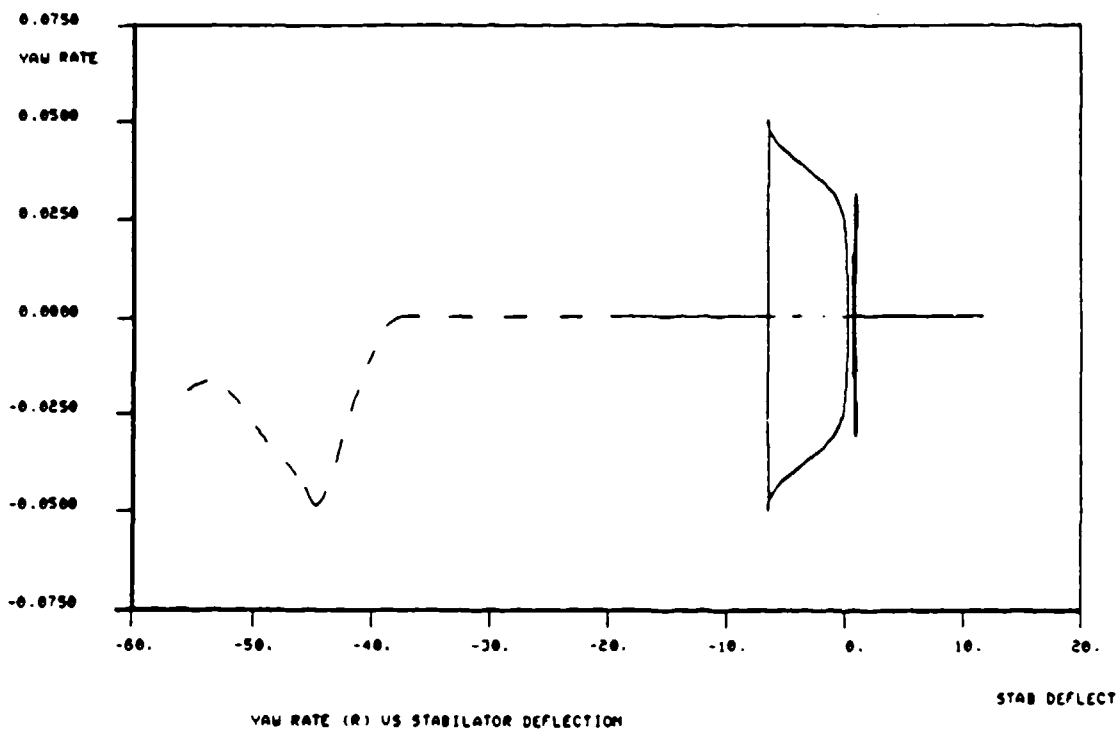
Figure C-5   Yaw Rate vs Stabilator Deflection (r vs δ_e)

106

PITCH ANGLE (THETA) VS STAB DEFLECTION
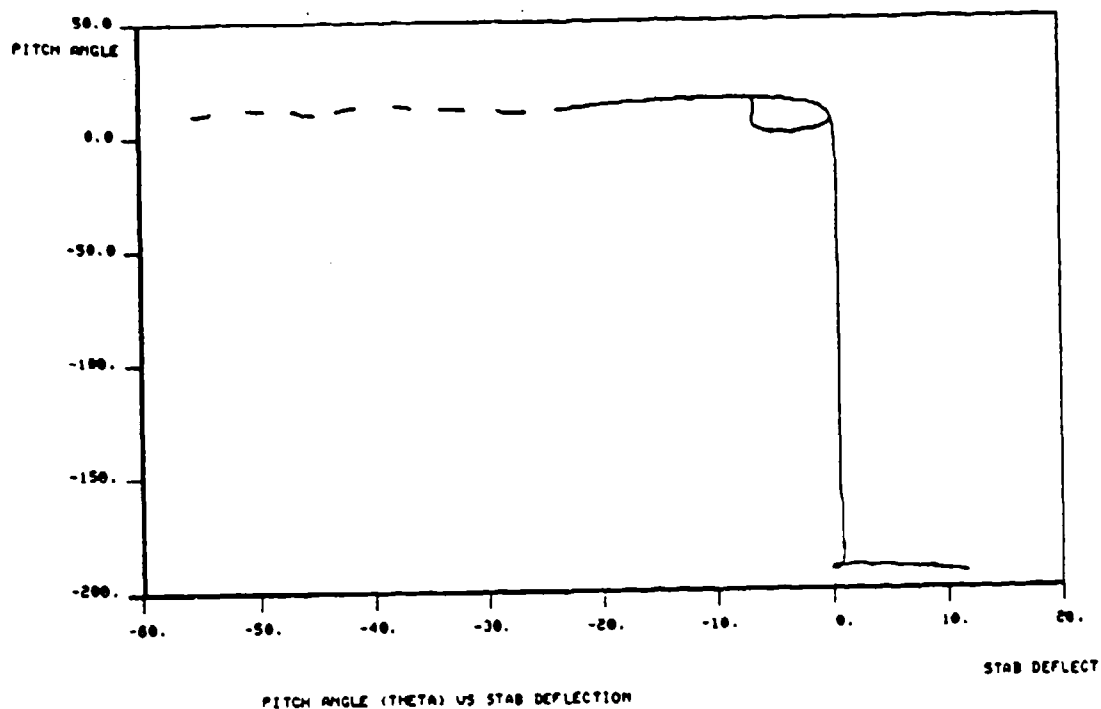
Figure C-6   Pitch Angle vs Stabilator Deflection (θ vs δ_e)

BANK ANGLE (PHI) VS STAB DEFLECTION
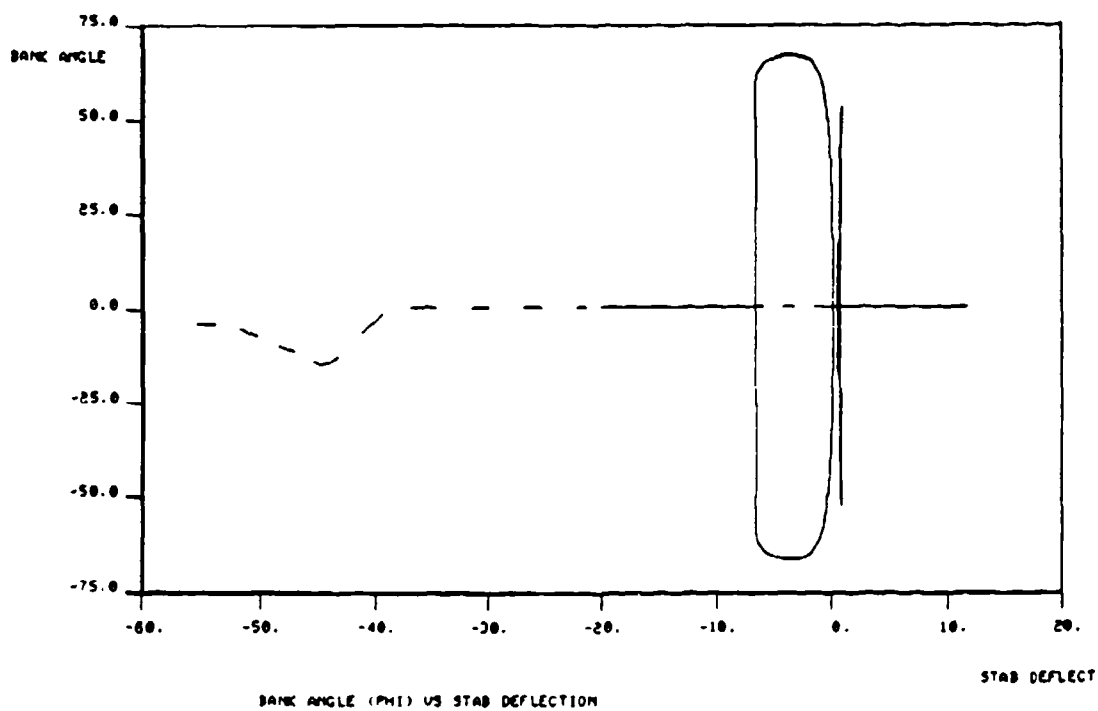
Figure C-7   Bank Angle vs Stabilator Deflection (ϕ vs δ_e)

107

TRUE VELOCITY (U) VS STAB DEFLECTION
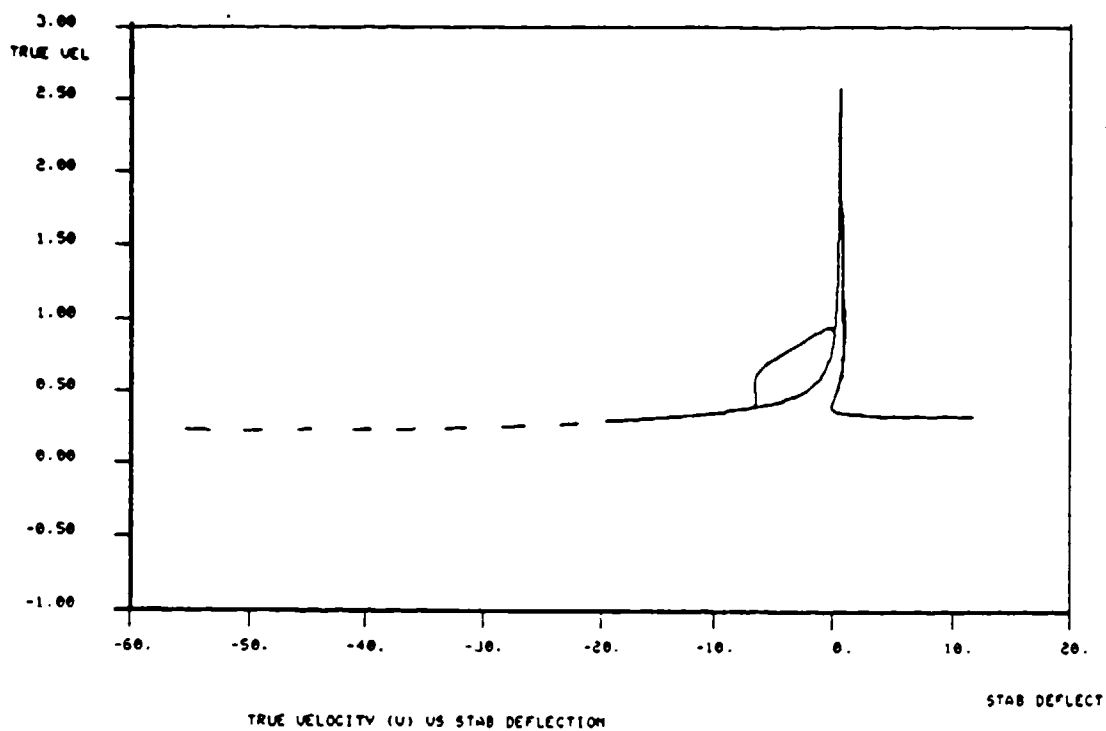
Figure C-8   Velocity vs Stabilator Deflection (V vs δe)

STABILATOR DEFLECTION VS ANGLE OF ATTACK
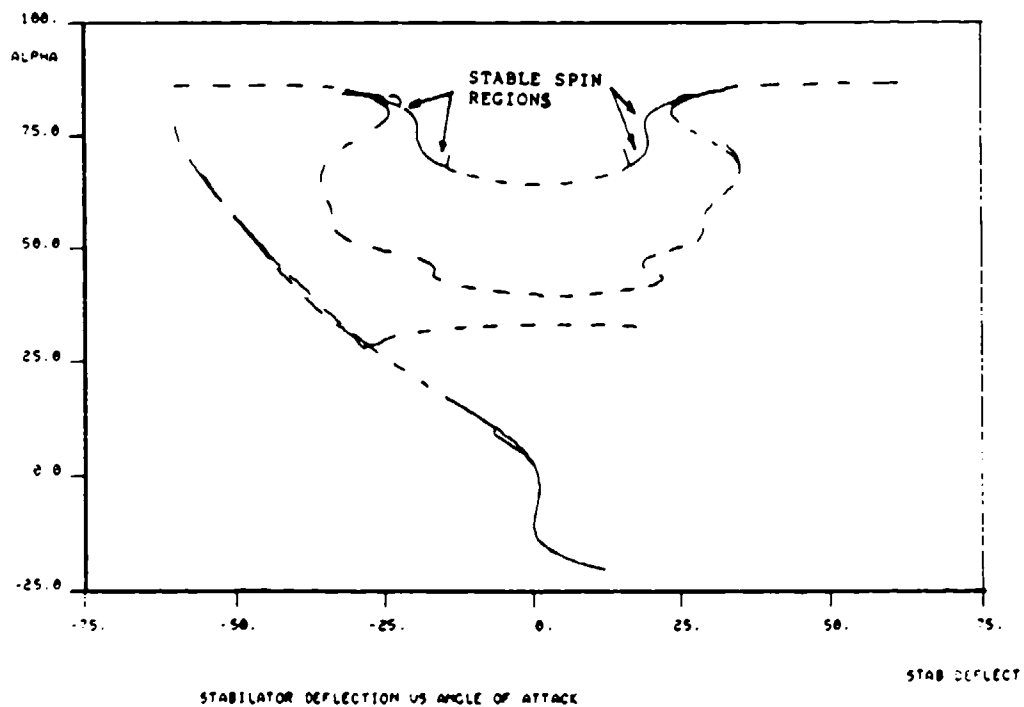
Figure C-9   Stabilator Sweeps ($\delta_r = \delta_a = \delta_{Le} = 0°$)

108

The following table is a compilation of stable low α equilibrium states (for plots C-1 through C-8) calculated for the F-15B as a function of stabilator deflection (δ_e). Aileron, rudder and differential stabilator deflections ($\delta_a, \delta_r, \delta_{\Delta e}$) are set equal to 0°, thrust is fixed constant at 8300 lbs (Mil Power) and altitude is fixed at 20,000 feet.

Table VII. Tabulation of Low α Equilibrium Conditions

Point	Stabilator Deflection δ_e Degrees	Angle of Attack α Degrees	Sideslip Angle β Degrees	Roll Rate p Rad/sec
1	-9.923545E+00	1.343360E+01	-3.286E-19	-1.873E-21
2	-1.004614E+01	1.353066E+01	-3.214E-19	-1.763E-21
3	-1.016881E+01	1.362758E+01	-2.930E-19	-1.549E-21
4	-1.029155E+01	1.372435E+01	-2.473E-19	-1.263E-21
5	-1.041435E+01	1.382099E+01	-1.890E-19	-9.323E-22
6	-1.053721E+01	1.391750E+01	-1.226E-19	-5.851E-22
7	-1.066011E+01	1.401388E+01	-5.283E-20	-2.443E-22
8	-1.078305E+01	1.411013E+01	1.593E-20	7.141E-23
9	-1.090602E+01	1.420626E+01	7.991E-20	3.477E-22
10	-1.102902E+01	1.430227E+01	1.360E-19	5.747E-22
11	-1.115204E+01	1.439816E+01	1.818E-19	7.469E-22
12	-1.127508E+01	1.449394E+01	2.156E-19	8.622E-22
13	-1.139812E+01	1.458962E+01	2.367E-19	9.218E-22
14	-1.152116E+01	1.468519E+01	2.492E-19	9.456E-22
15	-1.167496E+01	1.480452E+01	2.518E-19	9.263E-22
16	-1.182875E+01	1.492369E+01	2.424E-19	8.652E-22
17	-1.198251E+01	1.504272E+01	2.222E-19	7.702E-22
18	-1.213623E+01	1.516162E+01	1.928E-19	6.498E-22
19	-1.228991E+01	1.528038E+01	1.562E-19	5.123E-22
20	-1.244352E+01	1.539903E+01	1.144E-19	3.654E-22
21	-1.259708E+01	1.551755E+01	6.948E-20	2.163E-22
22	-1.275056E+01	1.563597E+01	2.355E-20	7.155E-23
23	-1.290396E+01	1.575429E+01	-2.145E-20	-6.361E-23
24	-1.305727E+01	1.587252E+01	-6.377E-20	-1.847E-22
25	-1.321048E+01	1.599065E+01	-1.019E-19	-2.884E-22
26	-1.336358E+01	1.610871E+01	-1.344E-19	-3.723E-22
27	-1.351657E+01	1.622668E+01	-1.605E-19	-4.352E-22
28	-1.366945E+01	1.634459E+01	-1.794E-19	-4.764E-22
29	-1.382219E+01	1.646244E+01	-1.933E-19	-5.028E-22
30	-1.401293E+01	1.660968E+01	-2.027E-19	-5.143E-22
31	-1.420345E+01	1.675684E+01	-2.042E-19	-5.057E-22

32	-1.439374E+01	1.690394E+01	-1.981E-19 -4.792E-22
33	-1.458379E+01	1.705099E+01	-1.850E-19 -4.372E-22
34	-1.477359E+01	1.719800E+01	-1.656E-19 -3.825E-22
35	-1.496312E+01	1.734499E+01	-1.409E-19 -3.181E-22
36	-1.515238E+01	1.749197E+01	-1.120E-19 -2.473E-22
37	-1.534136E+01	1.763895E+01	-8.030E-20 -1.733E-22
38	-1.553006E+01	1.778594E+01	-4.687E-20 -9.898E-23
39	-1.571846E+01	1.793296E+01	-1.299E-20 -2.684E-23
40	-1.590656E+01	1.808001E+01	2.043E-20 4.136E-23
41	-1.614126E+01	1.826390E+01	6.018E-20 1.188E-22
42	-1.637546E+01	1.844789E+01	9.674E-20 1.863E-22
43	-1.660917E+01	1.863200E+01	1.292E-19 2.431E-22
44	-1.684237E+01	1.881626E+01	1.567E-19 2.885E-22
45	-1.707506E+01	1.900070E+01	1.789E-19 3.224E-22
46	-1.730722E+01	1.918532E+01	1.952E-19 3.450E-22
47	-9.434075E+00	1.304385E+01	-2.510E-20 -1.691E-22
48	-9.556290E+00	1.314152E+01	4.576E-20 2.949E-22
49	-9.678611E+00	1.323903E+01	1.076E-19 6.643E-22
50	-9.801033E+00	1.333639E+01	1.567E-19 9.289E-22
51	-9.923545E+00	1.343360E+01	1.910E-19 1.089E-21
52	-1.004614E+01	1.353066E+01	2.097E-19 1.150E-21
53	-1.016881E+01	1.362758E+01	2.130E-19 1.126E-?1
54	-1.029155E+01	1.372435E+01	2.021E-19 1.032E-?1
55	-1.041435E+01	1.382099E+01	1.792E-19 8.843E-22
56	-1.053721E+01	1.391750E+01	1.467E-19 7.004E-22
57	-1.066011E+01	1.401388E+01	1.074E-19 4.967E-22
58	-1.078305E+01	1.411013E+01	6.418E-20 2.877E-22
59	-1.090602E+01	1.420626E+01	1.975E-20 8.595E-23
60	-1.102902E+01	1.430227E+01	-2.332E-20 -9.856E-23
61	-1.115204E+01	1.439816E+01	-6.283E-20 -2.582E-22
62	-1.127508E+01	1.449394E+01	-9.699E-20 -3.878E-22
63	-1.139812E+01	1.458962E+01	-1.244E-19 -4.846E-22
64	-1.152116E+01	1.468519E+01	-1.468E-19 -5.570E-22
65	-1.167496E+01	1.480452E+01	-1.662E-19 -6.114E-22
66	-1.182875E+01	1.492369E+01	-1.768E-19 -6.311E-22
67	-1.198251E+01	1.504272E+01	-1.787E-19 -6.196E-22
68	-1.213623E+01	1.516162E+01	-1.725E-19 -5.813E-22
69	-1.228991E+01	1.528038E+01	-1.588E-19 -5.210E-22
70	-1.244352E+01	1.539903E+01	-1.389E-19 -4.437E-22
71	-1.259708E+01	1.551755E+01	-1.139E-19 -3.547E-22
72	-1.275056E+01	1.563597E+01	-8.519E-20 -2.588E-22
73	-1.290396E+01	1.575429E+01	-5.415E-20 -1.606E-22
74	-1.305727E+01	1.587252E+01	-2.217E-20 -6.423E-23
75	-1.321048E+01	1.599065E+01	9.411E-21 2.665E-23
76	-1.336358E+01	1.610871E+01	3.938E-20 1.091E-22
77	-1.351657E+01	1.622668E+01	6.666E-20 1.807E-22
78	-1.366945E+01	1.634459E+01	9.033E-20 2.398E-22
79	-1.382219E+01	1.646244E+01	1.111E-19 2.889E-22
80	-1.401293E+01	1.660968E+01	1.319E-19 3.346E-22
81	-1.420345E+01	1.675684E+01	1.470E-19 3.640E-22
82	-1.439374E+01	1.690394E+01	1.561E-19 3.776E-22
83	-1.458379E+01	1.705099E+01	1.592E-19 3.762E-22

110

84	-1.477359E+01	1.719800E+01	1.563E-19	3.611E-22
85	-1.496312E+01	1.734499E+01	1.479E-19	3.339E-22
86	-1.515238E+01	1.749197E+01	1.345E-19	2.970E-22
87	-1.534136E+01	1.763895E+01	1.169E-19	2.524E-22
88	-1.553006E+01	1.778594E+01	9.585E-20	2.024E-22
89	-1.571846E+01	1.793296E+01	7.225E-20	1.493E-22
90	-1.590656E+01	1.808001E+01	4.756E-20	9.627E-23
91	-1.614126E+01	1.826390E+01	1.615E-20	3.188E-23
92	-1.637546E+01	1.844789E+01	-1.477E-20	-2.845E-23
93	-6.421912E+00	1.042375E+01	-4.268E-02	1.086E-02
94	-6.422383E+00	1.044356E+01	-4.259E-02	1.084E-02
95	-6.423676E+00	1.046077E+01	-4.235E-02	1.077E-02
96	-6.425619E+00	1.047573E+01	-4.199E-02	1.066E-02
97	-6.428061E+00	1.048874E+01	-4.149E-02	1.051E-02
98	-6.430869E+00	1.050007E+01	-4.087E-02	1.032E-02
99	-6.433929E+00	1.050994E+01	-4.012E-02	1.010E-02
100	-6.437148E+00	1.051855E+01	-3.925E-02	9.853E-03
101	-6.440450E+00	1.052608E+01	-3.827E-02	9.572E-03
102	-6.443775E+00	1.053266E+01	-3.717E-02	9.263E-03
103	-6.447078E+00	1.053844E+01	-3.597E-02	8.929E-03
104	-6.450325E+00	1.054353E+01	-3.466E-02	8.570E-03
105	-6.453494E+00	1.054803E+01	-3.325E-02	8.190E-03
106	-6.456571E+00	1.055202E+01	-3.174E-02	7.789E-03
107	-6.459549E+00	1.055559E+01	-3.014E-02	7.369E-03
108	-6.462428E+00	1.055880E+01	-2.845E-02	6.932E-03
109	-6.465209E+00	1.056171E+01	-2.669E-02	6.479E-03
110	-6.467898E+00	1.056437E+01	-2.484E-02	6.011E-03
111	-6.470503E+00	1.056682E+01	-2.293E-02	5.530E-03
112	-6.473031E+00	1.056910E+01	-2.094E-02	5.037E-03
113	-6.475490E+00	1.057124E+01	-1.890E-02	4.534E-03
114	-6.477886E+00	1.057327E+01	-1.680E-02	4.020E-03
115	-6.480224E+00	1.057522E+01	-1.466E-02	3.499E-03
116	-6.482507E+00	1.057709E+01	-1.247E-02	2.970E-03
117	-5.717336E+00	8.300828E+00	-1.980E-02	1.176E-03
118	-6.074053E+00	8.716746E+00	-2.249E-02	2.156E-03
119	-6.280097E+00	9.032906E+00	-2.500E-02	3.180E-03
120	-6.395281E+00	9.280496E+00	-2.733E-02	4.184E-03
121	-6.455888E+00	9.479154E+00	-2.947E-02	5.136E-03
122	-6.483826E+00	9.641531E+00	-3.143E-02	6.019E-03
123	-6.492522E+00	9.776117E+00	-3.323E-02	6.826E-03
124	-6.492752E+00	9.802286E+00	-3.360E-02	6.991E-03
125	-6.488953E+00	9.910892E+00	-3.520E-02	7.701E-03
126	-6.480309E+00	1.000274E+01	-3.663E-02	8.332E-03
127	-6.469735E+00	1.008089E+01	-3.791E-02	8.885E-03
128	-6.458999E+00	1.014768E+01	-3.903E-02	9.362E-03
129	-6.449121E+00	1.020499E+01	-4.000E-02	9.766E-03
130	-6.440642E+00	1.025429E+01	-4.082E-02	1.010E-02
131	-6.433794E+00	1.029681E+01	-4.148E-02	1.037E-02
132	-6.428613E+00	1.033355E+01	-4.200E-02	1.058E-02
133	-6.425019E+00	1.036534E+01	-4.237E-02	1.072E-02
134	-6.422862E+00	1.039288E+01	-4.260E-02	1.082E-02
135	-6.421965E+00	1.041677E+01	-4.269E-02	1.086E-02

136	-6.421912E+00	1.042375E+01	-4.268E-02	1.086E-02
137	-6.422383E+00	1.044356E+01	-4.259E-02	1.084E-02
138	-6.423676E+00	1.046077E+01	-4.235E-02	1.077E-02
139	-6.425619E+00	1.047573E+01	-4.199E-02	1.066E-02
140	-6.428061E+00	1.048874E+01	-4.149E-02	1.051E-02
141	-6.430869E+00	1.050007E+01	-4.087E-02	1.032E-02
142	-6.433929E+00	1.050994E+01	-4.012E-02	1.010E-02
143	-6.437148E+00	1.051855E+01	-3.925E-02	9.853E-03
144	-6.440450E+00	1.052608E+01	-3.827E-02	9.572E-03
145	-6.443775E+00	1.053266E+01	-3.717E-02	9.263E-03
146	-6.447078E+00	1.053844E+01	-3.597E-02	8.929E-03
147	-6.450325E+00	1.054353E+01	-3.466E-02	8.570E-03
148	-6.453494E+00	1.054803E+01	-3.325E-02	8.190E-03
149	-6.456571E+00	1.055202E+01	-3.174E-02	7.789E-03
150	-6.459549E+00	1.055559E+01	-3.014E-02	7.369E-03
151	-6.462428E+00	1.055880E+01	-2.845E-02	6.932E-03
152	-6.465209E+00	1.056171E+01	-2.669E-02	6.479E-03
153	-6.467898E+00	1.056437E+01	-2.484E-02	6.011E-03
154	-6.470503E+00	1.056682E+01	-2.293E-02	5.530E-03
155	-6.473031E+00	1.056910E+01	-2.094E-02	5.037E-03
156	-6.475490E+00	1.057124E+01	-1.890E-02	4.534E-03
157	-6.477886E+00	1.057327E+01	-1.680E-02	4.020E-03
158	-6.480224E+00	1.057522E+01	-1.466E-02	3.499E-03
159	-6.482507E+00	1.057709E+01	-1.247E-02	2.970E-03
160	-6.484735E+00	1.057891E+01	-1.024E-02	2.435E-03
161	-6.486905E+00	1.058068E+01	-7.985E-03	1.896E-03
162	-6.489012E+00	1.058242E+01	-5.703E-03	1.352E-03
163	-6.491045E+00	1.058412E+01	-3.402E-03	8.057E-04
164	-6.492993E+00	1.058579E+01	-1.089E-03	2.577E-04
165	-6.493874E+00	1.058656E+01	1.608E-09	-3.805E-10
166	-6.491972E+00	1.058491E+01	2.317E-03	-5.485E-04
167	-6.489977E+00	1.058322E+01	4.624E-03	-1.096E-03
168	-6.487903E+00	1.058150E+01	6.916E-03	-1.641E-03
169	-6.485762E+00	1.057975E+01	9.186E-03	-2.182E-03
170	-6.483561E+00	1.057795E+01	1.143E-02	-2.720E-03
171	-6.481303E+00	1.057611E+01	1.363E-02	-3.251E-03
172	-6.478991E+00	1.057420E+01	1.580E-02	-3.776E-03
173	-6.476623E+00	1.057221E+01	1.792E-02	-4.294E-03
174	-6.438693E+00	1.052221E+01	3.881E-02	-9.724E-03
175	-6.435426E+00	1.051413E+01	3.972E-02	-9.990E-03
176	-6.432281E+00	1.050488E+01	4.053E-02	-1.023E-02
177	-6.429342E+00	1.049426E+01	4.121E-02	-1.043E-02
178	-6.426713E+00	1.048207E+01	4.177E-02	-1.059E-02
179	-6.424517E+00	1.046806E+01	4.220E-02	-1.072E-02
180	-6.422899E+00	1.045194E+01	4.249E-02	-1.081E-02
181	-6.422019E+00	1.043340E+01	4.266E-02	-1.085E-02
182	-6.421912E+00	1.042375E+01	4.268E-02	-1.086E-02
183	-6.422446E+00	1.040092E+01	4.264E-02	-1.084E-02
184	-6.424178E+00	1.037462E+01	4.246E-02	-1.076E-02
185	-6.427292E+00	1.034426E+01	4.213E-02	-1.063E-02
186	-6.431951E+00	1.030919E+01	4.166E-02	-1.044E-02
187	-6.438261E+00	1.026863E+01	4.105E-02	-1.019E-02

188	-6.446230E+00	1.022162E+01	4.028E-02	-9.881E-03
189	-6.455700E+00	1.016704E+01	3.936E-02	-9.500E-03
190	-6.466245E+00	1.010347E+01	3.829E-02	-9.046E-03
191	-6.477021E+00	1.002920E+01	3.706E-02	-8.518E-03
192	-6.486537E+00	9.942043E+00	3.567E-02	-7.913E-03
193	-6.492302E+00	9.839201E+00	3.413E-02	-7.228E-03
194	-6.492752E+00	9.802286E+00	3.360E-02	-6.991E-03
195	-6.487000E+00	9.672882E+00	3.184E-02	-6.201E-03
196	-6.464168E+00	9.517156E+00	2.991E-02	-5.334E-03
197	-6.412155E+00	9.327274E+00	2.781E-02	-4.396E-03
198	-6.311292E+00	9.091681E+00	2.552E-02	-3.401E-03
199	-6.129087E+00	8.792579E+00	2.305E-02	-2.377E-03
200	-5.811713E+00	8.401748E+00	2.040E-02	-1.380E-03
201	-5.275754E+00	7.875753E+00	1.759E-02	-5.239E-04

Table VII. Tabulation of Low α Equilibrium Conditions
(Continued-)

Point	Pitch Rate q Rad/sec	Yaw Rate r Rad/sec	Pitch Angle θ Degrees	Bank Angle φ Degrees	True Velocity V kFt/sec
1	-7.159E-31	6.808E-21	1.538E+01	4.413E-18	3.384E-01
2	0.000E+00	6.413E-21	1.537E+01	4.142E-18	3.373E-01
3	2.031E-31	5.638E-21	1.537E+01	3.630E-18	3.362E-01
4	0.000E+00	4.597E-21	1.536E+01	2.950E-18	3.351E-01
5	-1.597E-30	3.396E-21	1.535E+01	2.173E-18	3.341E-01
6	-5.507E-32	2.133E-21	1.534E+01	1.360E-18	3.330E-01
7	6.609E-31	8.909E-22	1.533E+01	5.664E-19	3.320E-01
8	-2.809E-30	-2.606E-22	1.532E+01	-1.652E-19	3.310E-01
9	-3.359E-30	-1.270E-21	1.531E+01	-8.023E-19	3.300E-01
10	0.000E+00	-2.101E-21	1.530E+01	-1.323E-18	3.290E-01
11	0.000E+00	-2.733E-21	1.529E+01	-1.716E-18	3.280E-01
12	2.423E-30	-3.157E-21	1.527E+01	-1.976E-18	3.270E-01
13	-2.887E-25	-3.379E-21	1.526E+01	-2.108E-18	3.261E-01
14	3.552E-30	-3.469E-21	1.525E+01	-2.158E-18	3.251E-01
15	1.465E-29	-3.403E-21	1.523E+01	-2.109E-18	3.239E-01
16	-2.615E-30	-3.183E-21	1.521E+01	-1.965E-18	3.228E-01
17	6.939E-30	-2.838E-21	1.519E+01	-1.745E-18	3.216E-01
18	8.535E-30	-2.398E-21	1.516E+01	-1.469E-18	3.205E-01
19	-8.542E-30	-1.893E-21	1.514E+01	-1.156E-18	3.194E-01
20	0.000E+00	-1.353E-21	1.512E+01	-8.228E-19	3.183E-01
21	-9.569E-31	-8.023E-22	1.509E+01	-4.862E-19	3.172E-01
22	0.000E+00	-2.658E-22	1.507E+01	-1.605E-19	3.161E-01
23	-1.817E-30	2.367E-22	1.504E+01	1.424E-19	3.151E-01
24	-3.497E-30	6.888E-22	1.501E+01	4.130E-19	3.140E-01
25	3.084E-30	1.078E-21	1.498E+01	6.437E-19	3.130E-01
26	1.322E-30	1.394E-21	1.495E+01	8.298E-19	3.120E-01
27	1.239E-30	1.633E-21	1.492E+01	9.684E-19	3.109E-01
28	2.887E-26	1.791E-21	1.489E+01	1.059E-18	3.099E-01
29	-6.884E-30	1.895E-21	1.486E+01	1.116E-18	3.090E-01
30	2.049E-29	1.944E-21	1.482E+01	1.140E-18	3.077E-01
31	9.115E-30	1.917E-21	1.478E+01	1.119E-18	3.065E-01
32	-8.812E-31	1.823E-21	1.473E+01	1.059E-18	3.054E-01
33	0.000E+00	1.668E-21	1.469E+01	9.652E-19	3.042E-01

114

34	0.000E+00	1.464E-21	1.464E+01	8.434E-19	3.030E-01
35	0.000E+00	1.222E-21	1.459E+01	7.008E-19	3.019E-01
36	0.000E+00	9.533E-22	1.454E+01	5.445E-19	3.008E-01
37	1.101E-31	6.705E-22	1.449E+01	3.813E-19	2.996E-01
38	7.159E-31	3.843E-22	1.444E+01	2.176E-19	2.985E-01
39	-4.042E-25	1.046E-22	1.439E+01	5.897E-20	2.975E-01
40	-1.201E-29	-1.618E-22	1.434E+01	-9.081E-20	2.964E-01
41	0.000E+00	-4.668E-22	1.427E+01	-2.607E-19	2.951E-01
42	1.223E-29	-7.362E-22	1.420E+01	-4.089E-19	2.938E-01
43	0.000E+00	-9.654E-22	1.413E+01	-5.333E-19	2.925E-01
44	-1.074E-30	-1.152E-21	1.406E+01	-6.329E-19	2.912E-01
45	2.423E-30	-1.294E-21	1.399E+01	-7.073E-19	2.899E-01
46	-2.313E-30	-1.392E-21	1.392E+01	-7.569E-19	2.887E-01
47	-6.829E-30	6.141E-22	1.539E+01	4.033E-19	3.429E-01
48	0.000E+00	-1.071E-21	1.539E+01	-7.012E-19	3.418E-01
49	1.068E-29	-2.414E-21	1.539E+01	-1.575E-18	3.406E-01
50	3.442E-30	-3.376E-21	1.538E+01	-2.195E-18	3.395E-01
51	-3.948E-30	-3.958E-21	1.538E+01	-2.565E-18	3.384E-01
52	0.000E+00	-4.184E-21	1.537E+01	-2.703E-18	3.373E-01
53	4.640E-30	-4.098E-21	1.537E+01	-2.639E-18	3.362E-01
54	-9.087E-31	-3.757E-21	1.536E+01	-2.411E-18	3.351E-01
55	3.029E-30	-3.221E-21	1.535E+01	-2.061E-18	3.341E-01
56	0.000E+00	-2.553E-21	1.534E+01	-1.628E-18	3.330E-01
57	2.203E-30	-1.812E-21	1.533E+01	-1.152E-18	3.320E-01
58	3.001E-30	-1.050E-21	1.532E+01	-6.655E-19	3.310E-01
59	-3.848E-30	-3.139E-22	1.531E+01	-1.983E-19	3.300E-01
60	0.000E+00	3.603E-22	1.530E+01	2.269E-19	3.290E-01
61	4.172E-30	9.446E-22	1.529E+01	5.931E-19	3.280E-01
62	2.341E-31	1.420E-21	1.527E+01	8.889E-19	3.270E-01
63	-5.053E-25	1.776E-21	1.526E+01	1.108E-18	3.261E-01
64	-5.535E-30	2.044E-21	1.525E+01	1.271E-18	3.251E-01
65	-7.710E-31	2.246E-21	1.523E+01	1.392E-18	3.239E-01
66	2.258E-30	2.322E-21	1.521E+01	1.433E-18	3.228E-01
67	-1.239E-29	2.283E-21	1.519E+01	1.404E-18	3.216E-01
68	1.564E-29	2.145E-21	1.516E+01	1.314E-18	3.205E-01
69	1.057E-30	1.925E-21	1.514E+01	1.176E-18	3.194E-01
70	4.101E-31	1.643E-21	1.512E+01	9.992E-19	3.183E-01
71	-1.817E-30	1.315E-21	1.509E+01	7.971E-19	3.172E-01
72	0.000E+00	9.613E-22	1.507E+01	5.805E-19	3.161E-01
73	-1.101E-30	5.976E-22	1.504E+01	3.596E-19	3.151E-01
74	1.817E-30	2.395E-22	1.501E+01	1.436E-19	3.140E-01
75	0.000E+00	-9.958E-23	1.498E+01	-5.948E-20	3.130E-01
76	-7.297E-31	-4.084E-22	1.495E+01	-2.431E-19	3.120E-01
77	-5.232E-30	-6.780E-22	1.492E+01	-4.021E-19	3.109E-01
78	8.373E-25	-9.017E-22	1.489E+01	-5.329E-19	3.099E-01
79	1.804E-30	-1.089E-21	1.486E+01	-6.412E-19	3.090E-01
80	3.084E-30	-1.265E-21	1.482E+01	-7.415E-19	3.077E-01
81	-9.280E-30	-1.380E-21	1.478E+01	-8.056E-19	3.065E-01
82	0.000E+00	-1.436E-21	1.473E+01	-8.346E-19	3.054E-01
83	1.487E-30	-1.435E-21	1.469E+01	-8.305E-19	3.042E-01
84	7.770E-31	-1.382E-21	1.464E+01	-7.963E-19	3.030E-01
85	-3.458E-30	-1.283E-21	1.459E+01	-7.357E-19	3.019E-01

115

86	2.482E-30	-1.145E-21	1.454E+01	-6.537E-19	3.008E-01
87	5.783E-31	-9.762E-22	1.449E+01	-5.551E-19	2.996E-01
88	3.415E-30	-7.858E-22	1.444E+01	-4.449E-19	2.985E-01
89	-1.357E-24	-5.819E-22	1.439E+01	-3.281E-19	2.975E-01
90	-4.859E-30	-3.766E-22	1.434E+01	-2.114E-19	2.964E-01
91	-1.083E-31	-1.253E-22	1.427E+01	-6.997E-20	2.951E-01
92	4.025E-02	4.649E-02	9.922E+00	4.150E+01	4.401E-01
93	3.757E-02	4.622E-02	1.005E+01	4.105E+01	4.384E-01
94	3.497E-02	4.534E-02	1.043E+01	3.964E+01	4.333E-01
95	3.245E-02	4.439E-02	1.079E+01	3.823E+01	4.286E-01
96	3.002E-02	4.335E-02	1.113E+01	3.681E+01	4.241E-01
97	2.767E-02	4.225E-02	1.146E+01	3.539E+01	4.200E-01
98	2.542E-02	4.107E-02	1.178E+01	3.397E+01	4.161E-01
99	2.325E-02	3.983E-02	1.207E+01	3.254E+01	4.125E-01
100	2.117E-02	3.852E-02	1.235E+01	3.111E+01	4.091E-01
101	1.919E-02	3.715E-02	1.262E+01	2.968E+01	4.060E-01
102	1.730E-02	3.571E-02	1.287E+01	2.825E+01	4.030E-01
103	1.550E-02	3.423E-02	1.311E+01	2.681E+01	4.003E-01
104	1.379E-02	3.268E-02	1.333E+01	2.537E+01	3.977E-01
105	1.219E-02	3.109E-02	1.354E+01	2.393E+01	3.953E-01
106	1.068E-02	2.945E-02	1.373E+01	2.248E+01	3.931E-01
107	9.263E-03	2.776E-02	1.392E+01	2.104E+01	3.911E-01
108	7.948E-03	2.603E-02	1.408E+01	1.959E+01	3.892E-01
109	6.732E-03	2.426E-02	1.424E+01	1.814E+01	3.875E-01
110	5.614E-03	2.245E-02	1.438E+01	1.669E+01	3.859E-01
111	4.597E-03	2.061E-02	1.452E+01	1.524E+01	3.845E-01
112	3.681E-03	1.874E-02	1.463E+01	1.379E+01	3.832E-01
113	2.865E-03	1.683E-02	1.474E+01	1.233E+01	3.821E-01
114	2.151E-03	1.491E-02	1.483E+01	1.088E+01	3.811E-01
115	1.538E-03	1.296E-02	1.492E+01	9.424E+00	3.802E-01
116	9.327E-02	-4.453E-02	7.710E-01	-6.426E+01	6.548E-01
117	9.269E-02	-4.269E-02	2.926E-01	-6.542E+01	6.908E-01
118	9.083E-02	-4.223E-02	2.102E-01	-6.564E+01	6.997E-01
119	8.830E-02	-4.416E-02	6.564E-01	-6.452E+01	6.620E-01
120	8.541E-02	-4.569E-02	1.215E+00	-6.329E+01	6.316E-01
121	8.232E-02	-4.690E-02	1.822E+00	-6.202E+01	6.065E-01
122	7.912E-02	-4.786E-02	2.447E+00	-6.074E+01	5.852E-01
123	7.585E-02	-4.861E-02	3.075E+00	-5.944E+01	5.668E-01
124	7.514E-02	-4.918E-02	3.697E+00	-5.813E+01	5.506E-01
125	7.185E-02	-4.961E-02	4.307E+00	-5.682E+01	5.363E-01
126	6.857E-02	-4.968E-02	4.438E+00	-5.653E+01	5.334E-01
127	6.531E-02	-4.994E-02	5.030E+00	-5.520E+01	5.207E-01
128	6.208E-02	-5.006E-02	5.605E+00	-5.387E+01	5.093E-01
129	5.890E-02	-5.007E-02	6.162E+00	-5.252E+01	4.989E-01
130	5.578E-02	-4.997E-02	6.700E+00	-5.117E+01	4.893E-01
131	5.271E-02	-4.976E-02	7.218E+00	-4.981E+01	4.806E-01
132	4.971E-02	-4.945E-02	7.717E+00	-4.844E+01	4.725E-01
133	4.677E-02	-4.904E-02	8.196E+00	-4.706E+01	4.650E-01
134	4.391E-02	-4.854E-02	8.656E+00	-4.568E+01	4.581E-01
135	4.113E-02	-4.794E-02	9.097E+00	-4.429E+01	4.516E-01
136	4.025E-02	-4.726E-02	9.519E+00	-4.290E+01	4.457E-01
137	3.757E-02	-4.649E-02	9.922E+00	-4.150E+01	4.401E-01

138	3.497E-02	-4.622E-02	1.005E+01	-4.105E+01	4.384E-01
139	3.245E-02	-4.534E-02	1.043E+01	-3.964E+01	4.333E-01
140	3.002E-02	-4.439E-02	1.079E+01	-3.823E+01	4.286E-01
141	2.767E-02	-4.335E-02	1.113E+01	-3.681E+01	4.241E-01
142	2.542E-02	-4.225E-02	1.146E+01	-3.539E+01	4.200E-01
143	2.325E-02	-4.107E-02	1.178E+01	-3.397E+01	4.161E-01
144	2.117E-02	-3.983E-02	1.207E+01	-3.254E+01	4.125E-01
145	1.919E-02	-3.852E-02	1.235E+01	-3.111E+01	4.091E-01
146	1.730E-02	-3.715E-02	1.262E+01	-2.968E+01	4.060E-01
147	1.550E-02	-3.571E-02	1.287E+01	-2.825E+01	4.030E-01
148	1.379E-02	-3.423E-02	1.311E+01	-2.681E+01	4.003E-01
149	1.219E-02	-3.268E-02	1.333E+01	-2.537E+01	3.977E-01
150	1.068E-02	-3.109E-02	1.354E+01	-2.393E+01	3.953E-01
151	9.263E-03	-2.945E-02	1.373E+01	-2.248E+01	3.931E-01
152	7.948E-03	-2.776E-02	1.392E+01	-2.104E+01	3.911E-01
153	6.732E-03	-2.603E-02	1.408E+01	-1.959E+01	3.892E-01
154	5.614E-03	-2.426E-02	1.424E+01	-1.814E+01	3.875E-01
155	4.597E-03	-2.245E-02	1.438E+01	-1.669E+01	3.859E-01
156	3.681E-03	-2.061E-02	1.452E+01	-1.524E+01	3.845E-01
157	2.865E-03	-1.874E-02	1.463E+01	-1.379E+01	3.832E-01
158	2.151E-03	-1.683E-02	1.474E+01	-1.233E+01	3.821E-01
159	1.538E-03	-1.491E-02	1.483E+01	-1.088E+01	3.811E-01
160	1.028E-03	-1.296E-02	1.492E+01	-9.424E+00	3.802E-01
161	6.195E-04	-1.099E-02	1.499E+01	-7.968E+00	3.794E-01
162	3.139E-04	-9.002E-03	1.505E+01	-6.512E+00	3.788E-01
163	1.112E-04	-7.002E-03	1.509E+01	-5.056E+00	3.783E-01
164	1.136E-05	-4.992E-03	1.513E+01	-3.599E+00	3.779E-01
165	2.476E-17	-2.974E-03	1.515E+01	-2.142E+00	3.776E-01
166	5.149E-05	-9.508E-04	1.516E+01	-6.844E-01	3.775E-01
167	2.059E-04	1.404E-09	1.516E+01	1.011E-06	3.774E-01
168	4.632E-04	2.024E-03	1.516E+01	1.457E+00	3.775E-01
169	8.231E-04	4.045E-03	1.514E+01	2.914E+00	3.777E-01
170	1.286E-03	6.059E-03	1.511E+01	4.371E+00	3.781E-01
171	1.850E-03	8.064E-03	1.507E+01	5.828E+00	3.785E-01
172	2.517E-03	1.006E-02	1.502E+01	7.284E+00	3.791E-01
173	3.285E-03	1.203E-02	1.495E+01	8.740E+00	3.798E-01
174	2.226E-02	1.399E-02	1.487E+01	1.020E+01	3.806E-01
175	2.439E-02	1.593E-02	1.479E+01	1.165E+01	3.816E-01
176	2.660E-02	3.788E-02	1.248E+01	3.044E+01	4.076E-01
177	2.891E-02	3.922E-02	1.221E+01	3.187E+01	4.109E-01
178	3.130E-02	4.050E-02	1.192E+01	3.330E+01	4.144E-01
179	3.377E-02	4.170E-02	1.161E+01	3.473E+01	4.181E-01
180	3.634E-02	4.284E-02	1.129E+01	3.615E+01	4.221E-01
181	3.898E-02	4.391E-02	1.095E+01	3.757E+01	4.264E-01
182	4.025E-02	4.490E-02	1.060E+01	3.898E+01	4.310E-01
183	4.301E-02	4.582E-02	1.023E+01	4.039E+01	4.360E-01
184	4.585E-02	4.622E-02	1.005E+01	4.105E+01	4.384E-01
185	4.876E-02	4.702E-02	9.650E+00	4.245E+01	4.438E-01
186	5.174E-02	4.773E-02	9.234E+00	4.385E+01	4.497E-01
187	5.479E-02	4.836E-02	8.800E+00	4.524E+01	4.560E-01
188	5.789E-02	4.889E-02	8.346E+00	4.662E+01	4.627E-01
189	6.106E-02	4.933E-02	7.873E+00	4.800E+01	4.700E-01

117

190	6.427E-02	4.968E-02	7.381E+00	4.937E+01	4.779E-01
191	6.752E-02	4.992E-02	6.868E+00	5.073E+01	4.864E-01
192	7.080E-02	5.005E-02	6.337E+00	5.209E+01	4.957E-01
193	7.408E-02	5.008E-02	5.786E+00	5.343E+01	5.058E-01
194	7.514E-02	4.999E-02	5.217E+00	5.477E+01	5.169E-01
195	7.841E-02	4.978E-02	4.630E+00	5.610E+01	5.292E-01
196	8.163E-02	4.96?E-02	4.438E+00	5.653E+01	5.334E-01
197	8.475E-02	4.929E-02	3.830E+00	5.785E+01	5.474E-01
198	8.770E-02	4.875E-02	3.211E+00	5.916E+01	5.631E-01
199	9.032E-02	4.804E-02	2.584E+00	6.046E+01	5.810E-01
200	9.237E-02	4.713E-02	1.957E+00	6.175E+01	6.016E-01
201	9.330E-02	4.598E-02	1.344E+00	6.302E+01	6.257E-01

Table VIII. Stable Equilibrium States found by
rudder sweep for $\alpha < 40°$, $\delta_e = -19°$

Point	Rudder Deflection δ_r Degrees	Angle of Attack α Degrees	Sideslip Angle β Degrees	Roll Rate p Rad/sec
1	-1.631235E-02	2.082097E+01	4.085E-04	-8.902E-05
2	-1.701136E-01	2.081811E+01	4.257E-03	-9.284E-04
3	-4.159507E-01	2.080353E+01	1.039E-02	-2.265E-03
4	-6.555274E-01	2.077685E+01	1.636E-02	-3.552E-03
5	-8.855951E-01	2.073843E+01	2.207E-02	-4.759E-03
6	-1.103156E+00	2.068877E+01	2.745E-02	-5.855E-03
7	-1.305539E+00	2.062856E+01	3.241E-02	-6.810E-03
8	-1.490475E+00	2.055860E+01	3.687E-02	-7.588E-03
9	-1.575817E+00	2.052027E+01	3.890E-02	-7.901E-03
10	-1.731368E+00	2.043755E+01	4.249E-02	-8.35⊍3E-03
11	-1.801328E+00	2.039345E+01	4.404E-02	-8.477E-03
12	-1.925277E+00	2.030055E+01	4.659E-02	-8.508E-03
13	-1.979247E+00	2.025208E+01	4.758E-02	-8.402E-03
14	-2.027933E+00	2.020250E+01	4.837E-02	-8.206E-03
15	-2.071426E+00	2.015198E+01	4.896E-02	-7.914E-03
16	-2.109858E+00	2.010071E+01	4.933E-02	-7.520E-03
17	-2.143400E+00	2.004888E+01	4.948E-02	-7.016E-03
18	-2.172264E+00	1.999669E+01	4.941E-02	-6.395E-03
19	-2.196691E+00	1.994432E+01	4.911E-02	-5.649E-03
20	-2.216952E+00	1.989196E+01	4.858E-02	-4.771E-03
21	-2.233352E+00	1.983981E+01	4.781E-02	-3.753E-03
22	-2.246236E+00	1.978806E+01	4.680E-02	-2.584E-03
23	-2.255979E+00	1.973692E+01	4.555E-02	-1.256E-03
24	-2.262986E+00	1.968657E+01	4.405E-02	2.431E-04
25	-2.267691E+00	1.963720E+01	4.229E-02	1.923E-03
26	-2.270552E+00	1.958900E+01	4.029E-02	3.794E-03
27	-2.272046E+00	1.954214E+01	3.803E-02	5.868E-03
28	-2.272663E+00	1.949680E+01	3.552E-02	8.157E-03
29	-2.272904E+00	1.945311E+01	3.277E-02	1.067E-02
30	-2.273268E+00	1.941122E+01	2.977E-02	1.343E-02
31	-2.274252E+00	1.937124E+01	2.654E-02	1.643E-02
32	-2.276338E+00	1.933328E+01	2.307E-02	1.969E-02
33	-2.279990E+00	1.929742E+01	1.939E-02	2.322E-02
34	-2.285648E+00	1.926371E+01	1.549E-02	2.703E-02
35	-2.293720E+00	1.923218E+01	1.140E-02	3.112E-02
36	-2.304584E+00	1.920286E+01	7.101E-03	3.552E-02
37	-2.318585E+00	1.917572E+01	2.620E-03	4.021E-02
38	-2.336035E+00	1.915076E+01	-2.037E-03	4.522E-02

39	-2.357223E+00	1.912791E+01	-6.847E-03	5.055E-02
40	-2.382405E+00	1.910714E+01	-1.180E-02	5.621E-02
41	-2.411818E+00	1.908839E+01	-1.688E-02	6.220E-02
42	-2.435497E+00	1.907622E+01	-2.059E-02	6.669E-02
43	-2.456874E+00	1.906687E+01	-2.372E-02	7.053E-02`
44	-2.488484E+00	1.905524E+01	-2.802E-02	7.595E-02
45	-2.523239E+00	1.904479E+01	-3.241E-02	8.160E-02
46	-2.561256E+00	1.903546E+01	-3.689E-02	8.749E-02
47	-2.602658E+00	1.902726E+01	-4.145E-02	9.363E-02
48	-2.647577E+00	1.902014E+01	-4.611E-02	1.000E-01
49	-2.696155E+00	1.901410E+01	-5.087E-02	1.067E-01
50	-2.748547E+00	1.900913E+01	-5.573E-02	1.137E-01
51	-2.804922E+00	1.900521E+01	-6.070E-02	1.209E-01
52	-2.865467E+00	1.900235E+01	-6.578E-02	1.284E-01
53	-2.930386E+00	1.900056E+01	-7.099E-02	1.363E-01
54	-2.999904E+00	1.899985E+01	-7.632E-02	1.445E-01
55	-3.074267E+00	1.900024E+01	-8.179E-02	1.530E-01
56	-3.153742E+00	1.900176E+01	-8.740E-02	1.619E-01
57	-3.238621E+00	1.900446E+01	-9.316E-02	1.711E-01
58	-3.329222E+00	1.900838E+01	-9.909E-02	1.808E-01
59	-3.425886E+00	1.901359E+01	-1.052E-01	1.909E-01
60	-3.528977E+00	1.902015E+01	-1.115E-01	2.014E-01
61	-3.638887E+00	1.902815E+01	-1.179E-01	2.124E-01
62	-3.756030E+00	1.903767E+01	-1.246E-01	2.238E-01
63	-3.880839E+00	1.904884E+01	-1.315E-01	2.357E-01
64	-4.013769E+00	1.906176E+01	-1.386E-01	2.481E-01
65	-4.155295E+00	1.907657E+01	-1.459E-01	2.611E-01
66	-4.305903E+00	1.909342E+01	-1.534E-01	2.746E-01
67	-4.384770E+00	1.910265E+01	-1.572E-01	2.815E-01
68	-4.549950E+00	1.912285E+01	-1.650E-01	2.958E-01
69	-4.725498E+00	1.914550E+01	-1.731E-01	3.106E-01
70	-4.911957E+00	1.917081E+01	-1.813E-01	3.260E-01
71	-5.109891E+00	1.919897E+01	-1.898E-01	3.420E-01
72	-5.319894E+00	1.923022E+01	-1.984E-01	3.585E-01
73	-5.542601E+00	1.926479E+01	-2.073E-01	3.755E-01
74	-5.778698E+00	1.930293E+01	-2.162E-01	3.931E-01
75	-6.028937E+00	1.934494E+01	-2.254E-01	4.112E-01
76	-6.294153E+00	1.939110E+01	-2.346E-01	4.298E-01
77	-6.575274E+00	1.944176E+01	-2.440E-01	4.489E-01
78	-6.873334E+00	1.949727E+01	-2.535E-01	4.684E-01
79	-7.189472E+00	1.955803E+01	-2.632E-01	4.883E-01
80	-7.524926E+00	1.962446E+01	-2.730E-01	5.087E-01
81	-7.881005E+00	1.969703E+01	-2.830E-01	5.294E-01
82	-8.259029E+00	1.977627E+01	-2.933E-01	5.504E-01
83	-8.660231E+00	1.986271E+01	-3.040E-01	5.717E-01
84	-9.085586E+00	1.995696E+01	-3.153E-01	5.931E-01
85	-9.536172E+00	2.005966E+01	-3.275E-01	6.148E-01
86	-1.001564E+01	2.017139E+01	-3.401E-01	6.364E-01
87	-1.052638E+01	2.029275E+01	-3.529E-01	6.579E-01
88	-1.107040E+01	2.042435E+01	-3.661E-01	6.791E-01
89	-1.164954E+01	2.056673E+01	-3.797E-01	6.999E-01
90	-1.226529E+01	2.072037E+01	-3.937E-01	7.202E-01

120

Table VIII. Stable Equilibrium States found by
rudder sweep for α < 40°, δ_e = -19°
(Continued-)

Point	Pitch Rate q Rad/sec	Yaw Rate r Rad/sec	Pitch Angle Θ Degrees	Bank Angle φ Degrees	True Velocity V kFt/sec
1	1.330E-06	3.817E-04	1.313E+01	1.996E-01	2.784E-01
2	1.451E-04	3.985E-03	1.310E+01	2.085E+00	2.785E-01
3	8.780E-04	9.783E-03	1.299E+01	5.128E+00	2.790E-01
4	2.227E-03	1.552E-02	1.277E+01	8.167E+00	2.801E-01
5	4.186E-03	2.115E-02	1.245E+01	1.120E+01	2.816E-01
6	6.749E-03	2.664E-02	1.203E+01	1.422E+01	2.836E-01
7	9.904E-03	3.196E-02	1.150E+01	1.722E+01	2.862E-01
8	1.364E-02	3.707E-02	1.087E+01	2.020E+01	2.892E-01
9	1.572E-02	3.953E-02	1.052E+01	2.169E+01	2.910E-01
10	2.030E-02	4.427E-02	9.729E+00	2.463E+01	2.949E-01
11	2.279E-02	4.653E-02	9.291E+00	2.609E+01	2.971E-01
12	2.817E-02	5.083E-02	8.329E+00	2.899E+01	3.019E-01
13	3.104E-02	5.286E-02	7.804E+00	3.042E+01	3.045E-01
14	3.404E-02	5.481E-02	7.248E+00	3.185E+01	3.074E-01
15	3.716E-02	5.667E-02	6.661E+00	3.325E+01	3.103E-01
16	4.033E-02	5.845E-02	6.042E+00	3.465E+01	3.135E-01
17	4.374E-02	6.013E-02	5.390E+00	3.603E+01	3.169E-01
18	4.719E-02	6.173E-02	4.705E+00	3.739E+01	3.204E-01
19	5.074E-02	6.324E-02	3.986E+00	3.874E+01	3.241E-01
20	5.439E-02	6.466E-02	3.232E+00	4.007E+01	3.280E-01
21	5.813E-02	6.599E-02	2.443E+00	4.138E+01	3.321E-01
22	6.196E-02	6.723E-02	1.619E+00	4.266E+01	3.364E-01
23	6.587E-02	6.839E-02	7.575E-01	4.392E+01	3.410E-01
24	6.985E-02	6.947E-02	-1.414E-01	4.516E+01	3.457E-01
25	7.390E-02	7.046E-02	-1.079E+00	4.636E+01	3.506E-01
26	7.801E-02	7.138E-02	-2.055E+00	4.754E+01	3.558E-01
27	8.216E-02	7.224E-02	-3.070E+00	4.868E+01	3.611E-01
28	8.636E-02	7.302E-02	-4.125E+00	4.978E+01	3.667E-01
29	9.059E-02	7.376E-02	-5.220E+00	5.085E+01	3.724E-01
30	9.484E-02	7.444E-02	-6.354E+00	5.187E+01	3.784E-01
31	9.910E-02	7.508E-02	-7.527E+00	5.285E+01	3.845E-01
32	1.034E-01	7.569E-02	-8.737E+00	5.378E+01	3.907E-01
33	1.076E-01	7.628E-02	-9.984E+00	5.466E+01	3.971E-01
34	1.118E-01	7.686E-02	-1.127E+01	5.550E+01	4.036E-01
35	1.160E-01	7.743E-02	-1.258E+01	5.627E+01	4.103E-01
36	1.201E-01	7.802E-02	-1.393E+01	5.700E+01	4.169E-01
37	1.242E-01	7.863E-02	-1.530E+01	5.766E+01	4.237E-01
38	1.282E-01	7.927E-02	-1.670E+01	5.827E+01	4.305E-01

39	1.321E-01	7.994E-02	-1.813E+01	5.883E+01	4.372E-01
40	1.360E-01	8.068E-02	-1.957E+01	5.932E+01	4.440E-01
41	1.397E-01	8.147E-02	-2.103E+01	5.976E+01	4.507E-01
42	1.424E-01	8.208E-02	-2.209E+01	6.004E+01	4.555E-01
43	1.445E-01	8.261E-02	-2.296E+01	6.024E+01	4.594E-01
44	1.473E-01	8.338E-02	-2.416E+01	6.049E+01	4.646E-01
45	1.501E-01	8.421E-02	-2.536E+01	6.071E+01	4.698E-01
46	1.528E-01	8.511E-02	-2.657E+01	6.089E+01	4.749E-01
47	1.555E-01	8.607E-02	-2.779E+01	6.103E+01	4.799E-01
48	1.580E-01	8.711E-02	-2.900E+01	6.113E+01	4.849E-01
49	1.605E-01	8.823E-02	-3.022E+01	6.121E+01	4.897E-01
50	1.630E-01	8.944E-02	-3.144E+01	6.124E+01	4.944E-01
51	1.653E-01	9.073E-02	-3.266E+01	6.124E+01	4.991E-01
52	1.676E-01	9.213E-02	-3.388E+01	6.120E+01	5.036E-01
53	1.698E-01	9.362E-02	-3.510E+01	6.113E+01	5.079E-01
54	1.719E-01	9.523E-02	-3.632E+01	6.102E+01	5.122E-01
55	1.740E-01	9.696E-02	-3.753E+01	6.087E+01	5.163E-01
56	1.760E-01	9.881E-02	-3.873E+01	6.069E+01	5.202E-01
57	1.779E-01	1.008E-01	-3.993E+01	6.046E+01	5.241E-01
58	1.797E-01	1.029E-01	-4.112E+01	6.020E+01	5.277E-01
59	1.815E-01	1.052E-01	-4.230E+01	5.990E+01	5.312E-01
60	1.831E-01	1.076E-01	-4.347E+01	5.956E+01	5.345E-01
61	1.847E-01	1.102E-01	-4.463E+01	5.918E+01	5.376E-01
62	1.863E-01	1.130E-01	-4.577E+01	5.875E+01	5.406E-01
63	1.877E-01	1.160E-01	-4.689E+01	5.828E+01	5.433E-01
64	1.890E-01	1.192E-01	-4.799E+01	5.778E+01	5.459E-01
65	1.903E-01	1.225E-01	-4.908E+01	5.722E+01	5.482E-01
66	1.915E-01	1.261E-01	-5.013E+01	5.663E+01	5.503E-01
67	1.926E-01	1.299E-01	-5.116E+01	5.599E+01	5.522E-01
68	1.936E-01	1.340E-01	-5.216E+01	5.531E+01	5.539E-01
69	1.945E-01	1.383E-01	-5.313E+01	5.459E+01	5.553E-01
70	1.954E-01	1.428E-01	-5.407E+01	5.383E+01	5.564E-01
71	1.961E-01	1.476E-01	-5.497E+01	5.303E+01	5.573E-01
72	1.968E-01	1.527E-01	-5.584E+01	5.220E+01	5.580E-01
73	1.973E-01	1.580E-01	-5.666E+01	5.132E+01	5.583E-01
74	1.978E-01	1.635E-01	-5.745E+01	5.042E+01	5.584E-01
75	1.982E-01	1.694E-01	-5.820E+01	4.949E+01	5.582E-01
76	1.986E-01	1.755E-01	-5.890E+01	4.853E+01	5.578E-01
77	1.988E-01	1.819E-01	-5.956E+01	4.755E+01	5.570E-01
78	1.989E-01	1.885E-01	-6.019E+01	4.654E+01	5.560E-01
79	1.990E-01	1.954E-01	-6.077E+01	4.552E+01	5.546E-01
80	1.990E-01	2.026E-01	-6.131E+01	4.448E+01	5.530E-01
81	1.989E-01	2.101E-01	-6.181E+01	4.343E+01	5.510E-01
82	1.988E-01	2.179E-01	-6.227E+01	4.237E+01	5.487E-01
83	1.985E-01	2.259E-01	-6.269E+01	4.131E+01	5.461E-01
84	1.982E-01	2.342E-01	-6.307E+01	4.023E+01	5.431E-01
85	1.978E-01	2.428E-01	-6.341E+01	3.916E+01	5.397E-01
86	1.972E-01	2.516E-01	-6.371E+01	3.809E+01	5.360E-01
87	1.966E-01	2.606E-01	-6.398E+01	3.703E+01	5.317E-01
88	1.958E-01	2.697E-01	-6.421E+01	3.598E+01	5.271E-01
89	1.949E-01	2.790E-01	-6.439E+01	3.494E+01	5.220E-01
90	1.939E-01	2.884E-01	-6.455E+01	3.392E+01	5.165E-01

Bibliography

1. Mehra, R. K. and J. V. Carroll. <u>Bifurcation Analysis of Nonlinear Aircraft Dynamics</u>, Journal of Guidance, Vol. 5, No. 5, Sept. - Oct. 1982.

2. Zagaynov, G. I. and M. G. Goman. "Bifurcation Analysis of Critical Aircraft Flight Regimes," <u>International Council of the Aeronautical Sciences</u>, 84: 217-223, 1984.

3. Hawkins, Capt Carl A. <u>Application of Bifurcation and Catastrophe Theories to Near Stall Flight Mechanics.</u> MS Thesis. Massachusetts Institute of Technology, December 1985, (AD A167 697).

4. <u>SAS User's Guide: Statistics</u>, (Version 5 Edition). Cary, North Carolina: SAS Institute Inc., 1985.

5. Doedel, E. J. and J. P. Kernevez. <u>Software for Continuation Problems in Ordinary Differential Equations with Applications.</u>

6. Guicheteau, P. "Bifurcation Theory Applied to the Study of Control Losses on Combat Aircraft," <u>La Recherche Aerospatiale</u>, 1982.

7. McDonnell Aircraft Company. <u>F/TF-15 Stability Derivatives, Mass and Inertia Characteristics Flight Test Data Basis</u>. Report No. MDC A4172 Parts I and II, Rev. C, August 1976.

8. McDonnell Aircraft Company. <u>F-15 Stability and Control and Flying Qualities</u>. Report No. MDC A0503, 31 July 1972.

9. Planeaux, J. B. and Barth, T. J. <u>High-Angle-of-Attack Dynamic Behavior of a Model High-Performance Fighter Aircraft.</u> AIAA-88-4368

10. Seydel, R. <u>From Equilibrium to Chaos, Practical Bifurcation and Stability Analysis</u>. New York: Elsevier Science Publishing Co. Inc., 1988.

11. McRuer, D. et al. <u>Aircraft Dynamics and Automatic Control</u>. Princeton: Princeton University Press, 1973.

12. Barth, T. J. <u>Determination of High Angle-of-Attack Stability of the F-15B Aircraft Using Bifurcation Analysis</u>. MS Thesis. Wright-Patterson AFB, Ohio: School of Engineering, Air Force Institute of Technology, December 1987.

Bibliography
(Continued-)

13. Golubitsky, M. and Schaeffer, D. G. Singularities and
Groups in Bifurcation Theory, Vol. 51, New York: Springer-
Verlag, 1985.

14. Bifurcation Theory and Nonlinear Eigenvalue Problems.
Edited by Stuart Antman and Joeseph B. Keller. New York:
W. A. Benjamin, Inc., 1969.

15. Jordan, D. W. and Smith, P. Nonlinear Ordinary
Differential Equations. New York: Oxford University Press,
1977.

16. Bifurcation Analysis - Principles, Application and
Synthesis. Edited by Hazewinkel, M. et al. Dordrecht,
Holland: D. Reidel Publishing Company, 1985.

17. Doedel, E. J. and J. P. Kernevez. Software for
Continuation Problems in Ordinary Differental Equations with
Applications.

18. USAF Series F-15A/B Aircraft Flight Manual, TO 1F-
15A-1, 15 August 1980

19. Jahnke, C. C. and Culick, F. E. C. "Application of
Dynamical Systems Theory to Nonlinear Aircraft Dynamics,"
AIAA Atmospheric Flight Mechanics Conference. AIAA-88-
4372. Washington, D. C. American Institute of Aeronautics
and Astronautics, August 1988.

20. Cochran, J. E. and Ho, C. S. Stability of Aircraft
Motion in Critical Cases, Journal of Guidance, Vol. 6, No.
4, July - August 1983.

21. Young, J. W. et al. Prediction of Jump Phenomena in
Aircraft Maneuvers, including Nonlinear Aerodynamic Effects.
Journal of Guidance and Control, Vol. 1, No. 1, January -
February 1978.

22. Wilson, D. B. and Winters, C. P. F-15A Approach-to-
Stall / Stall / Post-Stall Evaluation, AFFTC-TR-75-32, Air
Force Flight Test Center, Edwards A.F.B., California,
January 1976

23. Doedel, E. AUTO: A Subroutine Package for the
Bifurcation Analysis of Autonomous Systems of Ordinary
Differential Equations, Concordia University, Montreal,
Canada.

124

Bibliography
(Continued-)

24. 1988 F-15 Aerobase, ASD/VFEF, Wright Patterson A.F.B.,
Ohio.

25. Burden, R. and J. Faires. Numerical Analysis, 3d ed.,
"Algorithm 3.5", Prindle, Webber and Schmidt - Kent, Boston
1985.

Vita

Captain Daniel D. Baumann was born on 16 February 1960 in Manhassett, New York. He graduated from Bellport Senior High School in 1978, and attended the University of Miami, Florida, from which he received the Bachelor of Science in Mechanical Engineering in June of 1982. He received his commission into the USAF through the Air Force Reserve Officer Training Corps (AFROTC) Detachment 155. His engineering experience included 5 years in the 3246 Test Wing, Eglin AFB in the Advanced Medium Range Air-To-Air Missile Joint Test Force (AMRAAM JTF). He is a licensed Professional Engineer (P.E.) in Mechanical Engineering. In addition he is a FAA licensed pilot with 600+ hours Pilot In Command time and owner of the following ratings; Glider, Single Engine Land, MultiEngine Land, Commercial, Instrument, and Certified Flight Instructor. He has also personally performed spin entry's and more importantly spin recoveries in the following Aircraft; Cessna T-37, Cessna 152 and Beechcraft BE-77's. He was the Board Recorder for the F-15D #84-0042 Flight Mishap Investigation Board. He entered the School of Engineering, Air Force Institute of Technology in June 1988.

Permanent Address: 1711 Daytonia Road
                     Miami Beach, Florida   33141

126

REPORT DOCUMENTATION PAGE

Form Approved
OMB No. 0704-0188

1a. REPORT SECURITY CLASSIFICATION UNCLASSIFIED	1b. RESTRICTIVE MARKINGS
2a. SECURITY CLASSIFICATION AUTHORITY	3. DISTRIBUTION/AVAILABILITY OF REPORT
2b. DECLASSIFICATION/DOWNGRADING SCHEDULE	Approved for public release. Distribution unlimited.

4. PERFORMING ORGANIZATION REPORT NUMBER(S) AFIT/GAE/ENY/89D-01	5. MONITORING ORGANIZATION REPORT NUMBER(S)

6a. NAME OF PERFORMING ORGANIZATION SCHOOL OF ENGINEERING	6b. OFFICE SYMBOL (If applicable) AFIT/ENY	7a. NAME OF MONITORING ORGANIZATION

6c. ADDRESS (City, State, and ZIP Code) AIR FORCE INSTITUTE OF TECHNOLOGY (AU) WRIGHT-PATTERSON AFB, OH 45433 - 6583	7b. ADDRESS (City, State, and ZIP Code)

8a. NAME OF FUNDING/SPONSORING ORGANIZATION F-15 SYSTEM PROGRAM OFFICE	8b. OFFICE SYMBOL (If applicable) ASD/VFEF	9. PROCUREMENT INSTRUMENT IDENTIFICATION NUMBER

| 8c. ADDRESS (City, State, and ZIP Code) AREA B BLDG. B WRIGHT-PATTERSON AFB, OH 45433 - 6585 | 10. SOURCE OF FUNDING NUMBERS |

PROGRAM ELEMENT NO.	PROJECT NO.	TASK NO	WORK UNIT ACCESSION NO.

11. TITLE (Include Security Classification)
F-15B HIGH ANGLE-OF-ATTACK PHENOMENA AND SPIN PREDICTION USING BIFURCATION ANALYSIS

12. PERSONAL AUTHOR(S)
DANIEL D. BAUMANN, B.S., P.E., CAPTAIN, USAF

13a. TYPE OF REPORT MS THESIS	13b. TIME COVERED FROM _____ TO _____	14. DATE OF REPORT (Year, Month, Day) 1989 DECEMBER	15. PAGE COUNT 140

16. SUPPLEMENTARY NOTATION

17. COSATI CODES			18. SUBJECT TERMS (Continue on reverse if necessary and identify by block number)
FIELD	GROUP	SUB-GROUP	AERODYNAMIC STABILITY, EQUATIONS OF MOTION, BIFURCATION, EQUILIBRIUM
12	01		

19. ABSTRACT (Continue on reverse if necessary and identify by block number)

THESIS CHAIRMAN: JAMES B. PLANEAUX, CAPTAIN, USAF
ASSISTANT PROFESSOR OF AERONAUTICAL ENGINEERING

20. DISTRIBUTION/AVAILABILITY OF ABSTRACT ☒ UNCLASSIFIED/UNLIMITED ☐ SAME AS RPT ☐ DTIC USERS	21. ABSTRACT SECURITY CLASSIFICATION UNCLASSIFIED
22a. NAME OF RESPONSIBLE INDIVIDUAL JAMES B. PLANEAUX, CAPTAIN, USAF	22b. TELEPHONE (Include Area Code) (513) 255 - 3517	22c. OFFICE SYMBOL AFIT/ENY

DD Form 1473, JUN 86   Previous editions are obsolete.

(BOX 19)

Modern fighter aircraft are being designed to be operated at higher and higher angles-of-attack. The resulting increase in maneuverability is offset however by an increase in susceptibility to departure from controlled flight. An investigation of the F-15B fighter aircraft was undertaken to predict high angle-of-attack phenomena such as flat spins. Aerodynamic forces and moments as a function of control surface deflections $(\delta_a, \delta_e, \delta_{\Delta e}, \delta_r)$ were modeled over a wide angle-of-attack range $(-20° \leq \alpha \leq +90°)$ and were then used to formulate a non-linear eight state $(\alpha, \beta, p, q, r, \theta, \phi, V)$ aircraft model. Equilibrium and periodic solutions to the resulting equations of motion were then computed using a bifurcation analysis package. A number of bifurcation points, limit points and Hopf bifurcation points were detected indicating changes in flight stability. Several stable equilibrium solution branches at angles-of-attack greater than 70 degrees were observed which correspond to flat spin behavior. Theoretically predicted flat spin conditions correlated well with empirical flight test data. In addition stable equilibrium and periodic solutions other than those corresponding to spin behavior were surveyed resulting in a global map of stability as a function of control surface deflection for the F-15B.

END

FILMED

3-90

DTIC